Dispersion of Water Sprays in a Transverse Air Jet and the Aging of Spray Nozzles

by

Shereen Eletribi

B.E., Mechanical Engineering
State University of New York at Stony Brook, 1997

Submitted to the Department of Mechanical Engineering
in partial fulfillment of the requirements for the degree of

Master of Science in Mechanical Engineering

at the

MASSACHUSETTS INSTITUTE OF TECHNOLOGY

February 1999

Author .....
Department of Mechanical Engineering
January 22, 1999

Certified by .....
Professor John H. Lienhard V
Associate Professor of Mechanical Engineering
Thesis Supervisor

Accepted by .....
Ain Sonin
Chairman of Graduate Studies
Mechanical Engineering

Dispersion of Water Sprays in a Transverse Air Jet and the Aging of Spray Nozzles

by

Shereen Eletribi

Submitted to the Department of Mechanical Engineering
on December 28, 1998, in partial fulfillment of the
requirements for the degree of
Master of Science in Mechanical Engineering

Abstract

This thesis explores spray cooling methods used in the manufacturing process of glass fibers. At the onset of the manufacturing process glass fibers are extruded from a pool of molten glass through an array of holes in a heated bushing plate. Before the fibers can be wound onto a spool, the fibers must be coated with a sizing compound. In order for the sizing compound to be applied, the glass fibers must be cooled to a temperature below 90°C or so. Heat losses through convection and radiation to the environment are not sufficient to achieve this temperature over a reasonable distance, so supplemental cooling in the form of water sprays is used in the manufacturing process. The sprays provide evaporative cooling to the fiber bundle.

This work explores ways to optimize the spray cooling process so the fibers can be cooled more uniformly and with lower water consumption. The spray atomization qualities and the spray dispersion patterns of the nozzles used on the glass production lines are examined. The droplet diameter, velocity and number flux are measured with a Phase Doppler Particle Analyzer.

When the fibers are pulled from the bushing plate, they move at very high velocities and generate a bulk air flow around the fiber bundle. This induced air flow appears to be a determining factor in the dispersion of the spray into the fiber bundle. An experimental apparatus was built to measure the entrainment of the spray into a transverse air jet (simulated fiber air flow). The spray nozzle operating pressure and the spray nozzle distance from the simulated bulk air flow were varied to determine the optimal spray configuration. Increasing the nozzle operating pressure from 276 kPa (40 psi) to 690 kPa (100 psi) was found to increase the quality of atomization, while further increases in pressure to 1000 kPa (145 psi) produced insignificant effects. The best spray dispersion was achieved at a separation of 15 cm between the spray nozzle and the edge of the fiber bundle. Furthermore, the characteristics of the spray interaction with the bulk air flow were compared to the behavior of the spray in still air.

The effect of aging on the spray nozzles is also examined. The spray characteristics were measured at three different positions within the spray cone for a range of operating pressures from 276 kPa (40 psi) to 1000 kPa (145 psi) for nozzles aged zero, two, four and six weeks on an actual glass fiber production line. It was found that increasing the nozzle operating pressure above 690 kPa (100 psi) did not provide significant improvement in spray atomization, as was also found in the bulk air flow case. Aging was found to cause inferior atomization and more scatter in the droplet parameters. Aging effects are due to corrosion of the spray nozzles and to scale deposits within the nozzle water passage.

Thesis Supervisor: John H. Lienhard V
Title: Associate Professor of Mechanical Engineering

Acknowledgments

I would like to express my gratitude to PPG Industries, Fiber Glass Research Center for sponsoring the research presented in this thesis. In particular, I would like to thank Dr. R. Allen Roach and Dr. Jerome A. Burgman for providing their insight and guidance.

I would also like to express my gratitude to Professor John H. Lienhard V for providing his guidance and assistance throughout this project. I want to thank Matthew Sweetland for his patience and help during the course of this work. I would also like to thank Megan Reese for providing me with assistance in completing this work. I also thank my labmates Marc Hodes, Sangjun Han, Hesham Younis, James Moran, Christa Ansbergs, Brett McKeone and Joachim Hadeler, for providing me with an open and friendly work environment.

Contents

List of Figures

List of Tables

Chapter 1

Introduction

Molten glass is extruded through orifices in a platinum bushing plate to form glass fibers. The bushing plate is heated electrically to maintain a constant glass temperature. On small production facilities, gas pressure is used to maintain a steady glass pressure at the orifice entrance. Large high volume production stations maintain a fixed molten glass depth to obtain a constant hydrostatic head. The glass that exits the orifices is pulled and wound onto a take-up reel. The resulting tension in the fiber causes the molten fiber to neck down until the glass sets at the final fiber diameter. The initial glass temperature at the bushing plate is about 1500 K (2240 °F) and the glass solidification temperature is 1390 K (2042 °F). Before the fibers are wound onto the take-up reel, they pass through a coating applicator. The fibers must be cooled to a temperature less than 367 K (200 °F) before the coating is applied.

For sufficient cooling the distance between the bushing plate and the coating applicator is of the order of 1 m. Typical fiber diameters vary between 5 μm and 30 μm with drawing speeds between 15 m/s and 90 m/s. Usually the smaller fibers are drawn at higher velocities than the larger fibers, but the same sized fiber may be pulled at different speeds on different production stations. Figure 1.1 illustrates a typical production station. Bushing plates contain an array of one hundred to several thousand orifices with the spacing between orifices varying from 0.6 cm to 1.0 cm. Multiple fibers are gathered into a bundle after the coating is applied and are then pulled onto the take-up reel.

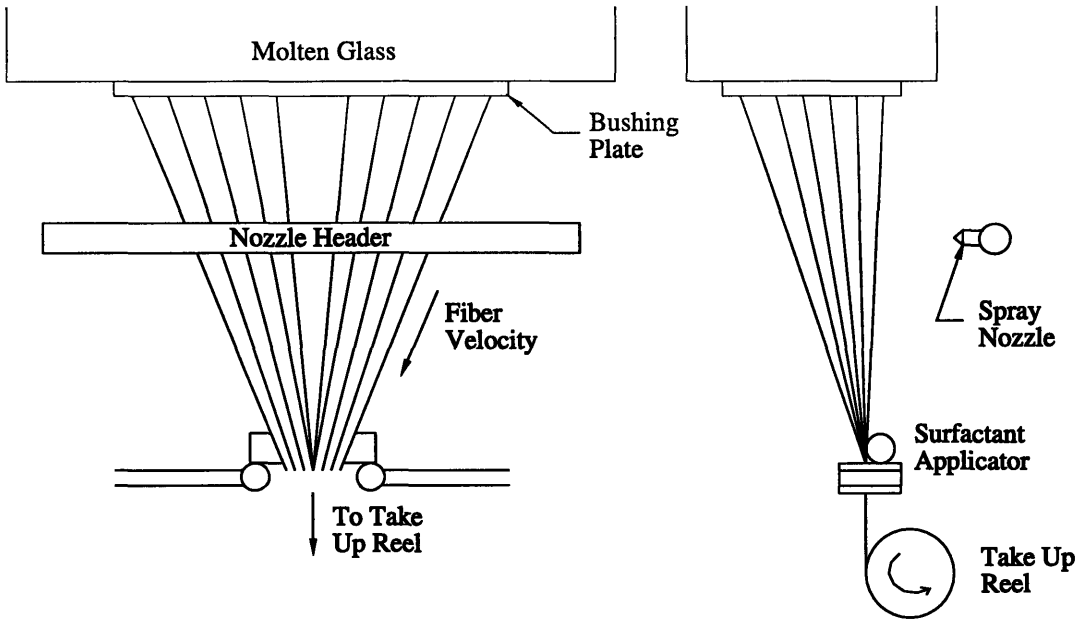

Figure 1.1: Glass fiber production station.[1]

These glass fibers have several applications. The fibers may be spun into fiberglass cloth for use in the automotive industry. They can be used in short lengths to reinforce plastics and in continuous strands for fibrous composites. Fibers are also used to form circuit boards by cutting them into short sections and imbedding them in epoxy.

The fiber heat transfer by convection and radiation to the environment is a significant factor in the production process. The fibers are spray cooled with a series of humidification nozzles to increase the heat transfer to the environment. Nozzle placement, number, type, and operating pressures vary between manufacturing stations and between production facilities.

A substantial amount of research has been performed on the various parts of the fiber forming process. Research on the initial drawing section where the fiber necks down and solidifies into the final diameter has received substantial attention because this area is also of interest to the fiber optics and textile industries. Some work has been performed on the evaluation of the velocity and thermal boundary layers of a long thin cylinder moving through still air. This work is mostly for lower velocity fibers (1-2 m/s) to

1. This figure has been adapted from the thesis, *Nozzle Analysis and Heat Transfer Model for Spray Cooling of Glass Fibers* by Sweetland [1].

quantify the effects of crossflow on the boundary layers. Some work also exists for spray cooling, but most is for the spray cooling of large heated surfaces, often involving boiling of the liquid at the surface. Sweetland [1] performed previous work on the spray nozzles described in this thesis. In this work, a series of clean nozzles were characterized based on droplet diameter and velocity distributions over a wide range of nozzle operating pressures in still air. Sweetland also developed an analytical heat transfer model for the spray cooling of glass fibers.[2]

This thesis consists of three parts pertaining to the analysis and characterization of the nozzles used on fiber production lines. The first section (Chapter 2) is a description of the nozzle testing chamber. The second part (Chapters 3 - 5) investigates the dispersion of the water sprays in a transverse air jet. This section includes the basic theory of air jet flow, a description of the bulk air flow simulating apparatus, a characterization of the bulk air flow field and an evaluation of the entrainment of spray in the air flow. The air velocity and turbulence intensity profiles in the vertical center plane of the spray, as measured with a hot film anemometer, are included. The dispersion measurements include the droplet size distribution and the droplet velocity profile along the vertical center plane of the spray for four different separations between the nozzle and the air jet and for three different jet exit velocities The third part (Chapter 6) describes the effect of aging on spray nozzles. The effect of nozzle pressure variations on spray characteristics is examined for nozzles that are aged zero, two, four and six weeks. Chapter 7 is a summary of the main findings of this work. The information on spray characteristics compiled in this thesis can be combined with an analytical heat transfer model such as the one developed by Sweetland [1], for a better representation of the actual glass fiber cooling rates.

---

2. The preceding paragraphs have been adapted from the thesis, *Nozzle Analysis and Heat Transfer Model for Spray Cooling of Glass Fibers* by Sweetland [1].

Chapter 2

Nozzle Theory and Test Equipment

This chapter covers the theoretical background of the type of nozzles used on the glass fiber production lines. An equation for nozzle flow rate is developed. Also covered in this chapter is a description of the equipment and procedure used to characterized nozzles.

2.1 Theoretical Background of Spray Nozzles

The spray nozzles tested are hollow cone pressure swirl atomizers, also known as simplex nozzles. These nozzles produce a wide spray angle compared with plain orifice atomizers. Simplex nozzles impart a high angular velocity to the liquid in a swirl chamber [Figure 2.1]. As the fluid exits the final orifice, the angular velocity causes the liquid to expand in a conical film which then breaks up into ligaments and drops. The evolution of fully developed spray produced by pressure swirl atomizers is described by Sweetland [1]. Fully developed spray produces a very short break-up length and fine atomization over a prescribed cone angle. The general spray structure of simplex nozzles consists of a sheath of large drops with high momentum surrounding a core of fine drops [1]. The trajectory angle of small drops in the sheath is less than for large drops. The decrease in mean velocity with axial distance is less in the central core than in the sheath due to entrained air.

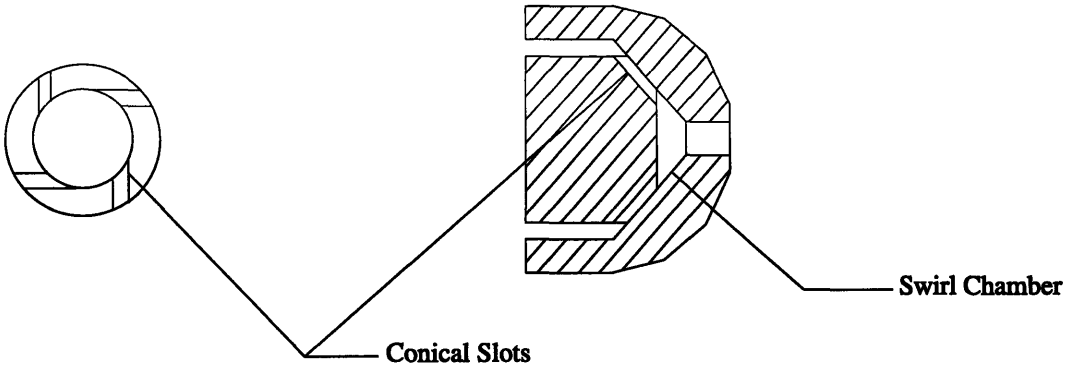

Figure 2.1: Pressure swirl atomizer.[3]

2.2 Flow Rate and Pressure

Basic inviscid theory can be used to develop a relationship between pressure and flow rate. Figure 2.2 is a diagram of inviscid flow inside a pressure-swirl nozzle. The equation derived from basic inviscid theory between pressure and flow rate for the Hago B-50 nozzle is,

$$Q = A_C\sqrt{\Delta P} \tag{2.1}$$

where A_c is a constant for a particular nozzle design, fluid and age, Q is the nozzle flow rate in ml/min and ΔP is the gage pressure in psi [1].

2.3 Diameter

The primary goal in the analysis of spray data is to obtain information necessary for a heat transfer model of the glass fiber production process. For this reason, the most applicable representative droplet diameter used to describe the droplet distribution is the Sauter mean diameter (SMD). The SMD is an indicator of the evaporation rate of the spray cloud and is a simple and explicit input into evaporation equations. The SMD is defined as the diameter of a drop with the same surface area to volume ratio as the whole spray cloud

3. This figure has been adapted from the thesis, *Nozzle Analysis and Heat Transfer Model for Spray Cooling of Glass Fibers* by Sweetland [1].

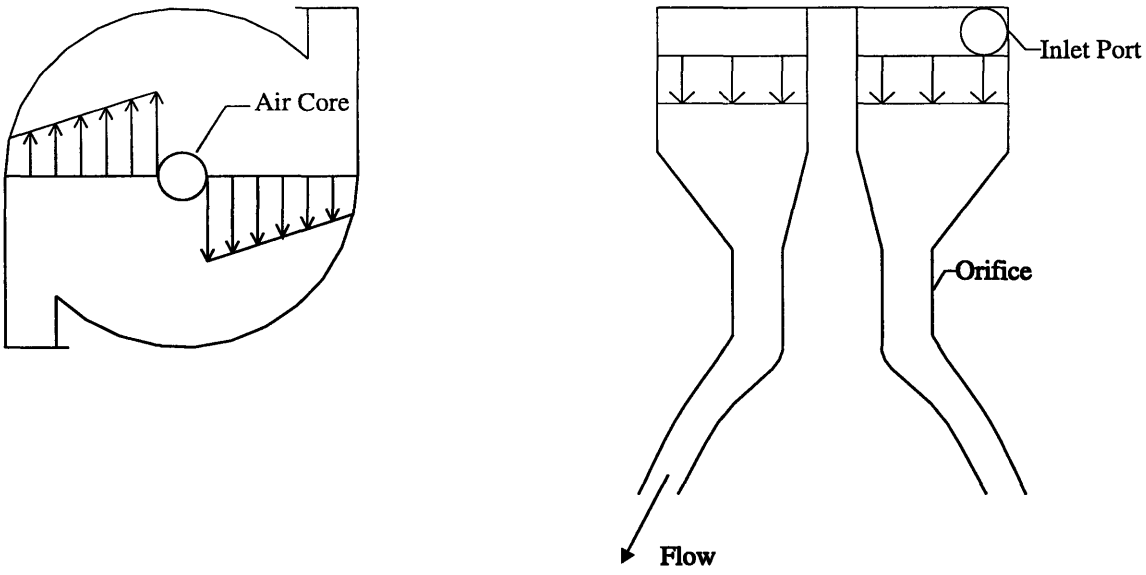

Figure 2.2: Inviscid flow in pressure-swirl atomizer.[4]

which is [2],

$$SMD = \frac{\sum n_i D_i^3}{\sum n_i D_i^2} \tag{2.2}$$

where n_i is the drop count in the bin with average diameter D_i.

Several empirical equations for the SMD of a pressure swirl atomizer have been established. However, these correlations are not reliable because they do not account for variability of the SMD across the spray cloud. Correlations are only useful to indicate general trends in the spray, but cannot be used to evaluate specific values at specific positions within the spray cloud [1].

4. This figure has been adapted from the thesis, *Nozzle Analysis and Heat Transfer Model for Spray Cooling of Glass Fibers* by Sweetland [1].

2.4 Equipment[5]

2.4.1 Test Chamber

The test apparatus for measuring the parameters of the PPG cooling nozzles is designed to simulate operating conditions of the production facility. The primary measurement tool is a phase doppler particle analyzer (PDPA) manufactured by Aerometrics Inc. Due to precise focusing requirements of the PDPA, the system is designed to move the spray nozzle through the field of the stationary PDPA. The size of the test chamber is limited by the optics of the PDPA and the length of an available linear rail system. Output from the PDPA is optimized by using forward scatter and a 30° offset angle between the transmitter and detector. The PDPA is mounted on a 24" by 48" optical table to aid in alignment and focusing, and to limit signal degradation due to thermal expansion of the mounting base during operation. The optical table is mounted on four cork/rubber anti-vibration pads.

The nozzle traverse and test chamber (Figure 2.3) are mounted on a transverse rail to allow motion perpendicular to the PDPA axis. The rail system is driven by a variable speed DC motor mounted to a lead screw. The system is capable of 44" of motion. Unlike most test chambers, the nozzle is mounted with a horizontal spray axis to preserve the effects of gravity present in PPG facilities. The nozzle rail is mounted to an X-Y traversing table that provides motion of the nozzle in a vertical plane. This system permits full motion of the spray around the PDPA measurement volume. The X-Y positions are controlled by hand cranks attached to 10 tpi lead screws. Positions in all three axes are measured relative to the PDPA measurement volume and are repeatable to ±1 mm.

The test chamber is constructed with 1/2" plexiglass sides. This provides a wide viewing area into the chamber while protecting the electronics and optics from water spray. Thick plexiglass was used to avoid warping and bending of the sides which would cause the detector to lose focus with the measurement

---

5. This section has been taken from the thesis, *Nozzle Analysis and Heat Transfer Model for Spray Cooling of Glass Fibers* by Sweetland [1].

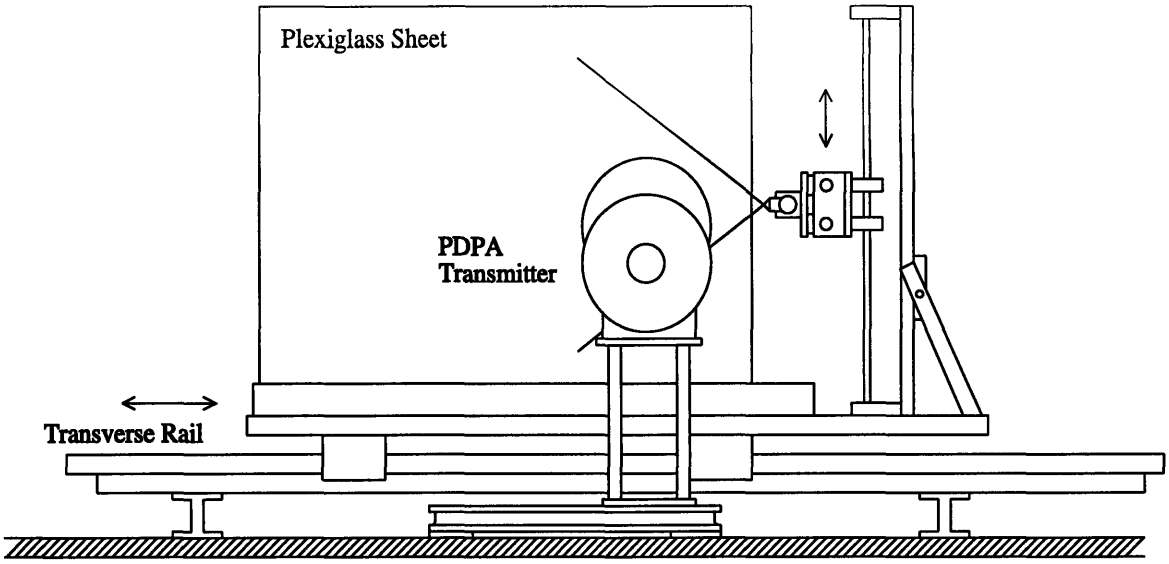

Figure 2.3: Side view of test chamber with flow loop removed.[6]

point. The internal dimensions of the chamber are 32" vertical by 36" horizontal. The base of the test chamber is a 3" deep aluminum pan for water collection. The chamber at the nozzle end is left open to the atmosphere to allow for air entrainment by the nozzle. The other end of the chamber is also left open to the atmosphere, but a sheet of lexan is placed at a slight angle to the horizontal with its base in the aluminum pan. This allows for entrained air to escape the test chamber, but catches most of the spray overshoot and returns it to the collection pan. The top of the chamber, a sheet of 1/8" lexan, is unattached and easily removed. The plexiglass and lexan sides are supported by a steel framework constructed from Dexion angle bracket.

2.4.2 Flow Loop

The flow loop (Figure 2.4) is a closed circuit designed which covers a wide range of operating conditions, from low pressure single nozzle operation to high pressure multiple nozzle flow. Water is stored in two 50 gallon reservoirs that feed into a common supply header for the pump. The pump is a gear pump powered by a 1 1/2 h.p., 230 VAC electric motor capable of pumping 5 gpm at 100 psi. Pump speed is fixed, so the

6. This figure has been adapted from the thesis, *Nozzle Analysis and Heat Transfer Model for Spray Cooling of Glass Fibers* by Sweetland [1].

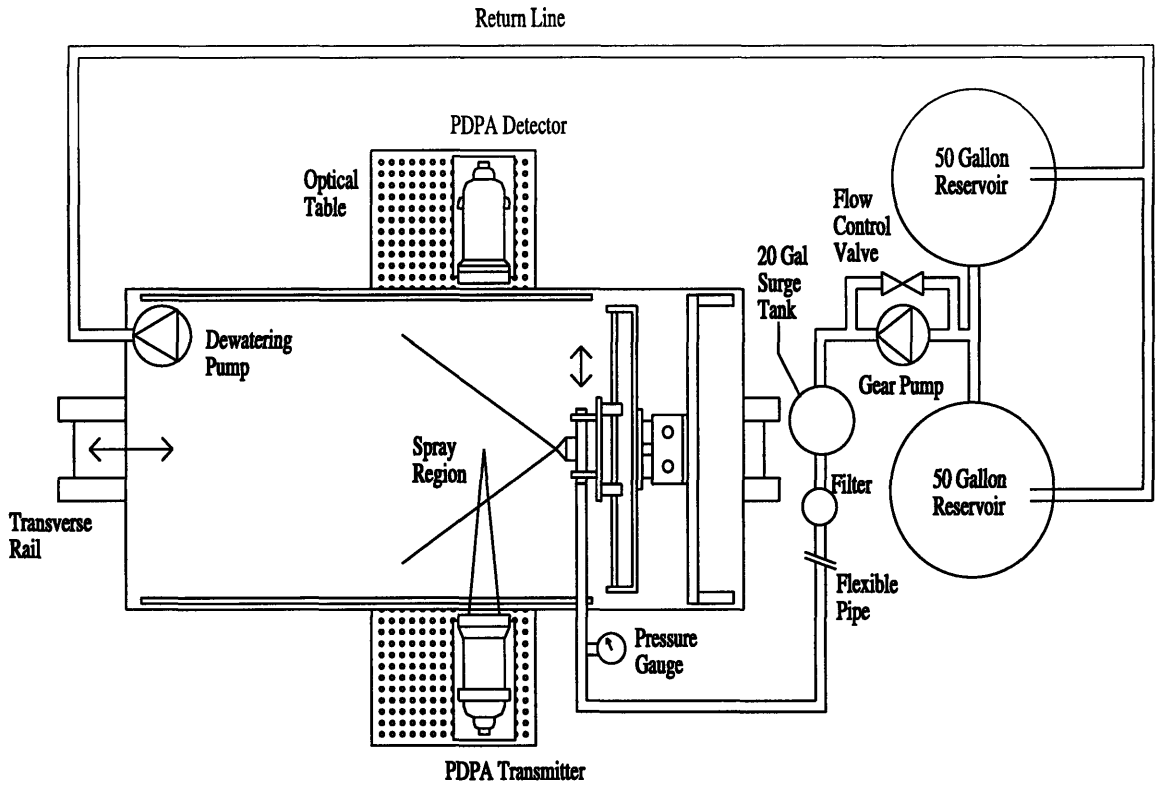

Figure 2.4: Test chamber and flow loop.[7]

flow rate is controlled via a bypass line from the pump exit to the pump intake. Pump pressure pulsations are reduced using a 20 gallon surge tank. The tank has an independent air supply line to vary the degree of capacitance. The flow is passed through two particle filters to remove contaminants before being piped to the nozzle header. Flow rate is measured using a rotameter accurate to ± 2.2 cc/min (±.034 GPH). A pressure gauge (±11 kPa/1.6 psi) and dial thermometer (±1.1°C/2°F) are mounted directly to the nozzle header. The high pressure system is constructed from 3/4" schedule 80 PVC pipe. Flow is returned to the reservoirs from the collection pan by a high volume, low pressure sump pump that is capable of pumping down to a 1/8" water depth.

2.4.3 Phase Doppler Particle Analyzer

The PDPA can be used for simultaneous measurements of particle size and velocity. An interference fringe

7. This figure has been adapted from the thesis, *Nozzle Analysis and Heat Transfer Model for Spray Cooling of Glass Fibers* by Sweetland [1].

pattern is produced by intersecting laser beams. When a particle traverses this pattern, refracted light produces a signal in the photomultiplier tubes. By measuring the frequency of the received signal and knowing the fringe pattern spacing from the laser wavelength, the particle velocity can be calculated. With the use of multiple detectors (three photomultiplier tubes) with fixed spacing, the phase shift of a particle signal from one detector to another can be used to calculate particle size. This calculation can be done with only two detectors, but by using three detectors, two separate size calculations can be made and compared. If the two values do not match, the signal is rejected. Accuracy of the diameter measurement varies with the optical set-up of the system and the range of particle diameters being measured.

The PDPA is a single particle measurement device. This means only one particle can be in the measurement volume at any one time for the measurement to be valid. Edwards and Marx [3] have described this restriction as a pair of Poisson filters acting on the data. The data point will be rejected if the particle spacing is sufficiently small that two particle are in the measurement volume at the same time. Also, the data point will be rejected if a particle in the measurement volume does not exit the space before another particle with a different velocity enters. These two effects cause increasing errors in the PDPA measurement of volume flux and particle density with increasing particle density and increasing particle velocity range. The actual measurement volume of the system varies depending on the particle size. Smaller particles must transit closer to the center of the measurement volume to produce a detectable signal. The combination of these effects can lead to large errors in volume flux and particle density calculations. Software algorithms attempt to correct for these effects, but become substantially less effective with increasing droplet density. It is important to note however, that as particle density and volume flux increase, the errors in diameter and velocity measurements do not change. While the number of rejections increase, as long as a sufficient number of valid samples are obtained, the diameter and velocity distributions will be correct. A final restriction on the PDPA is that the particles must be spherical for accurate size calculations. This leads to data rejection in regions of high velocity gradients where the drops are distorted by aerodynamic forces. If a particle is not rejected, the result is termed a validation. In still air and in bulk air flow the percentage of validations varies from 65% to 95%. The droplet validation rate (number/sec) can be used as an indicator of the droplet flux through a region.

The requirement of knowing the exact spacing from the measurement volume to the detectors for particle size measurements necessitates precise focusing of the detector on the measurement point. Loss of focus on this point will result in lost and incorrect data. For this reason, quality control of the received signal is critical. The two primary means of checking the data are through software monitoring of data rejection flags and by monitoring the data signals on oscilloscopes. The system software provides automatic monitoring of data validations as well as cumulative information of data rejections. If the detector is out of focus, the majority of data rejections will be due to excessive phase discrepancies between the multiple detectors. Data quality can also be monitored by observing the raw and processed signals from each photomultiplier tube on oscilloscopes. Two dual channel scopes are used in this set-up. One is a 60 MHz analog scope and the other is a 100 MHz digital scope. Signals from two separate photomultiplier tubes can be displayed on each screen and compared. The signals (both raw and processed) between detectors should have matching shapes with a phase shift. Large variations in shape or magnitude are good indicators that the detector is out of focus.

2.5 Experimental Procedure[8]

Water was supplied from the surge tank by applying compressed air at a set pressure. The pump was used for initially charging the tank with water. This method completely eliminated pressure pulsations from operating with the pump. Water temperature and pressure were measured at the nozzle header. Room temperature remained constant at 22°C (72°F), but the relative humidity varied with atmospheric conditions. Ambient temperature (±.6°C/1°F) and relative humidity (±3% in 20-90% range at 25°C) were measured with an Omega digital thermo-hygrometer (model RH-411).

Initial investigations of the spray yielded optimal settings for the PDPA [1]. The best results are found for the largest laser intersection angle and for a velocity offset of 5 m/s. The most accurate spray distribution information is found by inclusion of the largest drops in the measurement range [4]. Therefore, the specified maximum diameter was manually changed to accommodate the different positions in the spray

8. This section has been adapted from the thesis, *Nozzle Analysis and Heat Transfer Model for Spray Cooling of Glass Fibers* by Sweetland [1].

cone which had different size droplets.

A few measures are taken to eliminate corrosion and rust deposits from affecting nozzle performance and repeatability. The flow system is flushed each day before taking data. Also, if a noticeable change became apparent in the spray pattern of a particular nozzle, the nozzle would be replaced with a new nozzle. Changes are usually detected by a visual inspection of the spray cone, but an additional check was made each day by repeating points from the previous day's run and comparing values.

Chapter 3

Simulated Fiber Air Flow

This chapter describes the experimental apparatus used to simulate the bulk air motion induced by the moving fibers in PPG Industries glass fiber production lines. The bulk air flow is mainly due to the air that is entrained by the moving fibers, but it is also affected by a small duct located adjacent to the glass fiber manufacturing apparatus. The interaction of the spray with the bulk air motion will determine the spray distribution in the fiber bundle. Included in this chapter is the basic theory of air jet flow, a description of the equipment, a description of hot film anemometry, and a description of the procedure used to generate and measure air velocity and turbulence profiles. A description of the bulk air flow field including air velocity and turbulence intensity profiles, as measured with a pitot probe and hot film anemometer, is also included.

3.1 Bulk Air Flow Generating Apparatus

The experimental apparatus designed to generate velocity flow fields is illustrated in Figure 3.1. The test apparatus is designed to generate air velocity profiles for testing spray distributions. The results will be used to estimate spray distributions in actual fiber bundles.

A steel frame constructed from Dexion angle bracket was built around the existing nozzle testing chamber, described in Chapter 2. The plenum is mounted in this frame with four long arms to facilitate vertical movement. The housing is constructed from 0.5" plywood and has interior dimensions of 2' × 2' × 1'. The outside of the housing is protected from leaks with aluminum duct tape. Two stainless steel wire

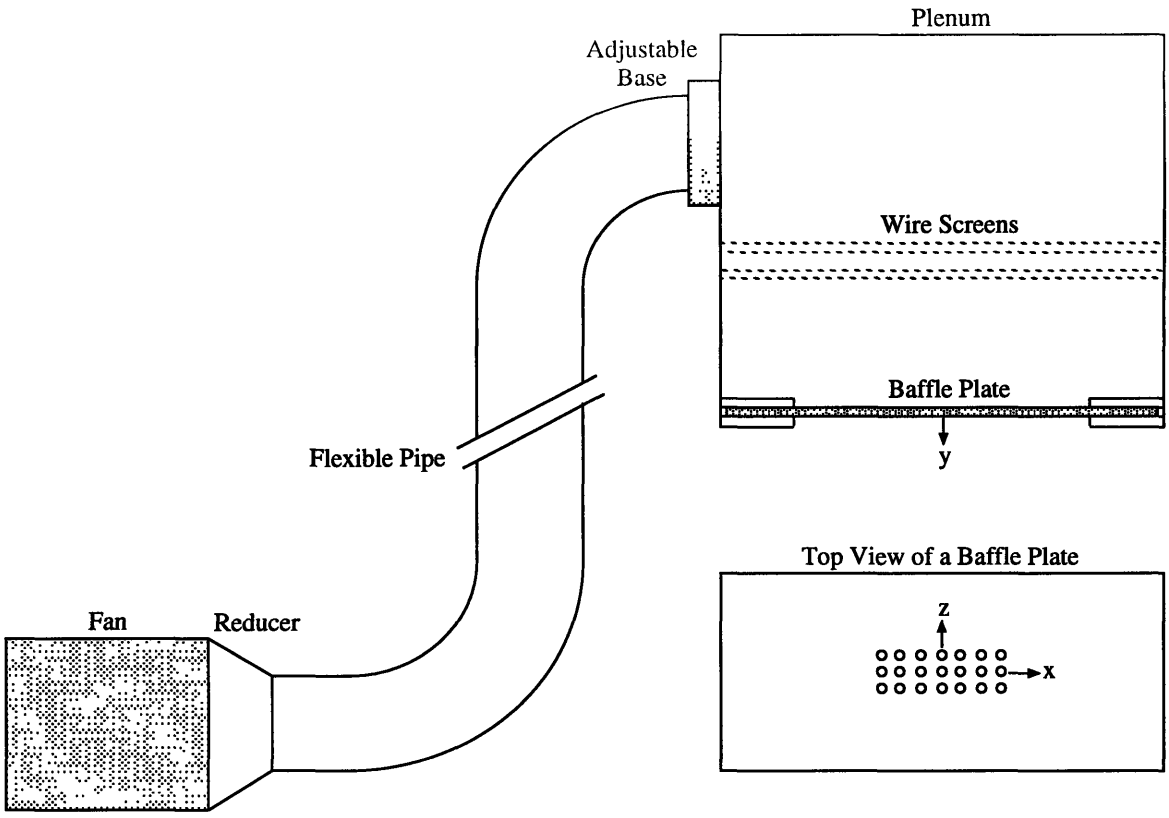

Figure 3.1: Experimental apparatus for generating velocity profiles.

screens (0.198 cm mesh, 38.9% open area) are mounted on shelves in the plenum just below the pipe opening to distribute the air flow uniformly before it reaches the baffle plate exit. The air flow exits through the baffle plate into the existing testing chamber.

A baffle plate is mounted in between two plywood shelves that are covered with polyurethane foam sheeting for leak prevention. Baffle plates are constructed from 0.25" Lexan and have dimensions of 1' × 2'. Several different baffle plates will be used, each with a different number of holes and variable spacing between holes, to generate various velocity profiles. The baffle plate used to generate the initial velocity profile has a 7 × 3 array of 1 cm diameter holes with a 2.5 cm center-to-center spacing.

Air flows from the fan to the plywood housing through corrugated flexible 6" aluminum pipe. The air source is a variable speed motor driven fan manufactured by INDUSTRIAL AIR (model 022D012NP). The fan can produce a range of volume flow rates from 20 to 90 cfm.

3.2 Pitot Probe Instrumentation

3.2.1 Theoretical Background

Pitot tubes measure differential pressures in fluid flows. The differential pressures are converted to velocities using the Bernoulli principle,

$$U_1 = \sqrt{\frac{2}{\rho}(P_2 - P_1)} \tag{3.1}$$

where ρ is the density of the air, P_2 is the stagnation point pressure ($U_2 = 0$), and (P_2 - P_1) is the differential pressure measured by the pitot tube. The air flow is considered incompressible and steady.

3.2.2 Equipment

A cylindrical pitot tube is used to take air velocity measurements. The pitot tube is attached to a 100 torr MKS Differential Baratron[R] pressure transducer which is used in conjunction with a Type 270 Signal Conditioner/Readout with a digital display. The pitot probe was calibrated using an inclined manometer. The accuracy of the pitot tube in measuring pressures is estimated at 5.0% with a sensitivity of 0.0005 inches of water. Using equation (3.1) the values of sensitivity and accuracy of the velocities are calculated to be 2.0% and 3.5%, respectively.

3.2.3 Procedure

The following analysis was done using the cylindrical pitot tube. Initial measurements were taken at various exit holes of the baffle plate to ensure uniformity of the exiting jets. Next, a linear relationship between fan speed and jet exit velocity was found. The velocities along the centerline of the jet array were measured at various heights to find the dependence of centerline velocity on the distance below the baffle plate.

Considering this data, three different combinations of height and fan speed were chosen which seemed likely to produce the desired velocity profile. The desired velocity range for the bulk air flow at the nozzle level is between 0.5 and 5.0 m/s (according to measurements taken in a glass fiber plant). The horizontal velocity profiles of these three combinations were measured in the positive x-direction (symmetry was assumed in the x- and z-directions since initial measurements of several holes' jet exit velocity yielded

uniformity of the exiting jets).

For a jet exit velocity of 13 m/s, the velocity flow field was measured on a 1 cm grid at horizontal planes normal to the air flow direction. The planes ranged from 10 to 40 cm below the baffle plate, at 10 cm intervals. The grid limits were defined by the sensitivity of the pitot probe, once velocities dropped below 0.5 m/s measurements were ceased.

Ambient temperature remained constant at 76°F. The moving air flow temperature was fairly steady at 75 ±.5°F. These measurements were made with an Omega digital thermo-hygrometer (model RH-411).

3.3 Hot Film Anemometry

3.3.1 Theoretical Background

Hot film anemometers measure fluid velocity by detecting changes in the heat loss from a small, electrically heated cylindrical film element placed in the fluid flow. The film resistance is kept constant by controlling the film temperature with a heating current provided by the anemometer electronics. The heat dissipated by convective cooling of the cylinder is balanced by electrical heating by varying the electric current through the film. Thus the voltage can be related to the velocity by using the following empirical relationship (King's Law),

$$\frac{V^2}{R} = (A + BU_a^{0.45}) \cdot (T - T_a) \tag{3.2}$$

where V is the film voltage, U_a is the gas velocity, T_a is the gas temperature, and A and B are constants. Since the film resistance, R, and the film temperature, T, are kept constant, equation (3.1) may be written as,

$$V^2 = C + DU_a^{0.45} \tag{3.3}$$

where C and D are constants that are obtained through calibration of the anemometer.

A major advantage of hot film anemometers over pitot tubes is their ability to measure rapid

fluctuations in velocity, thus enabling turbulence measurements. Turbulence intensity is defined as,

$$Tu = \frac{u'}{\overline{U}} \tag{3.4}$$

where $\overline{U}$ is the mean velocity and u' is the root mean square of the fluctuating component of velocity ($u = U - \overline{U}$). Hot film sensors measure turbulence accurately in flows with low to moderate turbulence intensities ($Tu < \sim 25\%$) [5].

The film sensor used in these experiments can measure velocities in the range of 0.15 to 100 m/s. Below 0.15 m/s natural convection effects are significant, above 100 m/s compressibility effects become an issue. Above a Reynolds number of 44 or a velocity of 13.6 m/s (air properties are taken at 300 K and are assumed constant), vortex shedding occurs and the cylindrical film probes generate a 1-2% turbulence of their own [5,6].

3.3.2 Equipment

A disposable TSI cylindrical hot film probe (model 1201-20) is used to take velocity and turbulence intensity measurements. This sensor has a diameter of 50.8 μm and is operated at a temperature of 250 °C. The maximum frequency that can be measured by the sensor is ~10 kHz. A TSI model 1150-6 standard probe support is used along with a 60 ft cable to connect the film probe to the anemometer. The TSI model 150 anemometer is housed in the TSI IFA-100 Master Cabinet (model 158) which is connected to a computer data acquisition system via a Keithley STA-16 screw terminal accessory board and a Keithley C-1800 ribbon cable. This cable is connected to the Keithley DAS-1601 data acquisition board which is installed inside the PC. Keithley Metrabyte Das 1600 Test & Control Panel software is used to acquire voltages. The cylindrical pitot tube was used to calibrate the anemometer.

3.3.3 Procedure

Initially, the hot film anemometer is set up and calibrated for measurements. The frequency response of the anemometer is optimized by performing a square-wave test with an HP dual channel 100 MHz digital oscilloscope [7]. A Nyquist frequency of 50 Hz is selected yielding a sampling frequency of 100 Hz. The

number of samples collected per data point is 600 which yields a frequency resolution of 0.17 Hz (100/600). Calibration is performed using a baffle plate with a 6 cm × 2.8 cm rounded slot in the center. The hot film anemometer is calibrated by comparison to the cylindrical pitot tube, both instruments mounted on the nozzle traverse. The air flow field (located 1.5 cm below the center of the baffle plate) was uniform with a turbulence intensity less than 1.5% and velocities ranging from 5.5 m/s to 13 m/s. The calibration constants in equation (3.2) were found to be, $C = 1.0522\ V^2$ and $D = 1.0644\ V^2/(\text{m/s})^{0.45}$.

The baffle plate with an array of holes described in Section 3.1 is used to simulate the air motion. For a jet exit velocity of 13 m/s, the velocity and turbulence flow field were measured on a 1.0 cm grid at a horizontal plane normal to the air flow 40 cm below the baffle plate. Measurements were also taken of the mean velocity (downward component) and turbulence intensity profiles occurring at an air jet exit velocity of 13 m/s in the vertical center plane of the spray nozzle for four different separations between the nozzle and the center of the bulk air flow: 10 cm, 15, cm, 19 cm, and 25 cm. The grid limits were defined by the measuring range of the film sensor. Near the edges of the jet, measurements were ceased when velocities dropped below 0.5 m/s.

Ambient temperature was 79± 2.0°F during these experiments. The moving air flow temperature was also fairly steady at 79± 2.0°F. Temperature measurements were made with an Omega digital thermo-hygrometer (model RH-411).

3.4 Theoretical Background of Air Jet Flow

Jets have the properties of conservation of momentum and a constant static pressure distribution throughout the flow. An instantaneous jet profile can be described by the three regions illustrated in Figure 3.2. The initial region close to the nozzle is characterized by uniform laminar flow. This region is designated by an ample potential flow core in the center, and a growing boundary layer on the edges of the jet. The velocity in the potential core remains constant. As distance from the exit increases the boundary layer grows, entraining air from the surroundings while the velocity of the jet itself is slowed down, thus conserving momentum. As the boundary layer grows, the non-viscous potential core diminishes and the cross-sectional area of the jet is increased. This stage is termed the transitional stage, identifying the shift from completely laminar flow to turbulent flow. The final region is fully developed turbulent flow. This region is

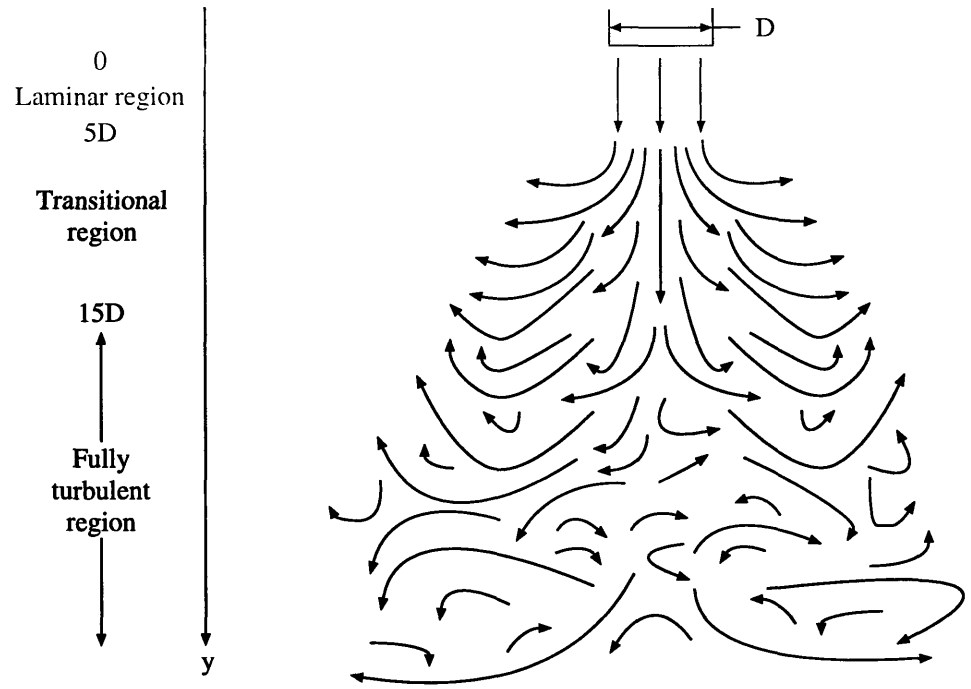

Figure 3.2: The instantaneous velocity profile of a jet.

characterized by large scale eddies, transverse velocities of the same magnitude as their longitudinal components, and random, disorderly flow. The turbulent region in Figure 3.2 illustrates instantaneous flow, the average bulk profile would be represented by uniform velocities of small magnitude in the principal y - direction.

Examination of the flow in the laminar region can be used to estimate the invasion profile of the spray jet and the profile trajectories of water drops. The turbulent region can be used to study the effect of turbulence on the droplet distribution within the fiber bundle. The flexibility of using different baffle plates permits the freedom to produce several velocity profiles with ease. The various possibilities of air flow generation include laminar flow, turbulent flow, uniform velocity flow, irregular flow, single jet flow or an array of jet flows. One possibility is designing a baffle plate with a single circular hole and investigating the regions of laminar and turbulent uniform flow. In the laminar region, uniform flow is present in the area between the jet exit and five diameters below this point. At distances greater than fifteen diameters, the velocity profile is uniformly turbulent. In the intermediate transitional region, the velocity distribution is

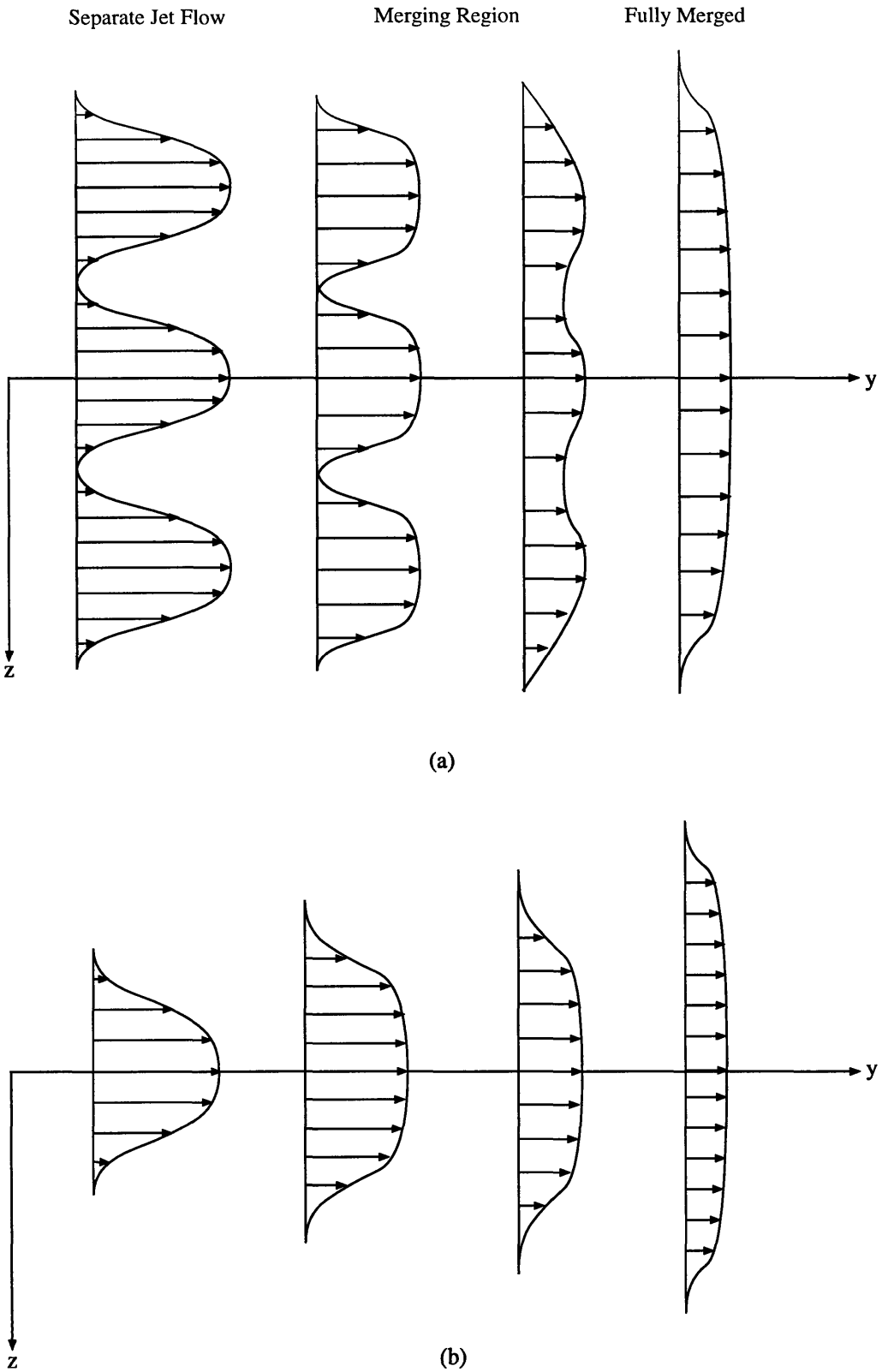

Figure 3.3: The average velocity profiles of (a) multiple jets and (b) a single jet.

non-uniform, with the highest velocities in the center and the velocities diminishing as distance from the centerline increases. The distances stated here are valid for axisymmetric jets, however similar distances are available for plane jets and can be found for other configurations. Irregular distributions of velocities could be made by designing a baffle plate with an array of several different hole diameters.

An initial baffle plate design with an array of holes was chosen to simulate the air motion caused by multiple moving fibers. Figure 3.3 compares the average velocity profiles of a single jet to that of multiple jets. In the initial region of multiple jet flow, the jets flow separately. However, the lower pressure in the confined region between the jets causes the jets to merge, until they eventually flow as a single jet. Eventually the fully merged flow behaves like a two-dimensional plane jet with a virtual origin at a point sufficiently downstream of the jet exit[8]. Therefore this baffle plate can be used to study the effect of a series of jets in the region close to the jet exits (approximately 12 diameters), or can be used to examine the effect of a plane jet velocity profile farther downstream. There are correlations available in the literature for axisymmetric and plane jet flow [8,9,10].

3.5 Bulk Air Column Characterization

To achieve the proper air velocities and bulk air column width at the spray nozzle level, the velocity profile and the spread of a jet were examined for the current baffle plate using the pitot probe. Once a velocity profile was found that was representative of the glass fiber making process, more detailed data describing the bulk air column was collected with the hot film anemometer. This section presents these pitot probe and hot film measurements. In the following Chapters 4 & 5, the dispersion of the droplets into this profiles examined. Different configurations of spray nozzles at various positions with different supply pressures were tested to find the optimal configuration.

3.5.1 Pitot Probe Results

3.5.1.1 Velocity Distribution

The jet exit velocities produced by the fan for the given baffle plate ranged from 6 to 25 m/s. Measurements of the centerline velocity at various distances below the baffle plate yielded a correlation for the centerline velocity at distances between 3 and 11 cm. This dependence is illustrated in Figure 3.4. The velocity, $U(y)$ at

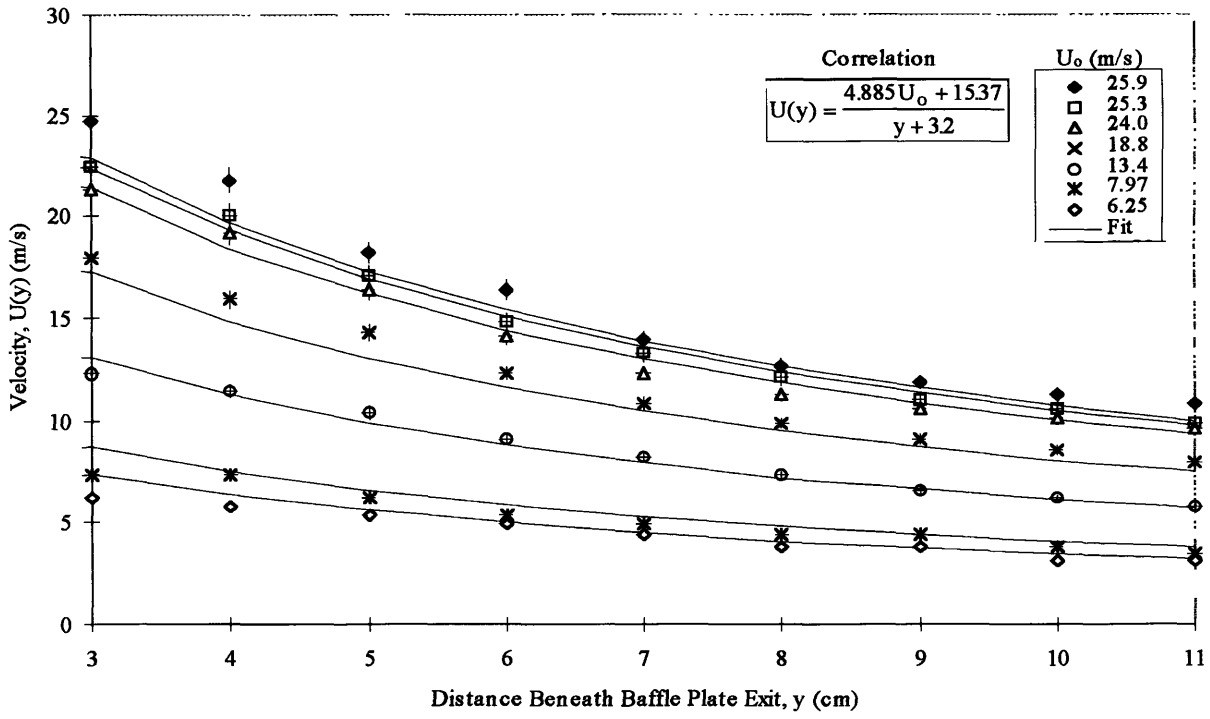

Figure 3.4: Centerline velocity empirical correlation.

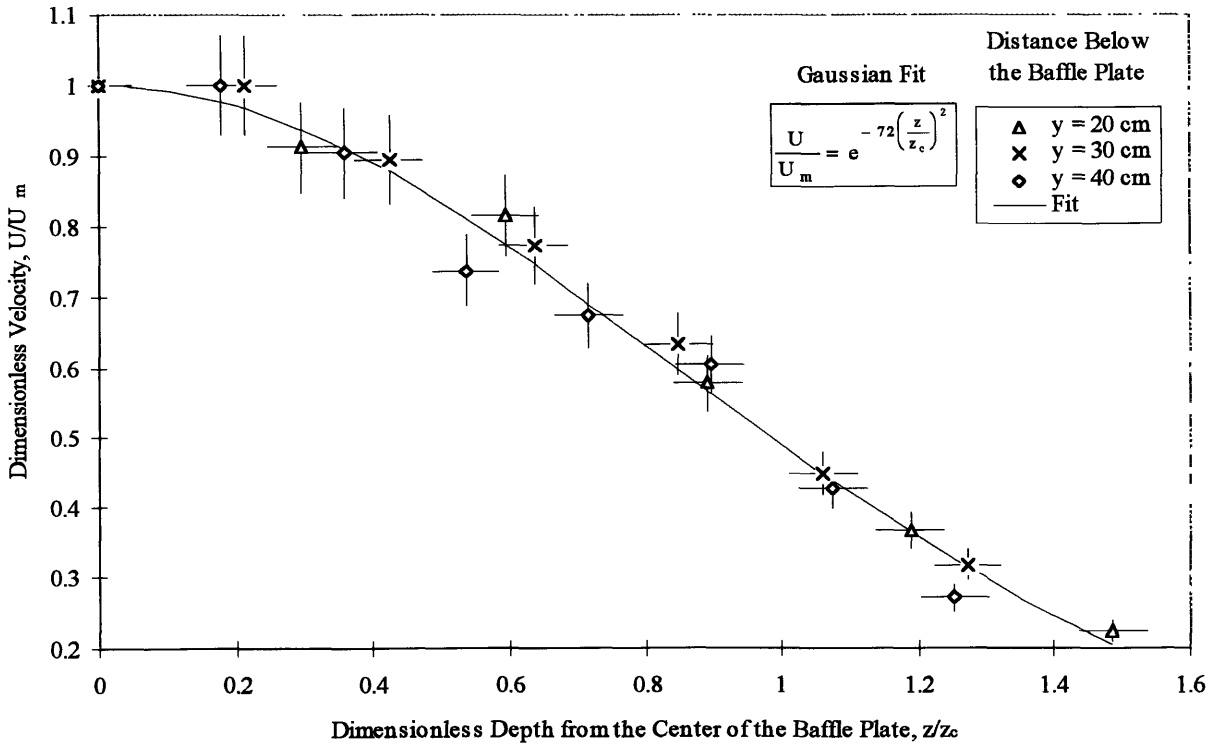

Figure 3.5: Similarity velocity profile.

a position y along the jet array centerline was found to vary according to the following correlation,

$$U(y) = \frac{4.885U_o + 15.37}{y + 3.2} \tag{3.5}$$

where U_o is the jet exit velocity. A different correlation is needed for the region following this because in this region the jets have started to merge with each other. In the region of the correlation, the jets appear to still behave as single axisymmetric jets. In the region between 3 cm and the baffle plate, the velocity remained fairly constant.

The velocity field produced by a jet exit velocity of 13 m/s at various horizontal planes is illustrated in Figure 3.6. This plot illustrates the effect of varying vertical distance from the baffle plate. At a distance of 10 cm below the baffle plate, the single axisymmetric jets had not yet completely merged as depicted by the spikes of high velocity present in the flow field. The peaks occurred at positions directly below one of the jet openings, the valleys are located under the spaces between the holes. As distance from the center of the baffle plate increases the velocity drops sharply for the 10 cm plane. However as the distance below the baffle plate is increased the deterioration of velocity becomes more gradual, yielding more uniform velocity profiles. The jets appear to have become fully merged at a distance between 11 cm and 20 cm.

The similarity velocity profile of the jet array is plotted in Figure 3.5. The 10 cm plane is not included in this plot because the jets have not yet merged at this point. Since the configuration of holes in the baffle plate resembled that of a plane jet, a comparison was made with the similarity profile of a plane jet. The profile of the plane jet is Gaussian,

$$\frac{U}{U_m} = e^{-c\left(\frac{z}{z_c}\right)^2} \tag{3.6}$$

where U_m is the centerline velocity, z is the depth from the center of the plate, z_c is the point at which the velocity is half the centerline velocity and c is an empirical constant. For the profiles of plane jets

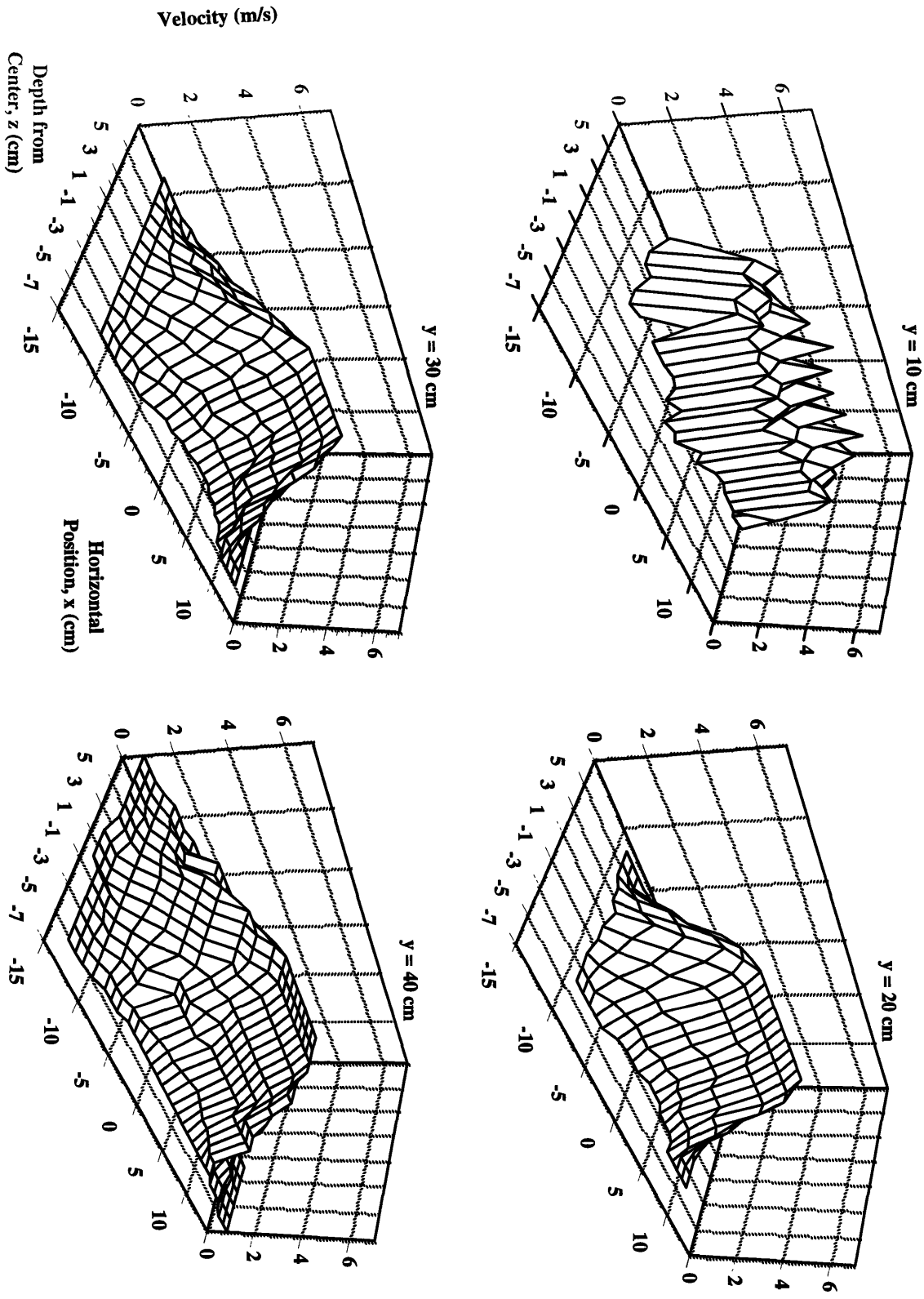

Figure 3.6: Bulk air velocity profiles
(The area of the baffle plate containing holes is 16 cm wide and 6 cm deep.
y is the distance beneath the baffle plate.)

c is equal to $\frac{\pi}{8}$ however, for the array of jets, c = 0.72 $\cong \frac{\pi}{4}$. Perhaps this discrepancy exists because the length to width ratio of the jet array is much less than that for regular plane jets

The repeatability of the velocity measurements was determined by collecting a second trial of data at a horizontal plane 20 cm below the baffle plate. The percent difference between the first and second data collection runs is shown in Table 3.1, Figure 3.7 illustrates this difference. The velocity measurements appear to be in good agreement for high values of velocity that occur towards the center of the baffle plate, however as the velocities become lower repeatability becomes poor.

3.5.1.2 Spread of Air Flow

The span the velocity air field covers is useful in finding a bulk air column width comparable to the air flow at PPG. As distance from the jet exit is increased the jets tend to spread out into larger regions. Figure 3.6 depicts the spreading of the array of jets. At a distance of 10 cm the area covered by the velocity field is only 10 cm × 3 cm, as opposed to the area at 40 cm of 15 cm × 7 cm.

3.5.2 Hot Film Anemometer Results

3.5.2.1 Air Flow Field Analysis in a Horizontal Plane

The velocity and turbulence intensity profile produced by a jet exit velocity of 13 m/s at a horizontal plane 40 cm below the baffle plate is illustrated in Figure 3.8. The velocity profile resembles that of a plane jet. Toward the center of the jet the turbulence intensity is low (Tu<0.15). However, as the distance from the center of the jet is increased, the measured turbulence intensity increases to a maximum value of Tu~65% and then starts to decrease again as the outer edges of the jet are approached. In reality, the turbulence intensity is known from laser-doppler measurements to reach a value of *unity* before it starts to decrease again. However, since the hot film anemometer is not accurate in measuring high turbulence levels, (owing to flow reversal) the present measurements do not reflect this behavior.

For turbulence intensity levels less than 35% repeatability of our hot-film velocity and turbulence measurements average 1.3% and 1.7%, respectively. For turbulence intensity levels ranging from 35% to 65%, repeatability became very poor. In the region of high turbulence, repeatability for velocity and turbulence intensity average 10.2% and 7.5%, respectively.

	Percent Difference Between Run 1 and Run 2					
	z = 0 cm	z = 1 cm	z = 2 cm	z = 3 cm	z = 4 cm	z = 5 cm
x = 0 cm	0.0%	0.0%	0.0%	0.0%	13.4%	18.4%
x = 1 cm	0.0%	0.0%	0.0%	0.0%	8.7%	29.3%
x = 2 cm	0.0%	0.0%	0.0%	0.0%	18.4%	13.4%
x = 3 cm	0.0%	4.9%	0.0%	0.0%	13.4%	29.3%
x = 4 cm	0.0%	0.0%	0.0%	0.0%	13.4%	50.0%
x = 5 cm	0.0%	4.9%	0.0%	22.5%	29.3%	42.3%
x = 6 cm	0.0%	5.4%	8.0%	0.0%	42.3%	0.0%
x = 7 cm	0.0%	8.0%	29.1%	6.5%	29.3%	0.0%
x = 8 cm	11.8%	0.0%	0.0%	0.0%	0.0%	0.0%
x = 9 cm	0.0%	18.3%	0.0%	29.3%	0.0%	0.0%
x = 10 cm	0.0%	41.4%	29.3%	0.0%	0.0%	0.0%

Table 3.1: Repeatability results of velocity measurements.

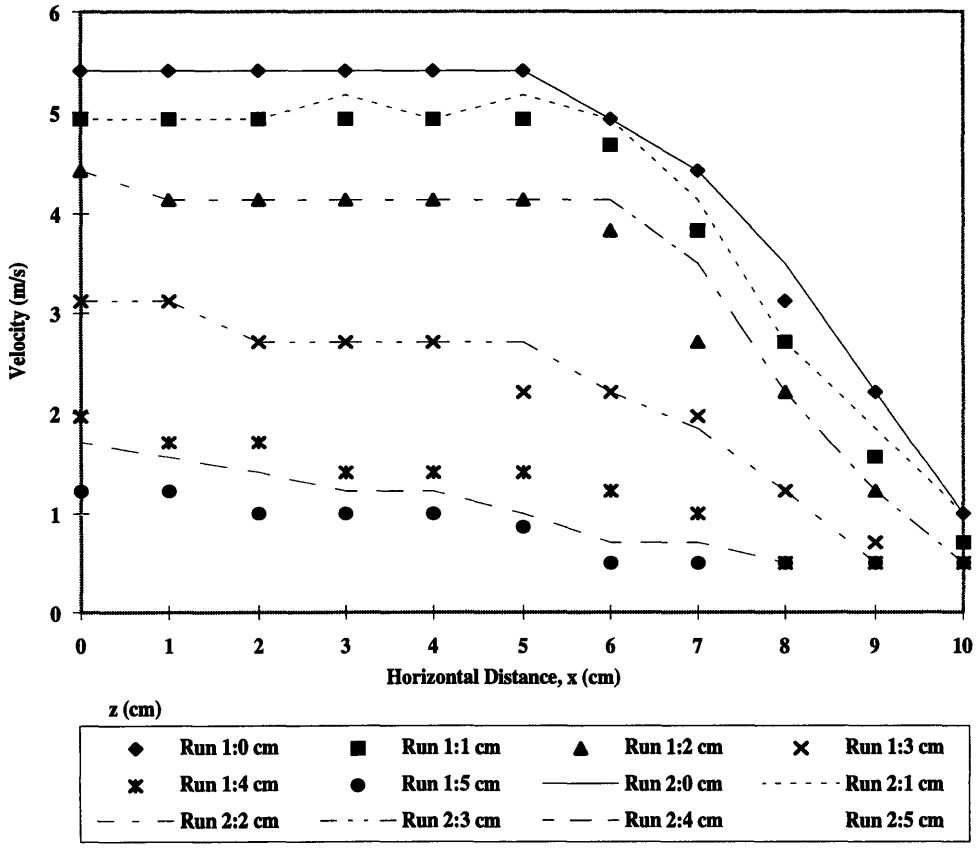

Figure 3.7: Repeatability results of velocity measurements.

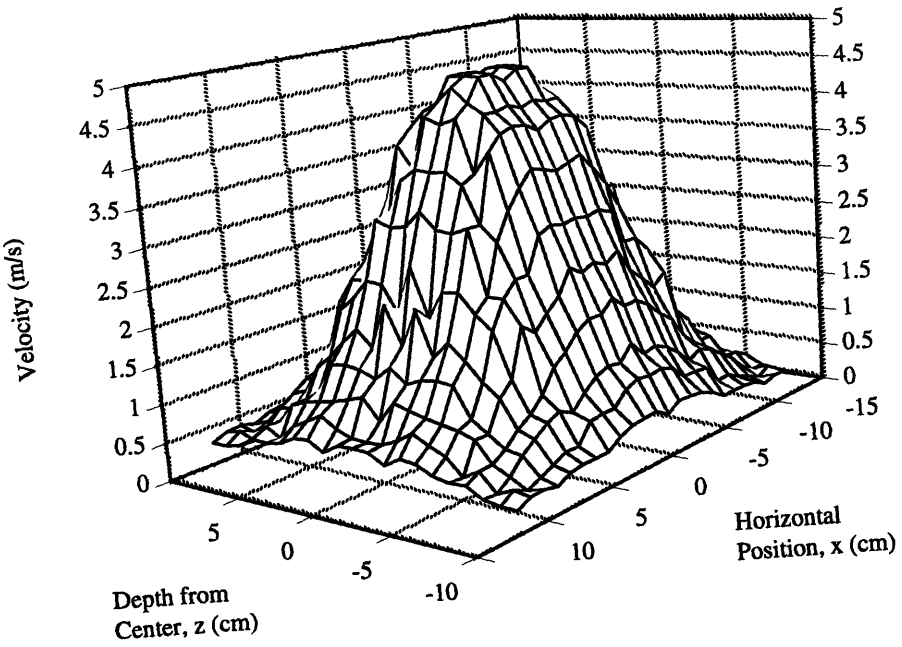

(a) Velocity Profile

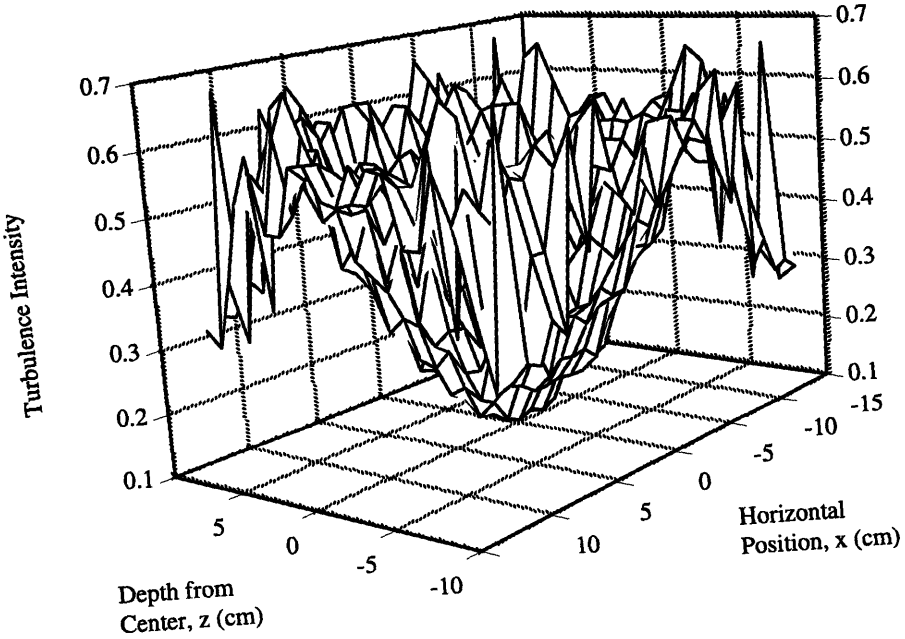

(b) Turbulence Intensity Profile

Figure 3.8: Bulk air velocity profile 40 cm below the baffle plate.
(Baffle plate centerline is at (0,0).)

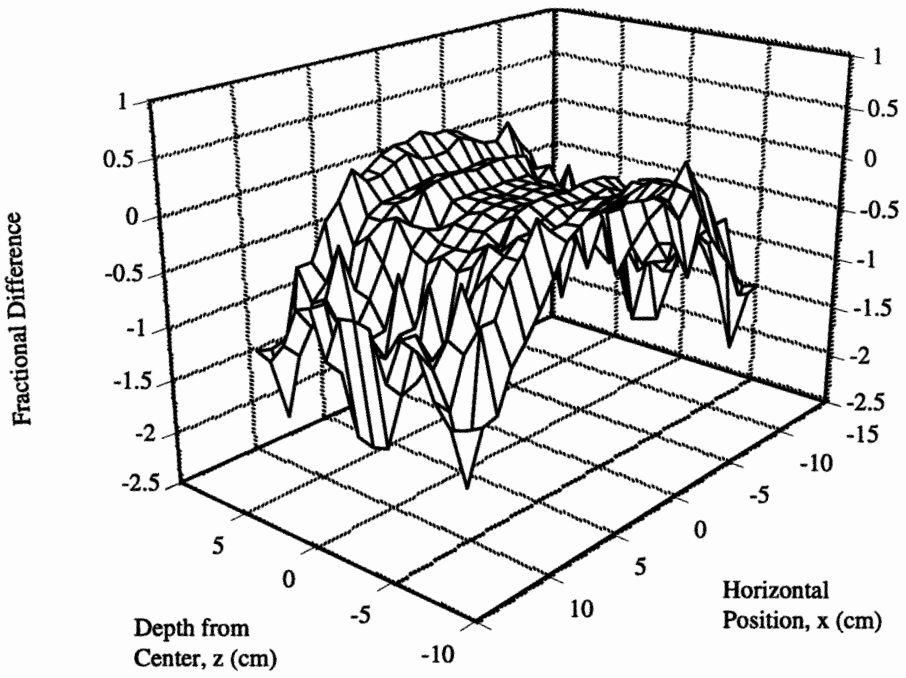

Figure 3.9: Fractional difference between hot film and pitot tube velocities, $(V_{hf}-V_{pt})/V_{hf}$.
(A fractional difference of 1 corresponds to a 100% difference.)

Figure 3.9 is a plot of the fractional difference between hot film and pitot tube mean velocity measurements. In the center region of the jet the fractional difference is less than 20%, however the difference increases rapidly in the outer regions of the jet to values close to -250%. The discrepancy is largely due to the fact that the pitot tube is not suitable for measurements in turbulent flows (neither is the hot-film when Tu > 25%).

Though the hot-film anemometer has limitations, it still serves as a very accurate measuring device in flows with Tu < 25%. The results of this hot-film indicate excellent repeatability when Tu < 35%. Thus the data obtained in all but the outer edges of the jet gives a good representation of the air flow field.

3.5.2.2 Air Flow Field Analysis in Vertical Planes

The air velocity and turbulence intensity profiles in the vertical center plane of the spray, as measured with a hot film anemometer, are included.

Figures 3.10, 3.11, 3.12, and 3.13 illustrate the mean velocity (downward component) and turbulence intensity profiles occurring at an air jet exit velocity of 13 m/s in the vertical center plane of the spray nozzle for the four different separations between the nozzle and the center of the bulk air flow: 10 cm,

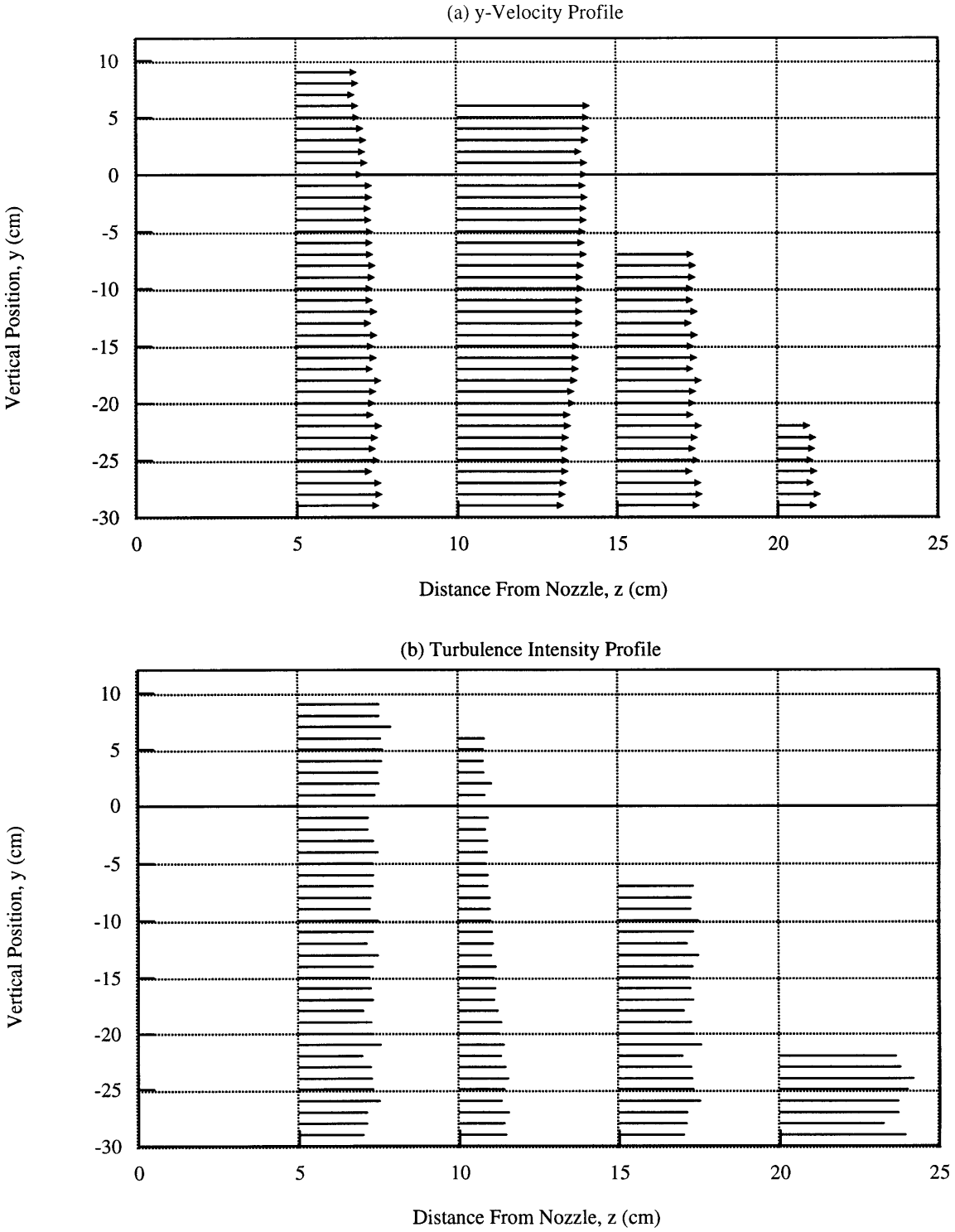

Figure 3.10: Bulk air y-velocity profile along the vertical center plane of the spray.
(Center of baffle plate is at z = 10 and y = 40 cm and jet exit velocity is 13 m/s.
The length of each line is proportional to (a) the velocity which ranges from 1.2 - 4.8 m/s and
(b) the turbulence intensity which ranges from 0.09 - 0.51).

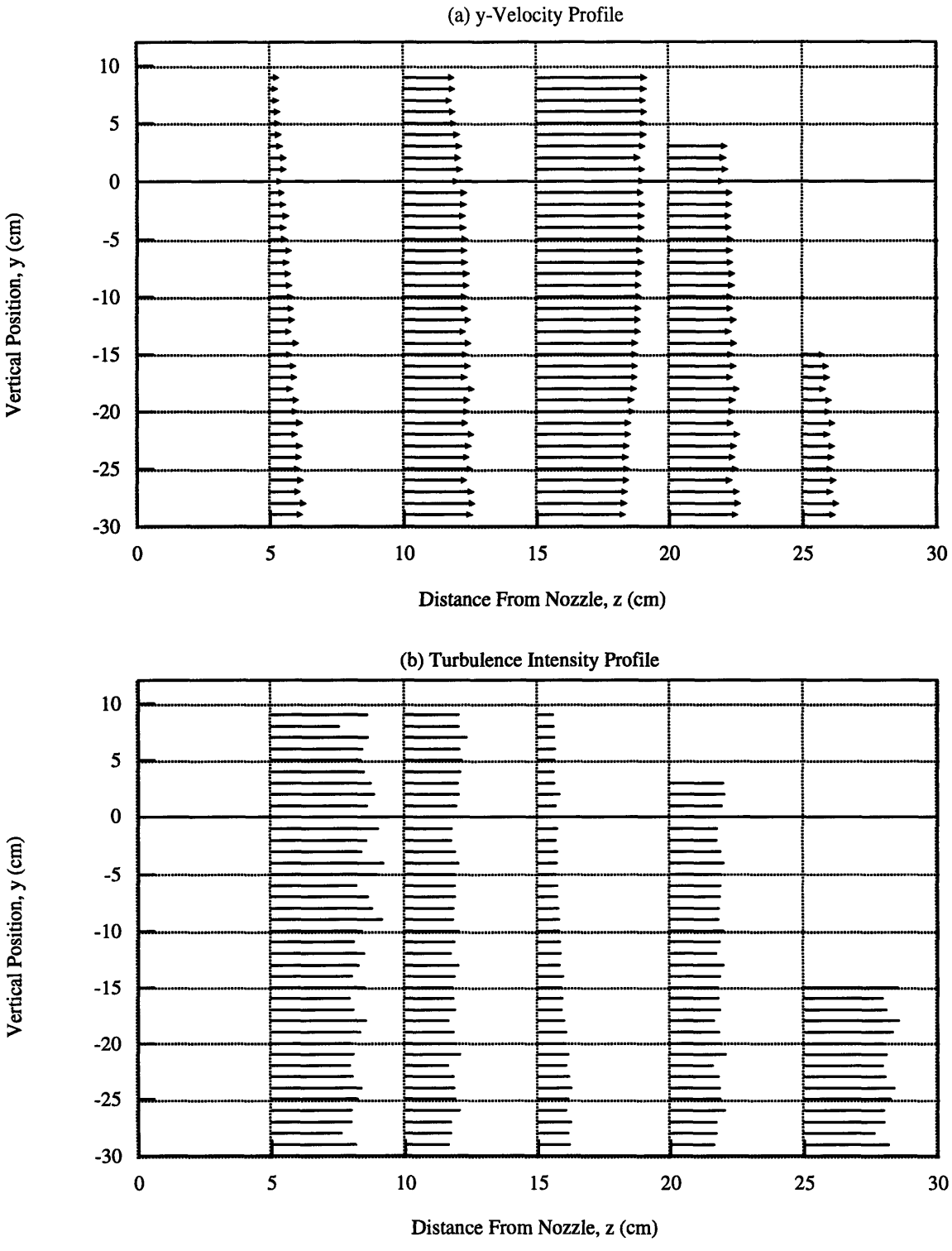

Figure 3.11: Bulk air y-velocity profile along the vertical center plane of the spray.
(Center of baffle plate is at z = 15 and y = 40 cm and jet exit velocity is 13 m/s.
The length of each line is proportional to (a) the velocity which ranges from 1.2 - 4.8 m/s and
(b) the turbulence intensity which ranges from 0.09 - 0.51).

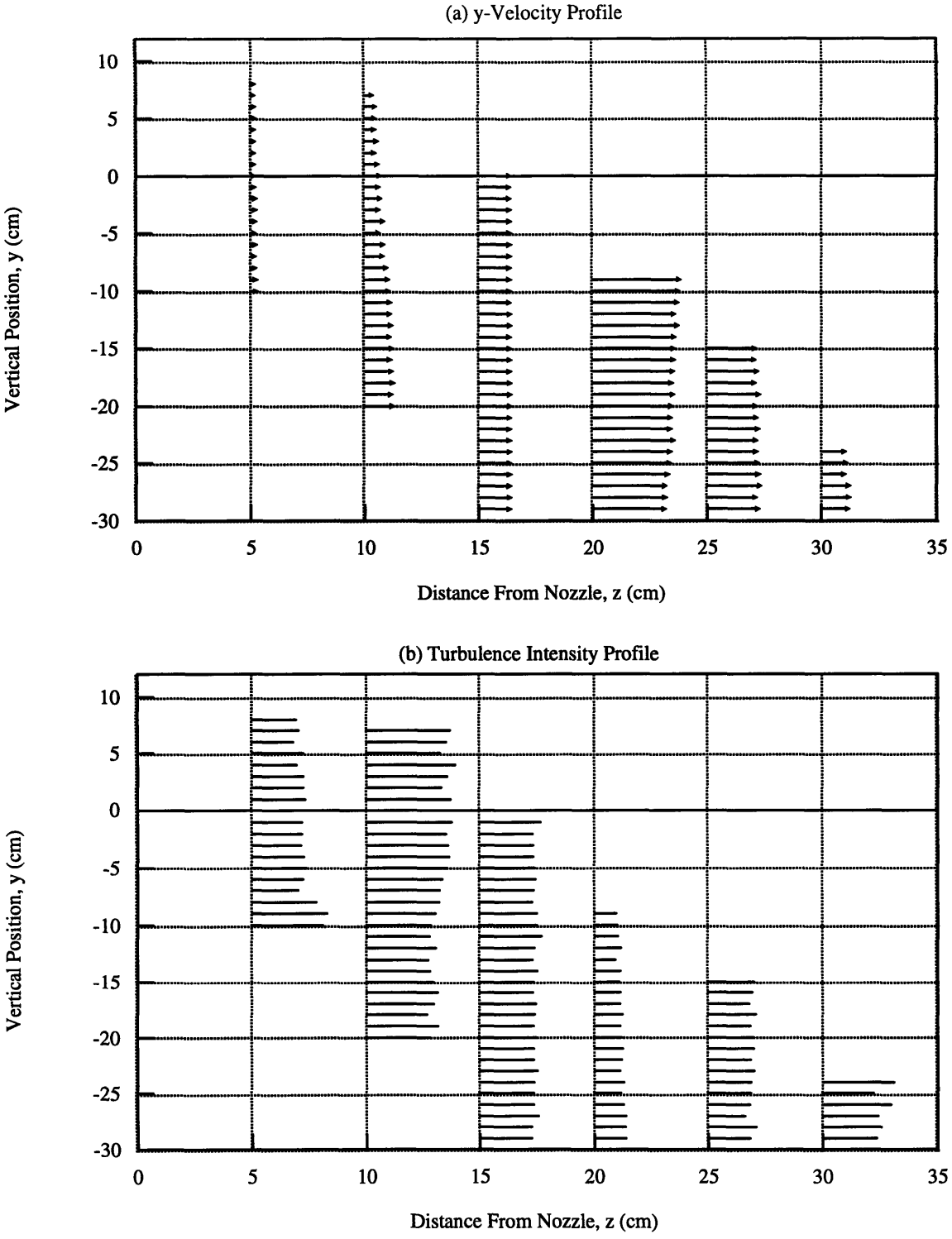

Figure 3.12: Bulk air y-velocity profile along the vertical center plane of the spray.
(Center of baffle plate is at z = 19 and y = 40 cm and jet exit velocity is 13 m/s.
The length of each line is proportional to (a) the velocity which ranges from 1.2 - 4.8 m/s and
(b) the turbulence intensity which ranges from 0.09 - 0.51).

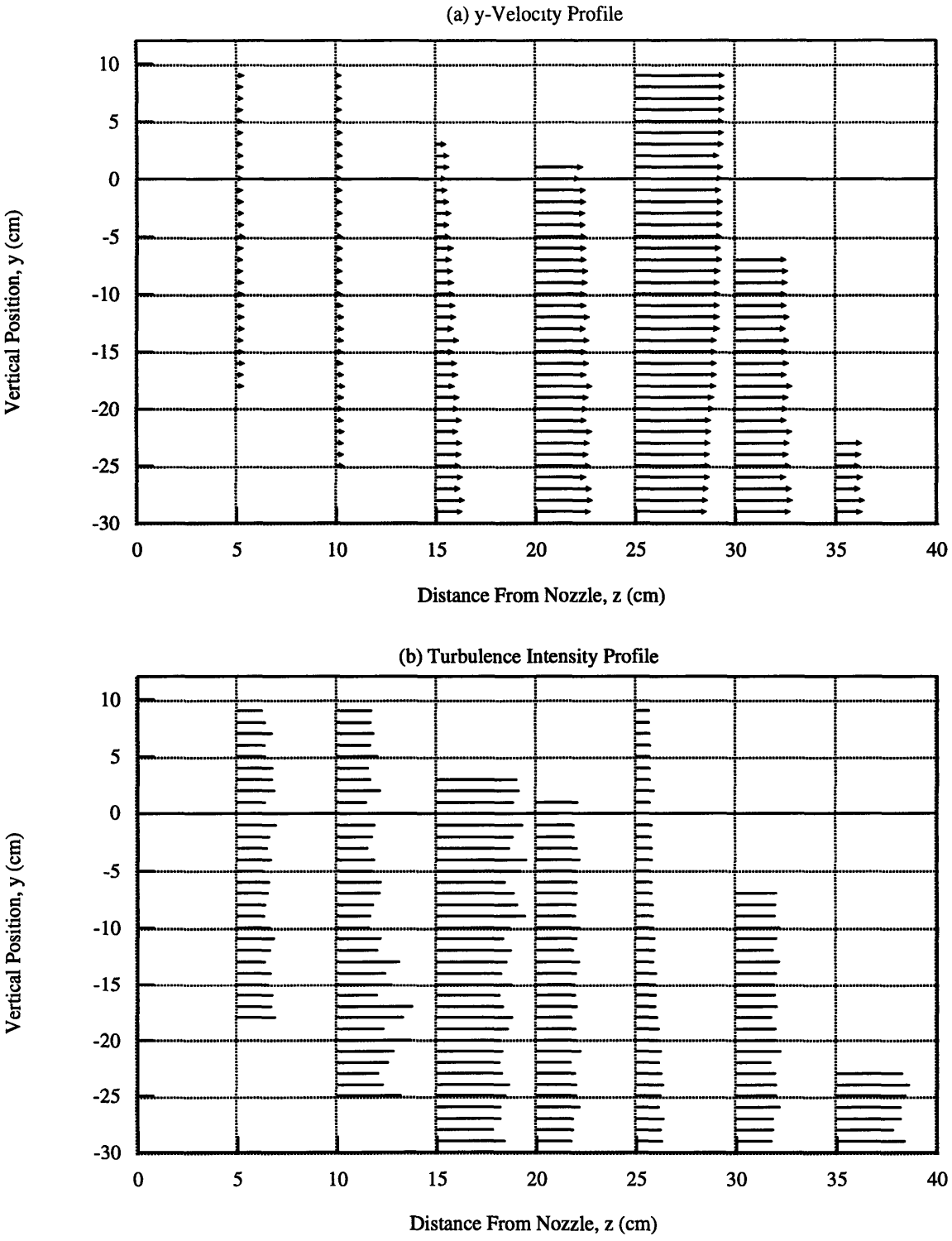

Figure 3.13: Bulk air y-velocity profile along the vertical center plane of the spray.
(Center of baffle plate is at z = 25 and y = 40 cm and jet exit velocity is 13 m/s.
The length of each line is proportional to (a) the velocity which ranges from 1.2 - 4.8 m/s and
(b) the turbulence intensity which ranges from 0.09 - 0.51).

15, cm, 19 cm, and 25 cm. For comparison to subsequent dispersion data, all measurements are plotted with respect to the distance from the spray nozzle. To locate these positions with respect to the center of the baffle plate from which the flow originated, subtract 40 cm from the y-coordinate and subtract the given z-separation from the z-coordinate. For example, in Figure 3.10, the position y = 0 cm and z = 15 cm (relative to the nozzle) would correspond to the position y = -40 cm and z = 5 cm relative to the center of the baffle plate. The measurements were taken with the hot film anemometer described in Section 3.3.

The mean velocity profiles show that velocity is only weakly affected by the y-distance more than 31 cm below the baffle plate. The maximum velocity of the air jet occurs in the center of the air jet and has a magnitude of about 5 m/s. The velocity decreases from the center of the jet to the edges.

Toward the center of the jet the turbulence intensity is low ($Tu<0.15$). However, as the distance from the center of the jet is increased, the measured turbulence intensity increases to a maximum value of $Tu\sim65\%$ and then starts to decrease again as the outer edges of the jet are approached. In reality, the turbulence intensity is known from laser-doppler measurements to reach a value near *unity* before it starts to decrease again. However, since the hot film anemometer is not accurate in measuring high turbulence levels (owing to flow reversal), the present measurements do not reflect this behavior. The relation of these measurements to the spray dispersion measurements will be discussed in Chapters 4 and 5.

Chapter 4

Spray Dispersion for Various Bulk Air Flows

A better understanding of the spray droplet distribution within the fiber bundle is necessary for improving the spray cooling of the glass fibers. The induced air flow appears to be a determining factor in the dispersion of the spray in the fiber bundle. This chapter examines the spray dispersion at separations of 10 cm, 15 cm, 19 cm and 25 cm; between the nozzle and the center of the bulk air flow for an initial air jet speed of 13 m/s. The spray dispersion is also examined for initial air jet velocities of 17.3 m/s and 21.4 m/s for the separation of 15 cm. Figure 4.1 is a spatial description of the experimental configuration used to examine spray dispersion into a bulk air flow column. Data was taken with the PDPA (described in the Chapter 2) at one centimeter intervals along the dashed vertical lines shown in Figure 4.1. Measurements were ceased when velocities became negative or when less than 1000 points could be collected in 500 seconds. A Hago B-50 nozzle was used for all tests. The results consist of the Sauter mean diameter distribution, the velocity profile, and the validation rate profile.

4.1 Spray Dispersion for Varying Separation of Nozzle and Air Flow

4.1.1 Droplet Diameter

Figures 4.2, 4.3, 4.4, and 4.5 compare the SMD distribution with and without air flow along the vertical center plane of the spray at four nozzle-to-bulk-air-flow separations (where the center of the baffle plate is 10 cm, 15 cm, 19 cm, and 25 cm from the nozzle, respectively). When the separation is 10 cm as shown in Figure 4.2 (b), it is evident that the spray cone has not become fully developed. A fully developed spray cone is characterized by a central core of small diameter droplets surrounded by a sheath of larger droplets

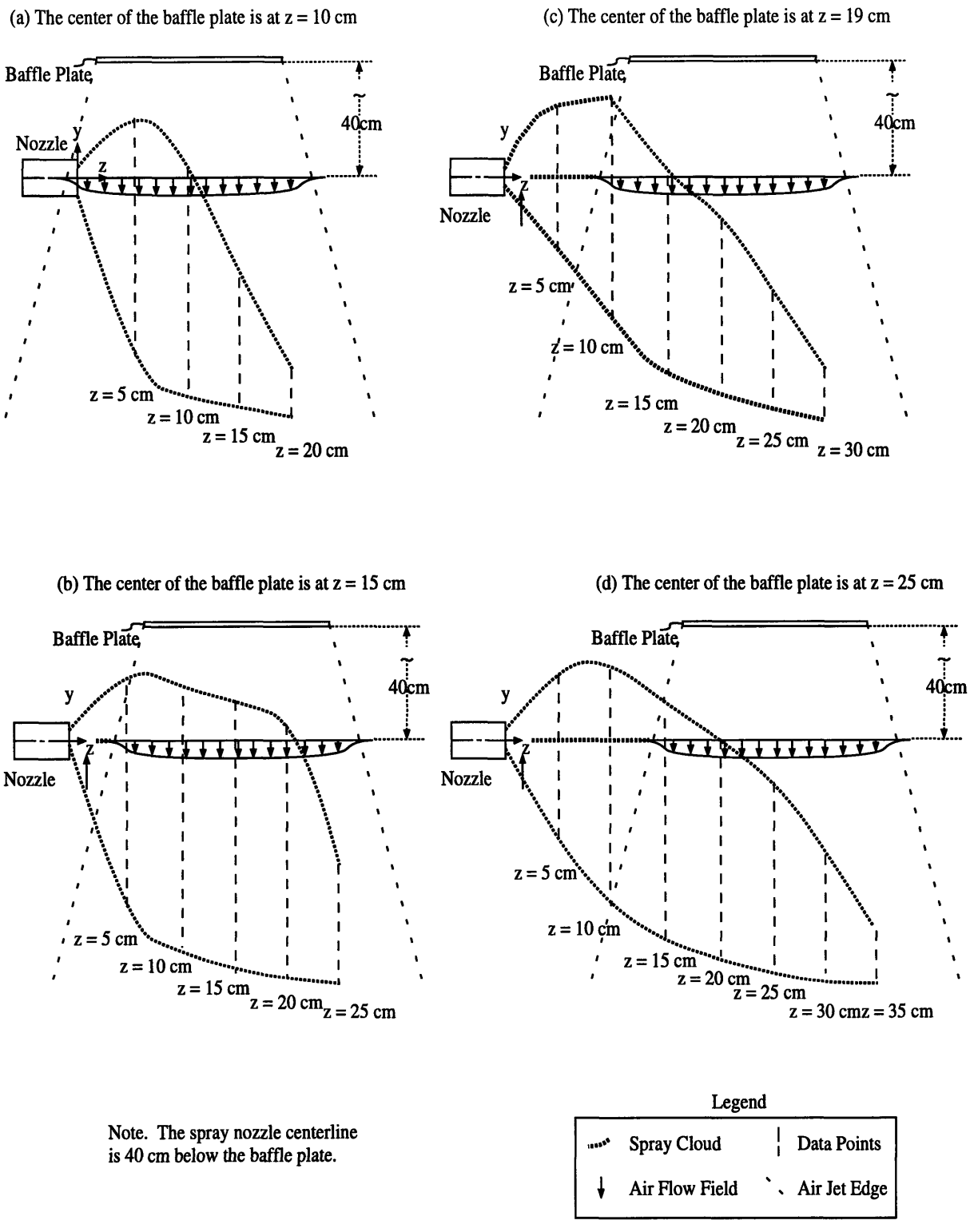

Figure 4.1: Flow Field Orientation
(The initial air jet velocity is 13 m/s)

(a) In Still Air

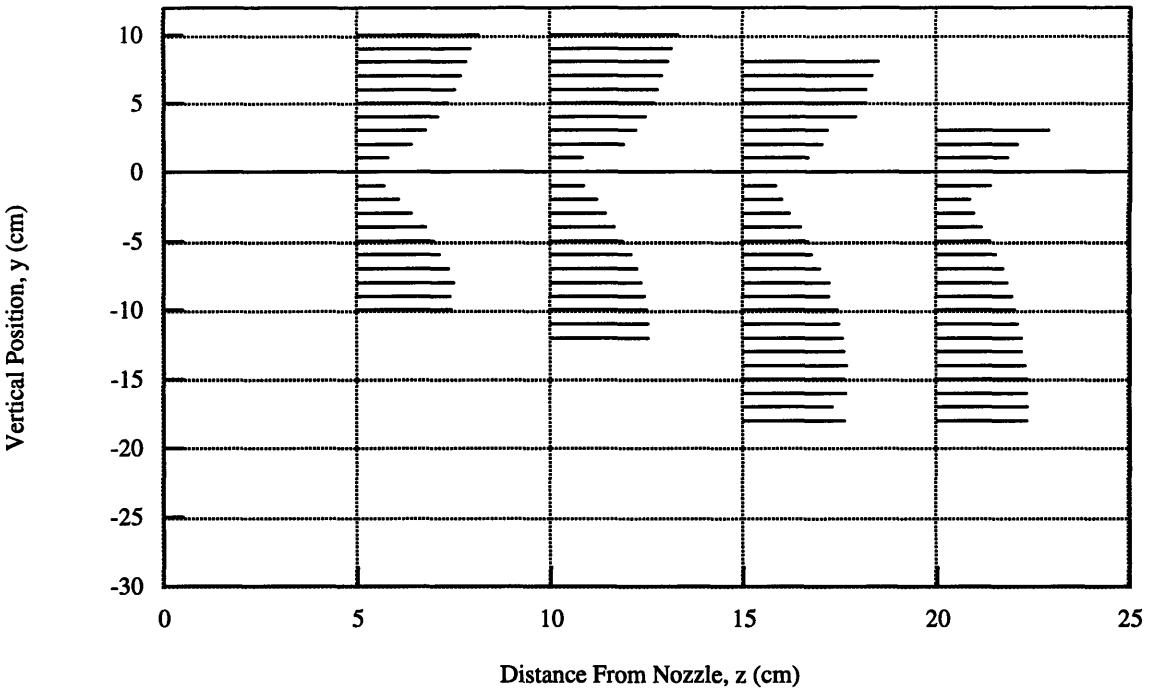

(b) In Bulk Air Flow (Center of Baffle Plate is at z = 10 and y = 40 cm and Initial Jet Velocity is 13 m/s)

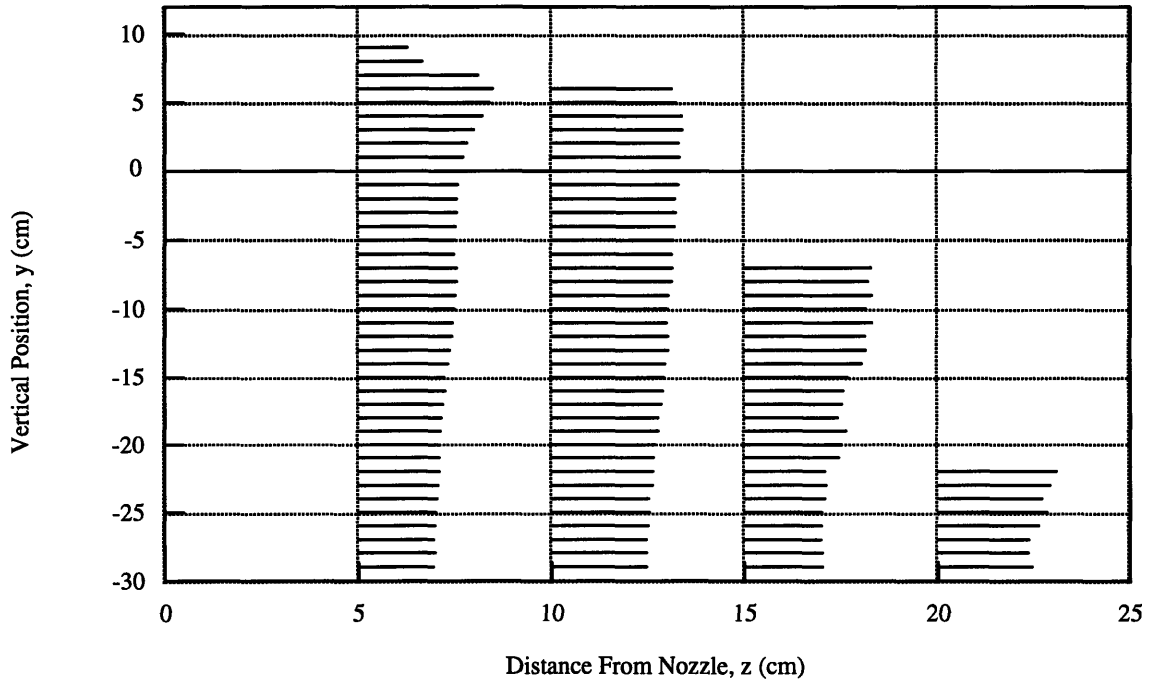

Figure 4.2: SMD distribution at 100 psi along the vertical center plane of the spray (B-50 clean nozzle). (The length of each line is proportional to the magnitude of the SMD which ranges from 14 - 107 microns.)

(a) In Still Air

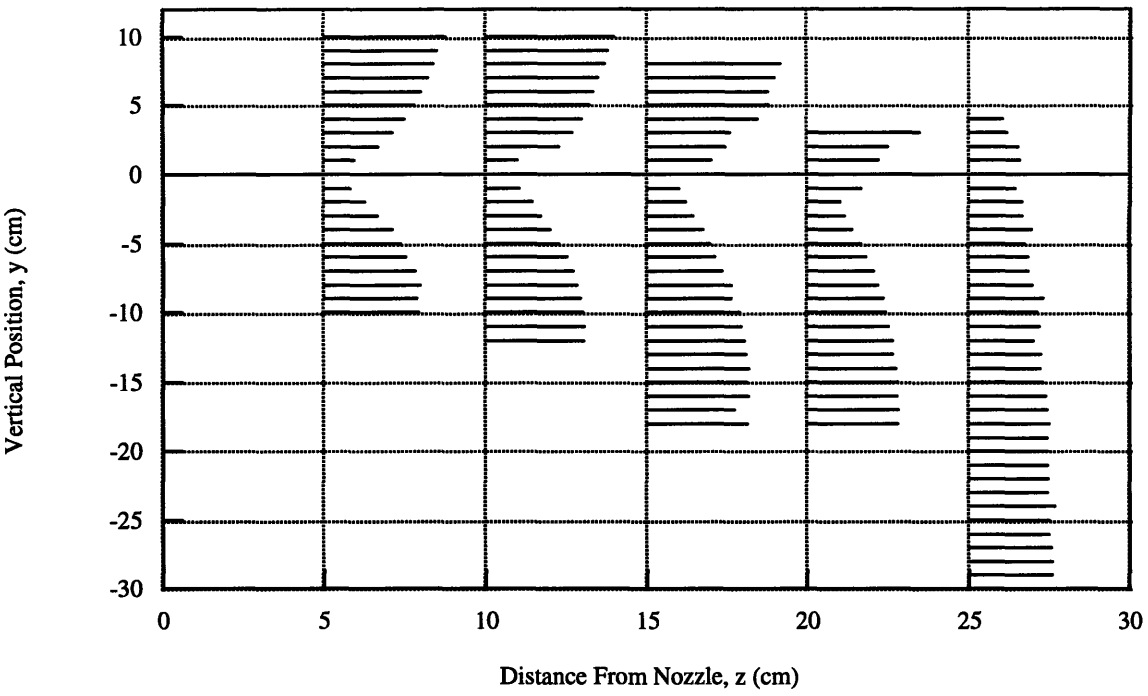

(b) In Bulk Air Flow (Center of Baffle Plate is at z = 15 and y = 40 cm and Initial Jet Velocity is 13 m/s)

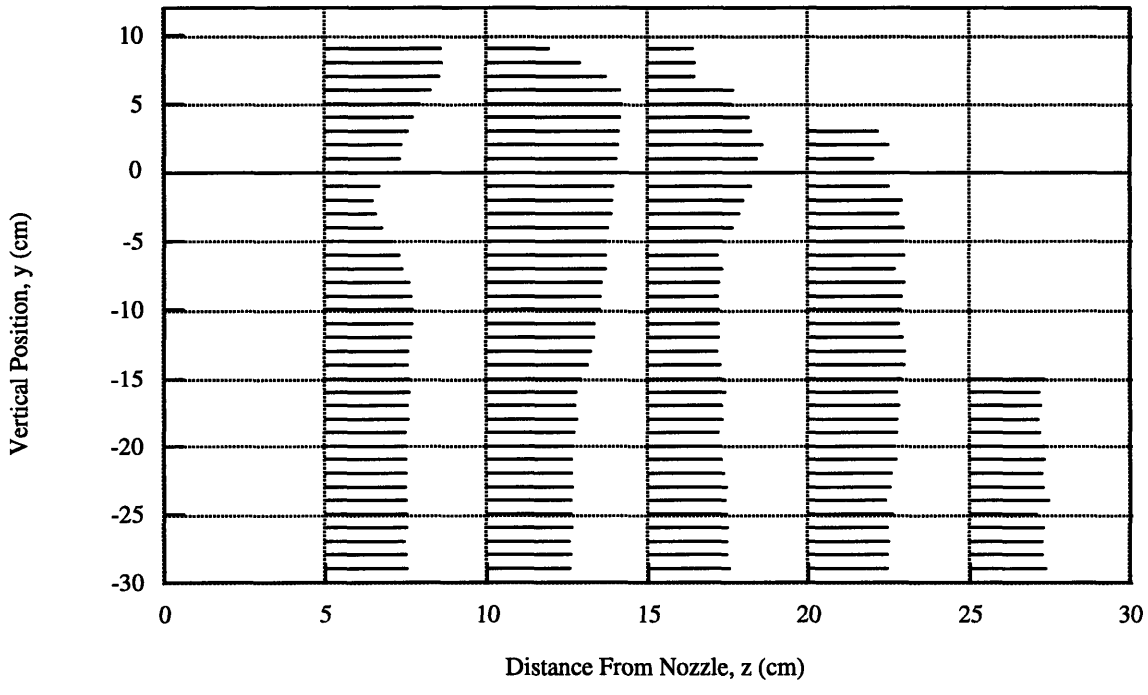

Figure 4.3: SMD distribution at 100 psi along the vertical center plane of the spray (B-50 clean nozzle). (The length of each line is proportional to the magnitude of the SMD which ranges from 14 - 107 microns.)

(a) In Still Air

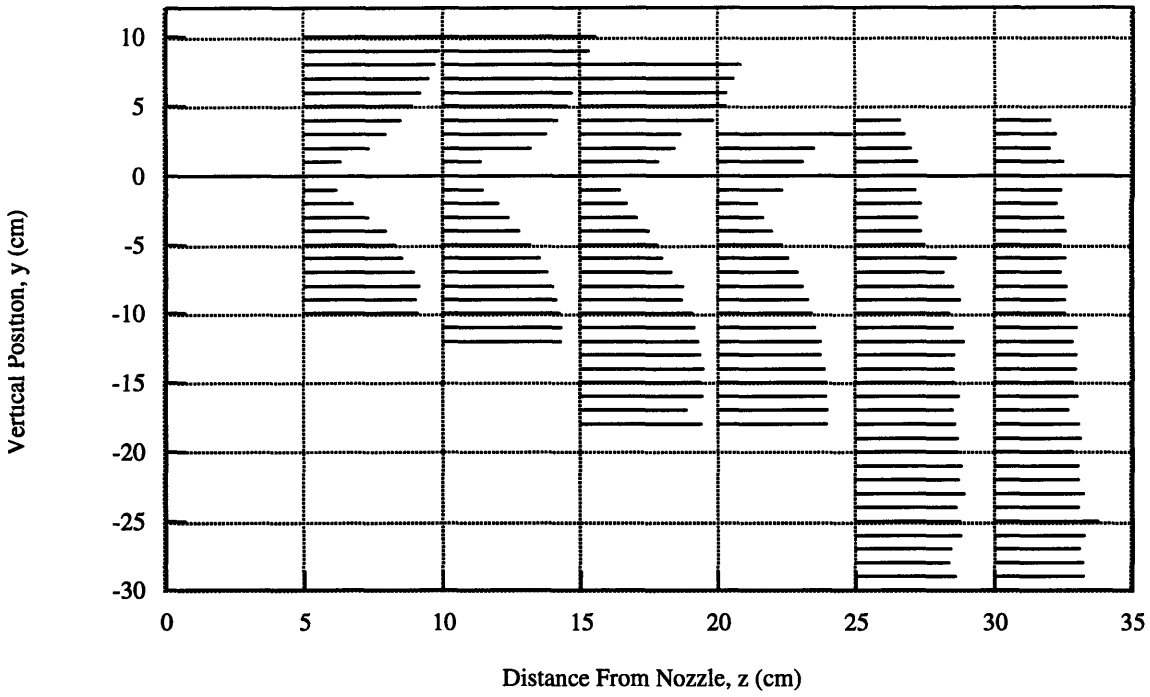

(b) In Bulk Air Flow (Center of Baffle Plate is at z = 19 and y = 40 cm and Initial Jet Velocity is 13 m/s)

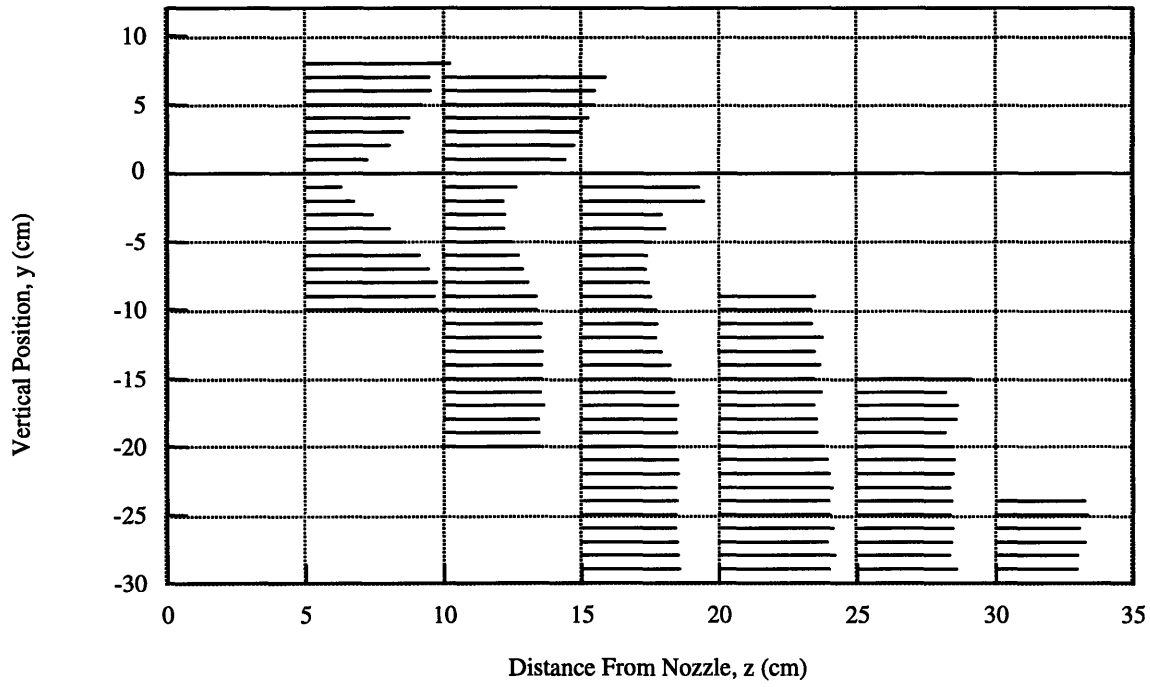

Figure 4.4: SMD distribution at 100 psi along the vertical center plane of the spray (B-50 clean nozzle). (The length of each line is proportional to the magnitude of the SMD which ranges from 14 - 107 microns.)

(a) In Still Air

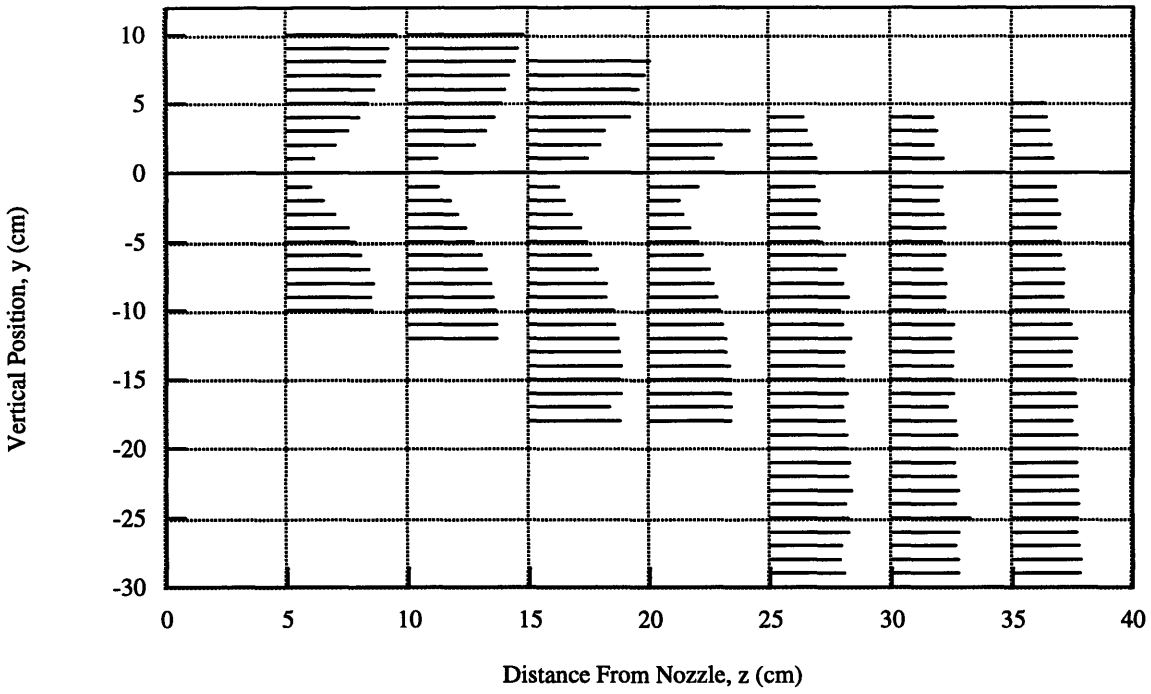

(b) In Bulk Air Flow (Center of Baffle Plate is at z = 25 and y = 40 cm and Initial Jet Velocity is 13 m/s)

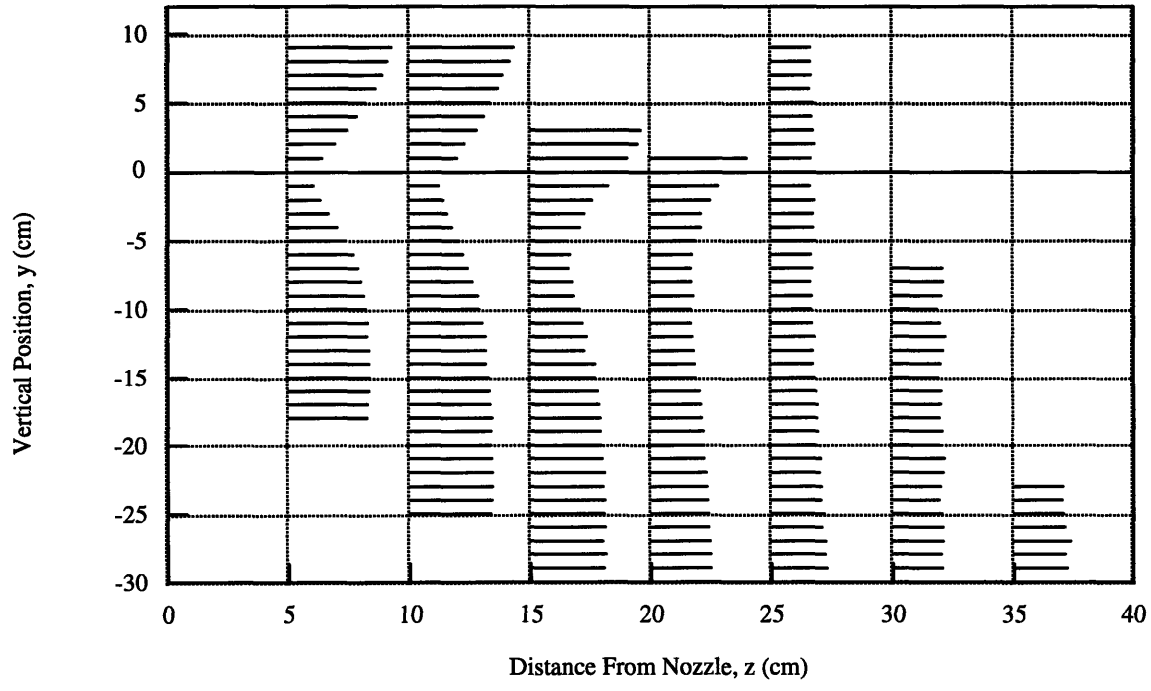

Figure 4.5: SMD distribution at 100 psi along the vertical center plane of the spray (B-50 clean nozzle). (The length of each line is proportional to the magnitude of the SMD which ranges from 14 - 107 microns.)

as depicted in Figure 4.2 (a). In contrast, for this case the SMD profiles have the largest SMD's at the top and gradually decrease to a minimum SMD at the bottom of the spray profile. The SMD profiles are fairly constant with an SMD range of 53 to 94.20 μm (with the exception of the 2 positions at the top of the spray cone at z = 5 cm). Figure 3.1(a) shows that a downward air velocity of about 3 m/s with a turbulence intensity of approximately 0.30 is acting on the spray at a distance of 5 cm from the nozzle. This high velocity (the y-velocity of the air is of the same magnitude as the droplet z-velocity in still air) in the close vicinity of the nozzle appears to prevent the spray cone from becoming fully developed.

For separations of 15 cm, 19 cm, and 25 cm the spray became fully developed before it was affected by the air flow. As the bulk air column is moved farther from the nozzle, the spray has more space to develop. Traces of a fully developed spray cone exist until z = 20 cm at a separation of 25 cm, until z = 15 cm at a separation of 19 cm, but only at z = 5 cm at a separation of 15 cm. The closer the bulk air flow is located to the nozzle, the earlier the SMD profiles became constant.

The SMD profiles in Figure 4.5 (b) at a separation of 25 cm are very similar to the corresponding profiles in still air, except that the profiles in the bulk air flow have been pushed down farther due to the additional drag force of the air column. At a distance of z = 35 cm from the nozzle, the top of the spray cone is at y = 5 cm for still air as opposed to y = -23 cm in bulk air flow.

4.1.2 Droplet Velocity

Figures 4.6, 4.7, 4.8, and 4.9 compare the z-velocity profile with and without air flow along the vertical center plane of the spray at four nozzle to bulk air flow separations (where the center of the baffle plate is 10 cm, 15 cm, 19 cm, and 25 cm from the nozzle, respectively). The velocity profiles generally have a maximum velocity at the center and decrease as distance from the center increases. For all four separations, the velocity profiles evolve from well defined peak(s) into nearly flat profiles of negligible velocity (less than 0.3 m/s). This final constant velocity profile occurs at a distance from the nozzle of z = 20 cm, 25 cm, 30 cm, and 35 cm for separations of 10 cm, 15 cm, 19 cm and 25 cm, respectively. Thus, as the separation increases between the nozzle and the bulk air column, a greater distance from the nozzle is necessary for these flat profiles to develop.

Figures 3.11, 3.12 and 3.13 show that the downward velocities in the close vicinity of the spray are

(a) In Still Air

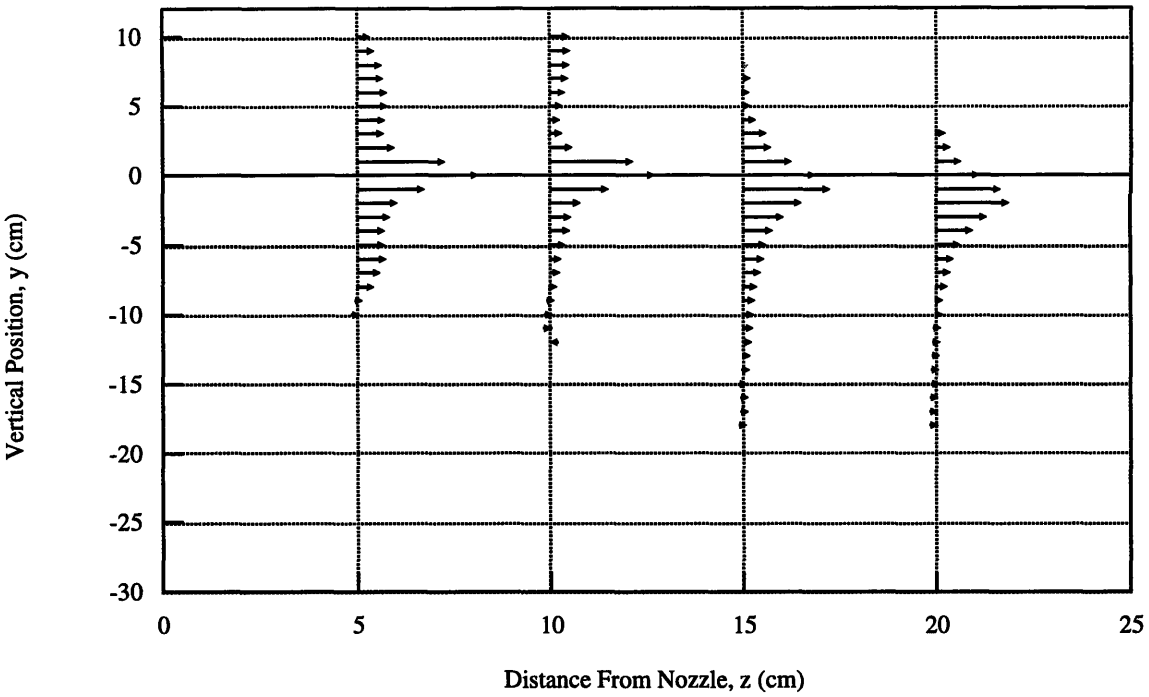

(b) In Bulk Air Flow (Center of Baffle Plate is at z = 10 and y = 40 cm and Initial Jet Velocity is 13 m/s)

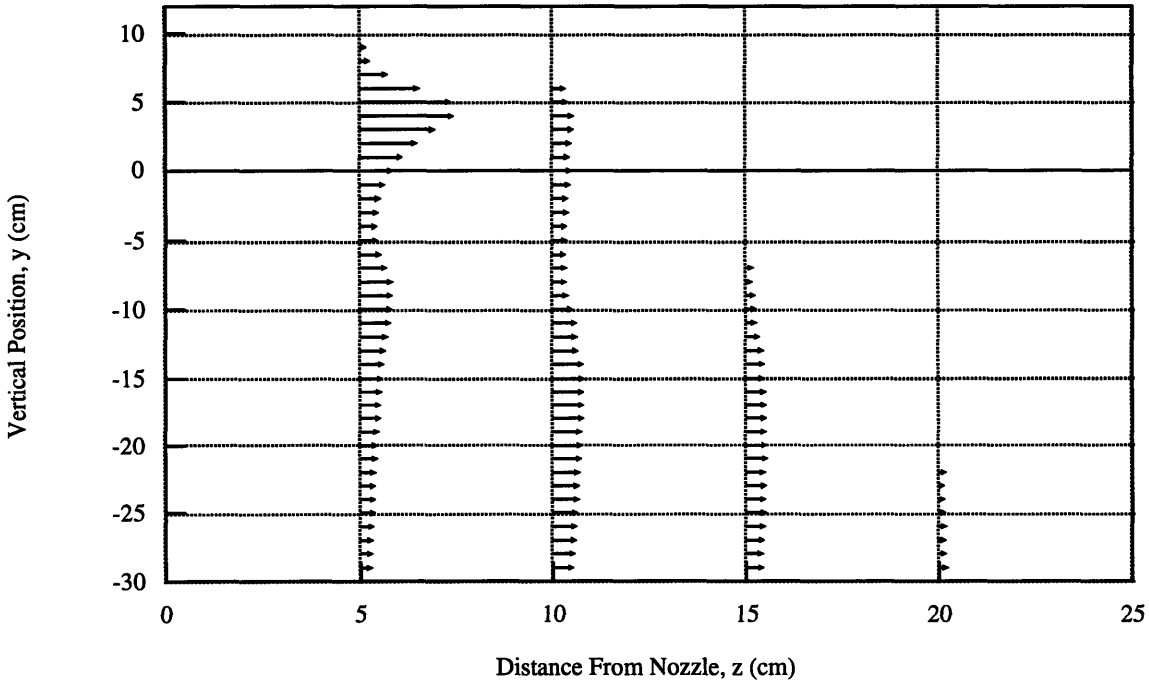

of

Figure 4.6: z-Velocity distribution at 100 psi along the vertical center plane of the spray (B-50 clean nozzle). (The length of each line is proportional to the magnitude of the velocity which ranges from 0 - 3.5 m/s.)

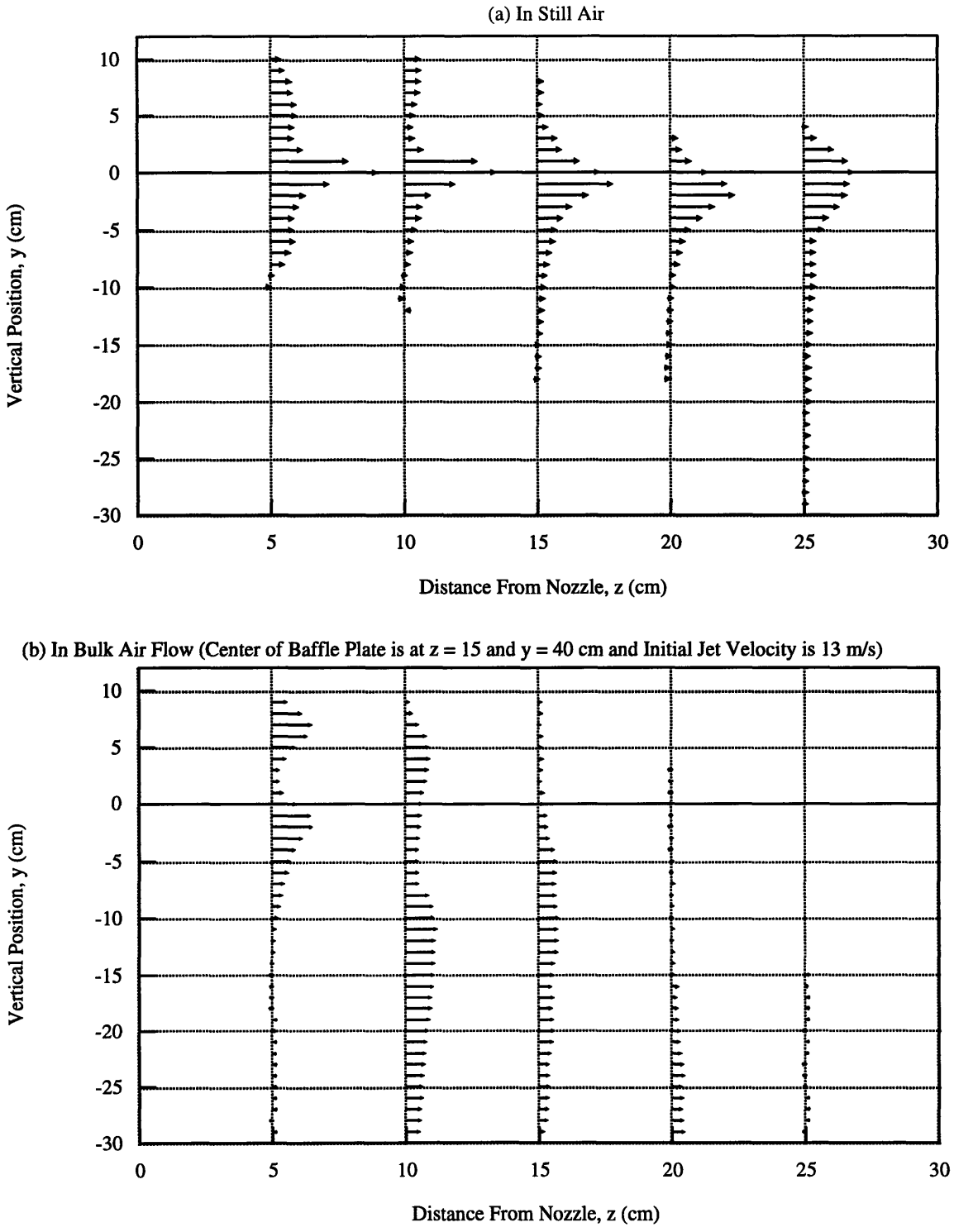

Figure 4.7: z-Velocity distribution at 100 psi along the vertical center plane of the spray (B-50 clean nozzle). (The length of each line is proportional to the magnitude of the velocity which ranges from 0 - 3.5 m/s.)

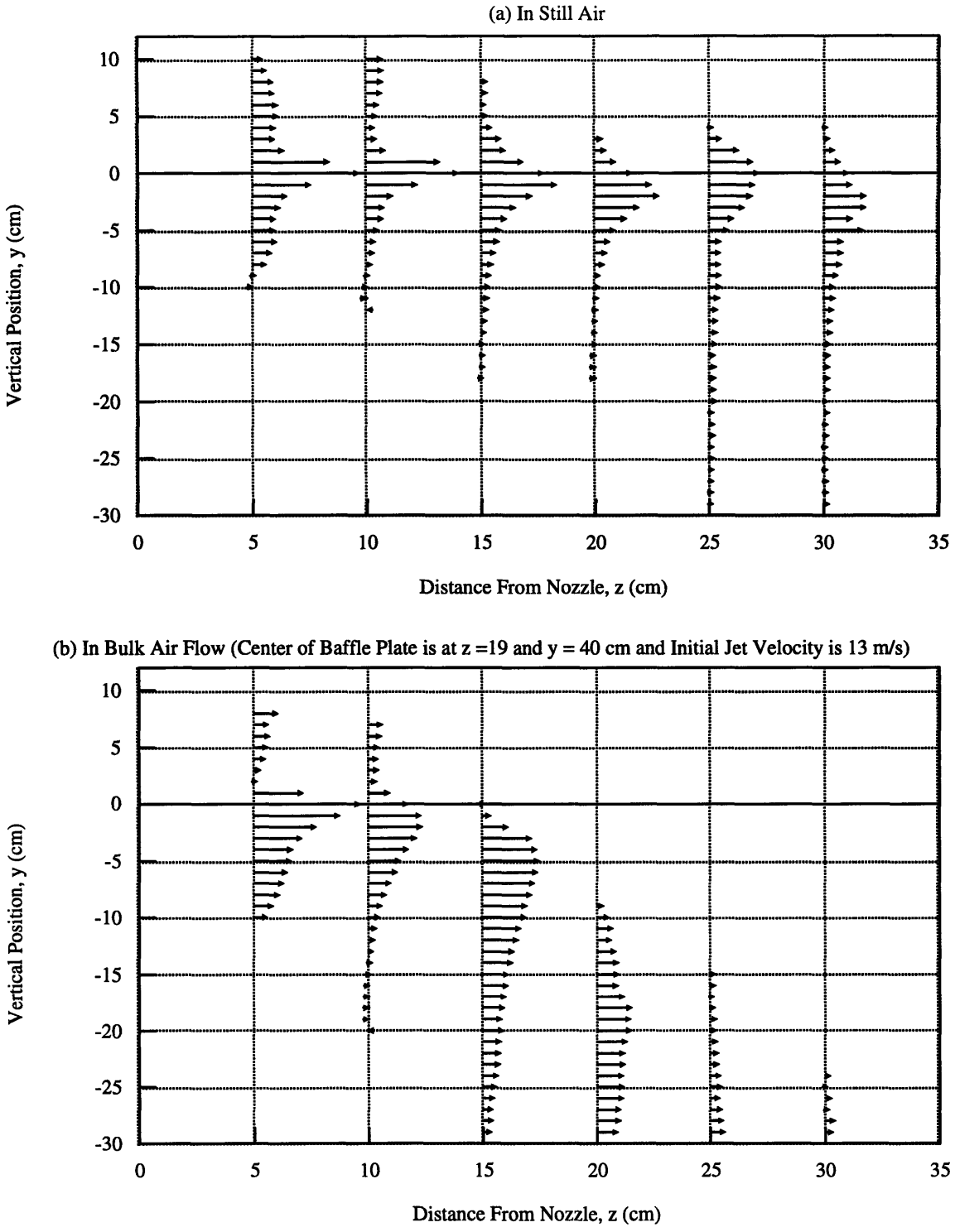

Figure 4.8: z-Velocity distribution at 100 psi along the vertical center plane of the spray (B-50 clean nozzle). (The length of each line is proportional to the magnitude of the velocity which ranges from 0 - 3.5 m/s.)

(a) In Still Air

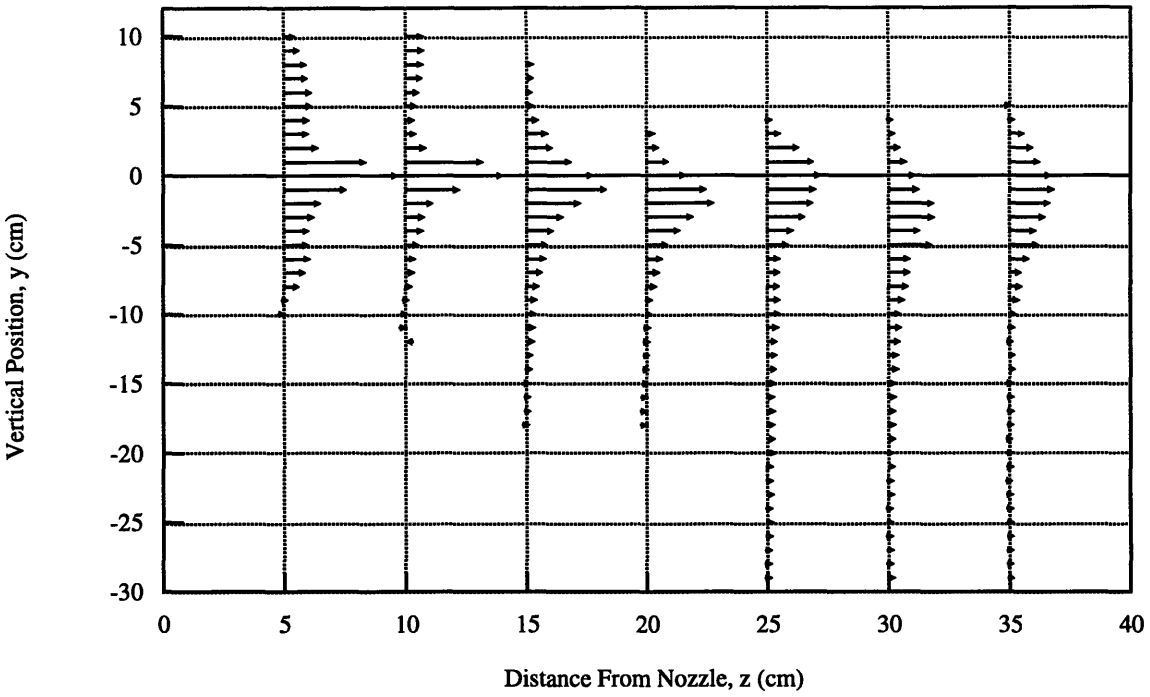

(b) In Bulk Air Flow (Center of Baffle Plate is at z = 25 and y = 40 cm and Initial Jet Velocity is 13 m/s)

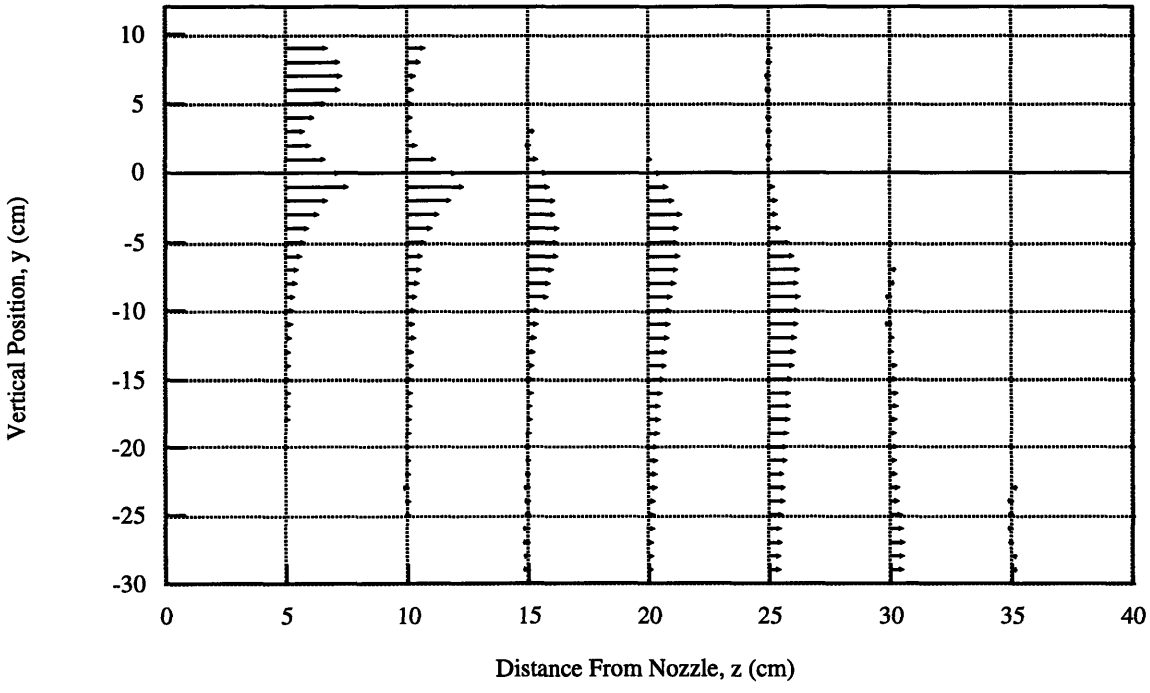

Figure 4.9: z-Velocity distribution at 100 psi along the vertical center plane of the spray (B-50 clean nozzle). (The length of each line is proportional to the magnitude of the velocity which ranges from 0 - 3.5 m/s.)

small magnitude compared to the corresponding droplet z-velocities in still air. This observation explains why a fully developed spray structure was seen close to the nozzle at the corresponding separations of 15 cm, 19 cm and 25 cm. After the spray passes the maximum y-velocity center of the bulk air flow, the droplets exhibit the constant profile of very small velocities for all separations.

The drag force of the bulk air force causes the maximum velocity peak to shift downward for all four configurations. As the separation increases, the downward shift of the maximum velocity peak occurs more gradually. At a distance of z = 15 cm from the nozzle, the maximum velocity occurs at y = -20 cm, y = -10, y = -5, and y = -4 for separations of 10 cm, 15 cm, 19 cm and 25 cm, respectively.

The double peaks seen at a distance of z = 5 cm from the nozzle for separations of 15 cm and 25 cm are independent of the bulk air flow effects. Rather they are a consequence of nozzle aging. All measurements were taken with the same nozzle, the last measurements taken were at separations of 15 cm and 25 cm. This explanation was verified by retaking the still air data with this nozzle at z = 5 cm; that data also exhibited dual peaks.

4.1.3 Droplet Validation Rate

Figures 4.10, 4.11, 4.12, and 4.13 compare the validation profile with and without air flow along the vertical center plane of the spray at four nozzle to bulk air flow separations (where the center of the baffle plate is 10 cm, 15 cm, 19 cm, and 25 cm from the nozzle, respectively). For all four separations, as distance from the nozzle is increased the profiles shift downward and flatten. As the separation from the nozzle increases, the distance from the nozzle at which this occurs increases. For all four separations, the droplet flux greatly decreases after passing the center of the bulk air column, where the highest air velocities occur (Figures 3.10, 3.11, 3.12, and 3.13).

Again it is evident that at a separation of 10 cm, the spray is not fully developed before reaching the bulk air column. For the other three separations the validation profile starts out with most of the droplets in the center of the cone, as distance from the center increases, the number of drops decreases. This fully developed structure is similar to the still air case. The farther the separation between the nozzle and the air jet, the greater this fully developed structure is preserved. Eventually this fully developed structure evolves into a flat profile with increasing flux corresponding to increasing distance below the nozzle.

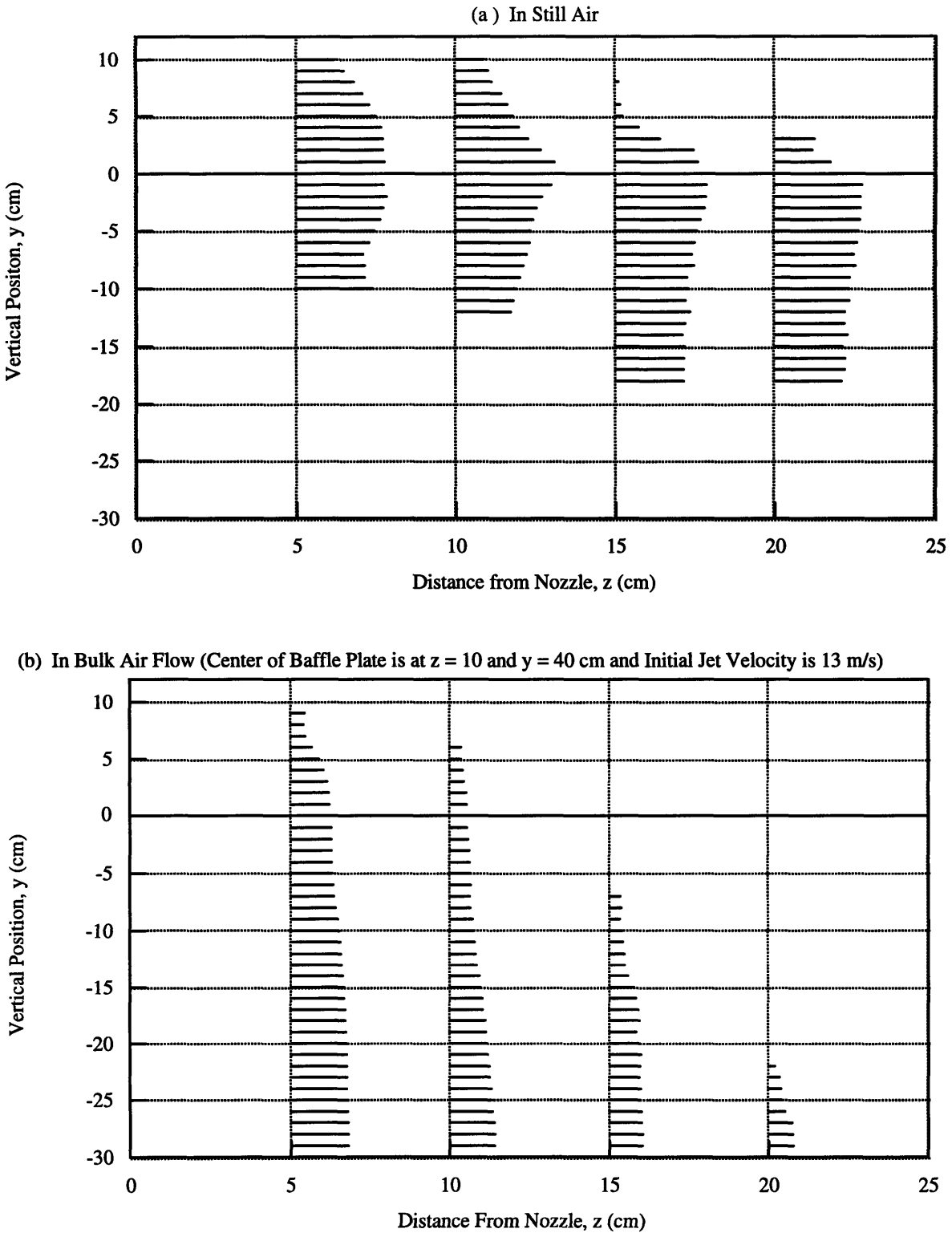

Figure 4.10: Validation Rate Profile at 100 psi along the vertical center plane of the spray (B50 clean nozzle)
(The length of each line is proportional to the magnitude of
the Log_{10}(validations/sec) which ranges from 0 - 3.5.)

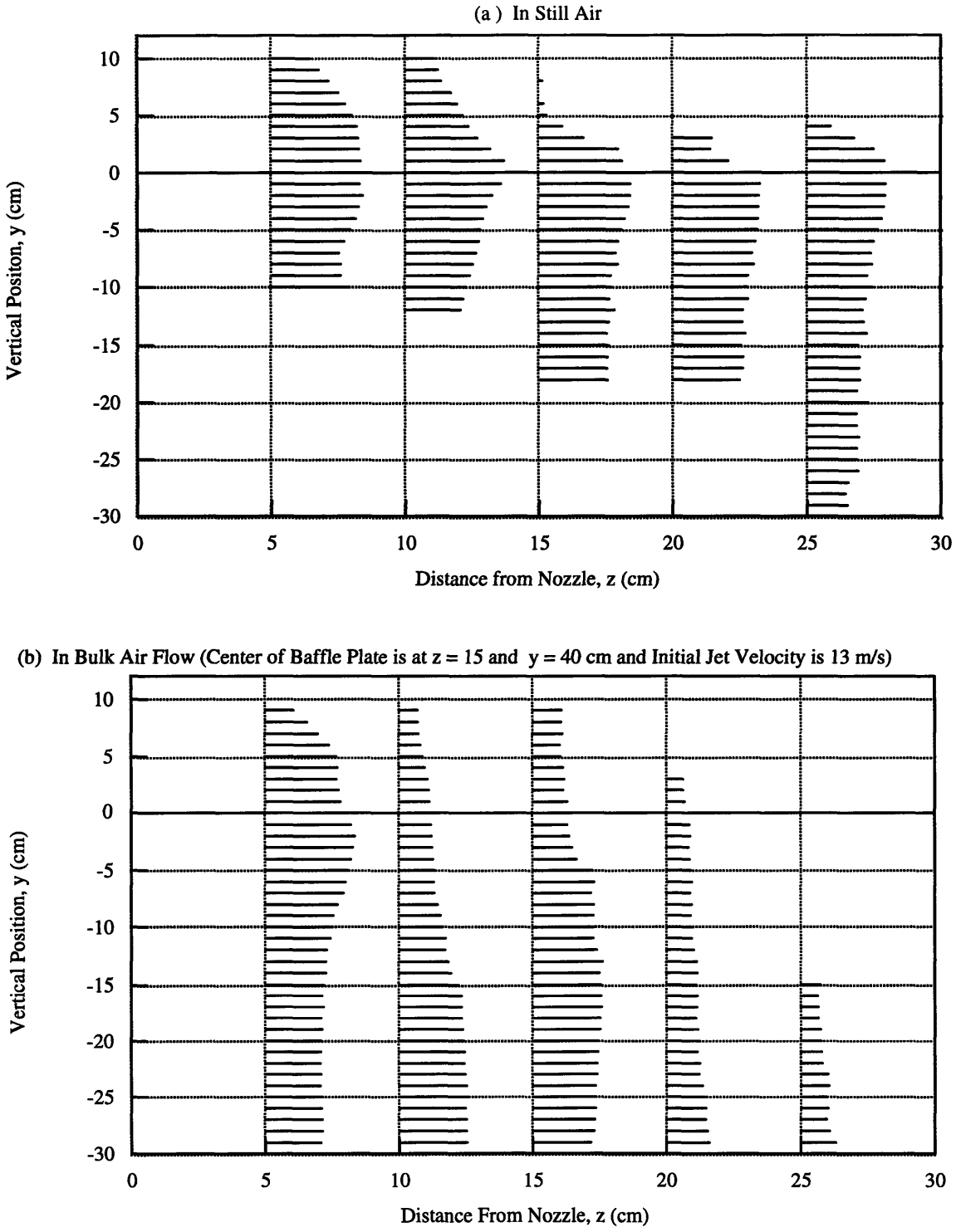

Figure 4.11: Validation Rate Profile at 100 psi along the vertical center plane of the spray (B50 clean nozzle)
(The length of each line is proportional to the magnitude of
the Log_{10}(validations/sec) which ranges from 0 - 3.5.)

(a) In Still Air

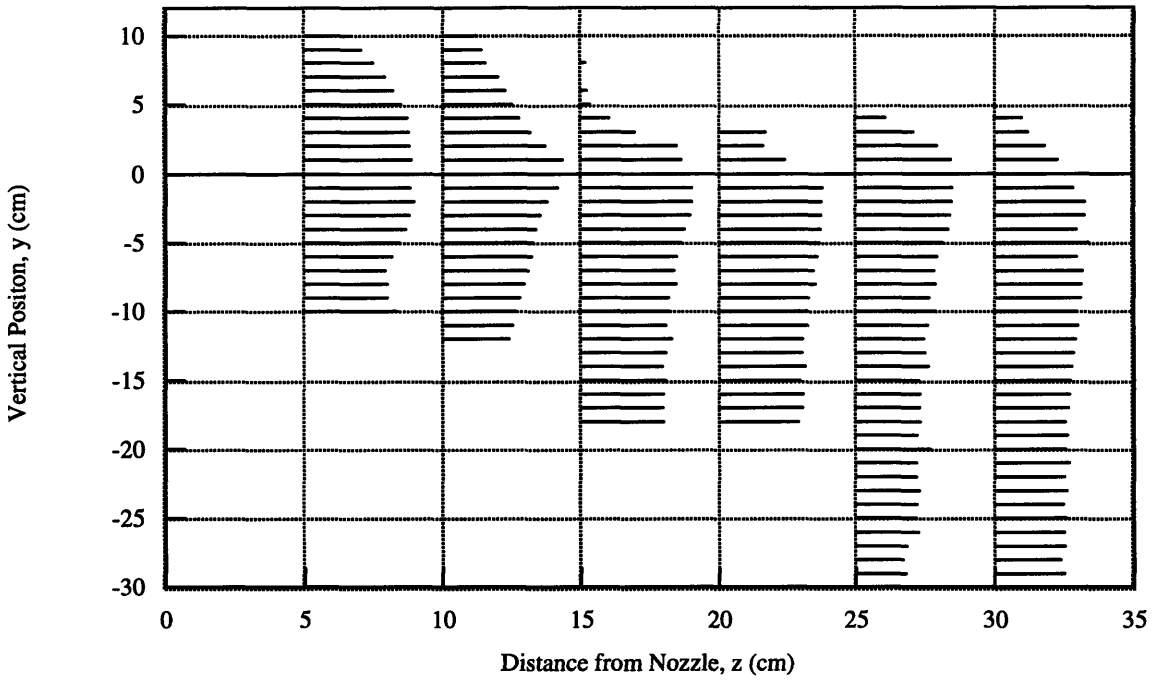

(b) In Bulk Air Flow (Center of Baffle Plate is at z = 19 and y = 40 cm and Initial Jet Velocity is 13 m/s)

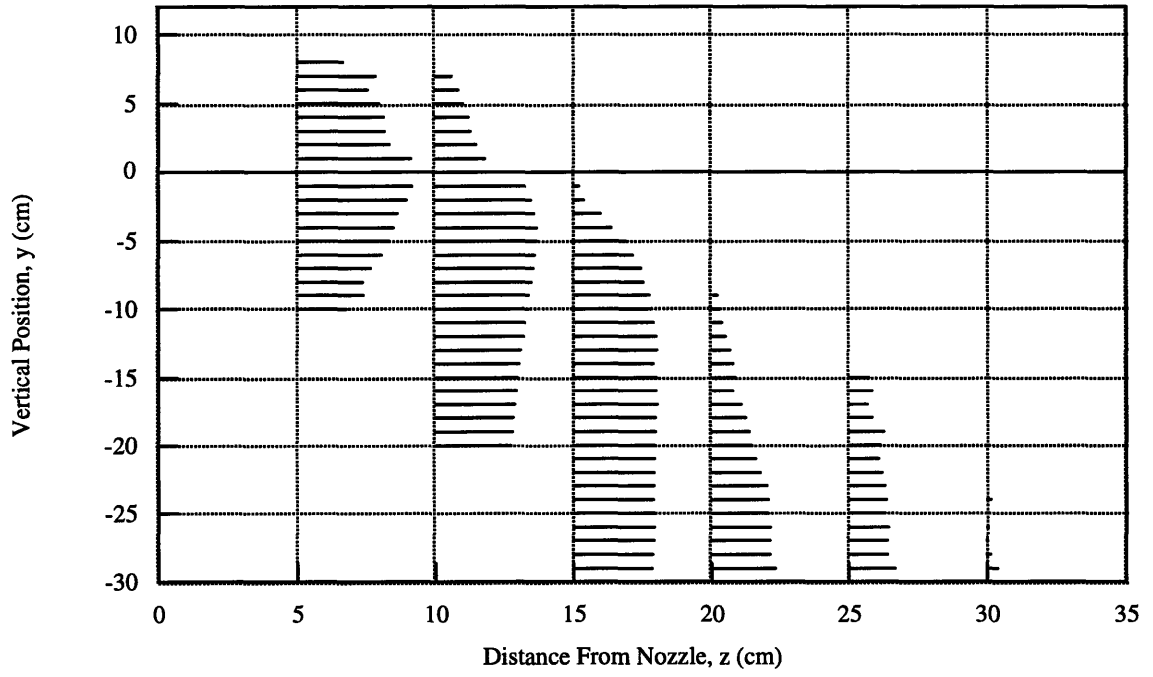

Figure 4.12: Validation Rate Profile at 100 psi along the vertical center plane of the spray (B50 clean nozzle)
(The length of each line is proportional to the magnitude of
the Log_{10}(validations/sec) which ranges from 0 - 3.5.)

(a) In Still Air

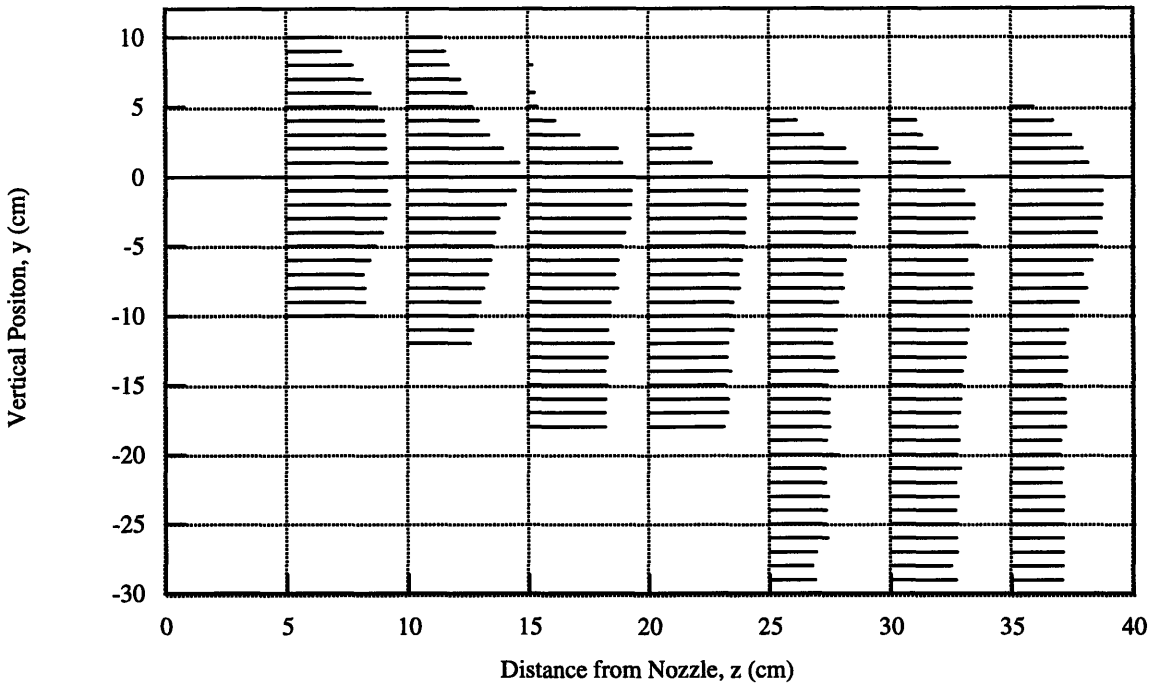

(b) In Bulk Air Flow (Center of Baffle Plate is at z = 25 and y = 40 cm and Initial Jet Velocity is 13 m/s)

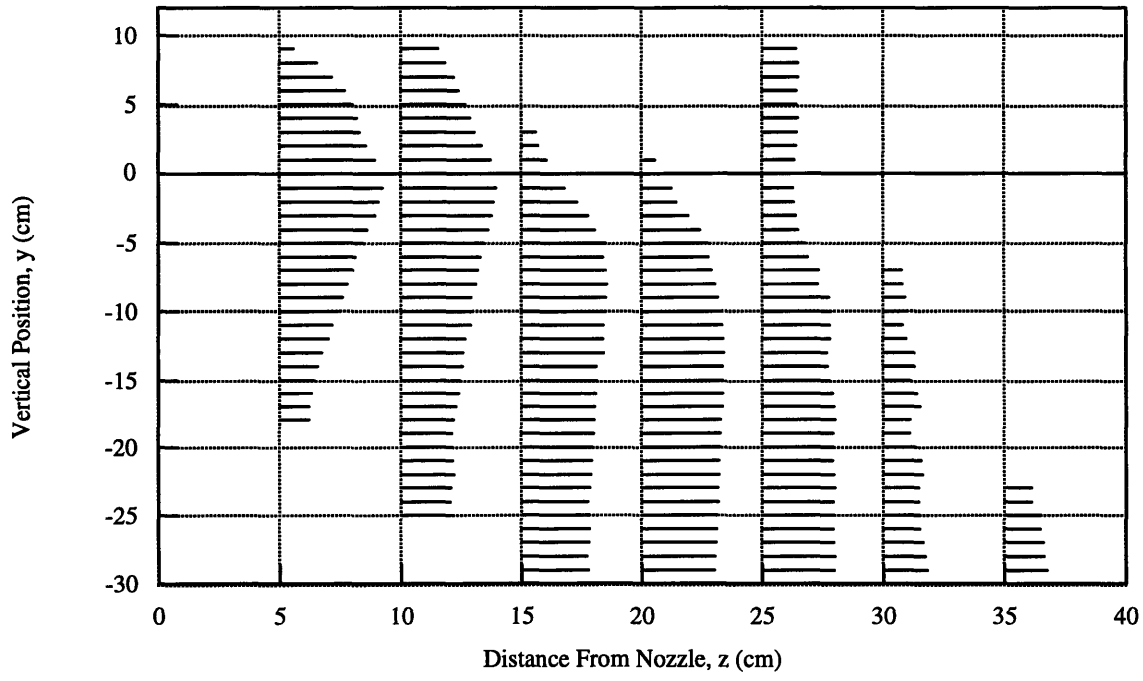

Figure 4.13: Validation Rate Profile at 100 psi along the vertical center plane of the spray (B50 clean nozzle)
(The length of each line is proportional to the magnitude of
the Log_{10}(validations/sec) which ranges from 0 - 3.5.)

If the center of the baffle plate is taken as the edge of the fiber bundle, the best droplet dispersion is obtained if the separation between the nozzle and the center of the bulk air flow is 15 cm. As seen in Figure 4.10 (b), the dispersion of the droplets at z = 15 cm spans a large y-range of y = -29 to y = 9 cm, and the flux is distributed fairly uniformly, with an average flux around 13 validations/sec between y = -4 and y = 9 cm and a flux of about 130 validations/sec between y = -29 and y = -5 cm. The separation of 15 cm yields the best results because the spray is given enough room to become fully developed, yet it is placed close enough to the air column that there is still high flux available when it enters the column. Perhaps the high turbulence intensity (Tu between 0.39 and 0.64) close to the spray nozzle seen in Figure 3.11 (b) contributes to the favorable distribution observed at this separation.

4.2 Spray Dispersion for Varying Air Jet Velocity

4.2.1 Droplet Diameter

Figures 4.3, 4.14 and 4.15 compare the SMD distribution with and without air flow along the vertical center plane of the spray at three initial air jet velocities (13 m/s, 17.3 m/s, and 21.4 m/s, respectively). The SMD profiles are very similar in shape and magnitude for these three air speeds at distances of z = 10 cm and greater from the nozzle. These profiles have the following characteristics. At distances of z = 20 cm and z = 25 cm the SMD profiles are nearly constant with values ranging from 50 - 80 μm. At a distance of z = 15 cm, the SMD profile is constant except for the region between y = ± 5 cm, where there are larger droplets than the rest of the profile. At z = 10 cm, the SMD profiles have the largest SMD's at the top and gradually decrease to a minimum SMD at the bottom of the spray profile.

However, there are differences in the SMD profiles at a distance of z = 5 cm from the nozzle. When the initial velocity is 21.4 m/s as shown in Figure 4.15 (b), it is evident that the spray cone has not become fully developed. This is due to higher air velocities at the edges of the faster air jet not allowing the spray enough space to develop. A fully developed spray cone is characterized by a central core of small diameter droplets surrounded by a sheath of larger droplets as depicted in Figures 4.2 (b) and 4.14 (b) for the other two speeds at z = 5 cm. The SMD profile at z = 5 cm for the highest air speed is fairly constant with an SMD range of 50 to 60 μm (with the exception of the 4 positions at the top of the spray cone at z = 5 cm).

(a) In Still Air

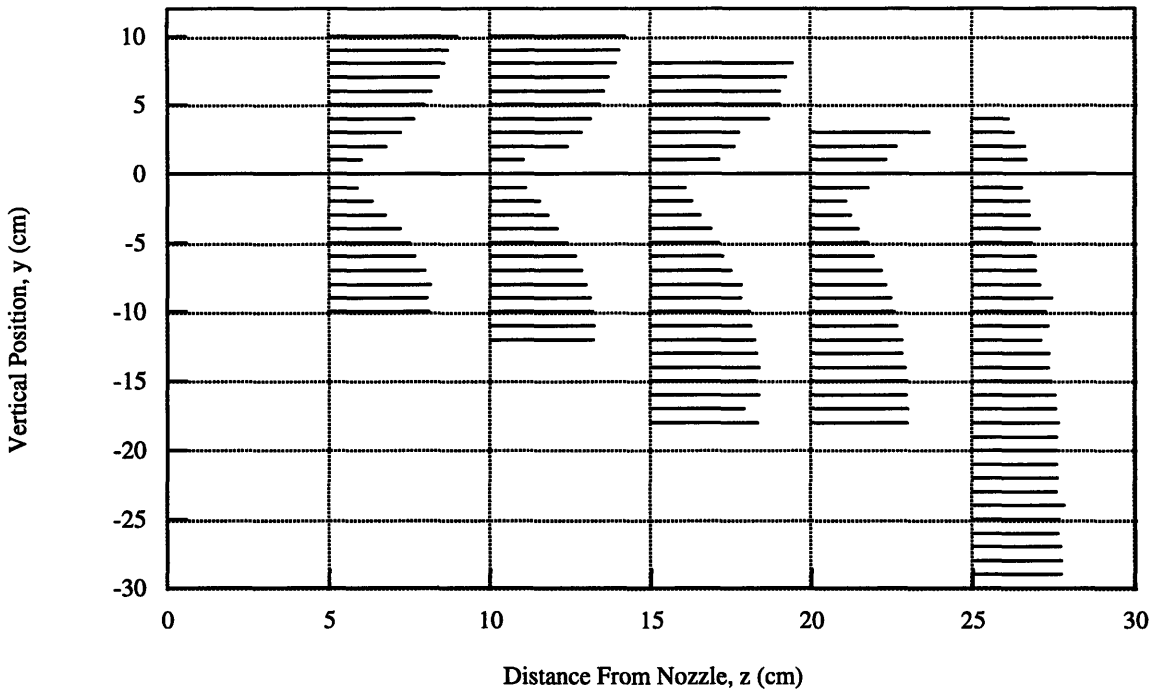

(b) In Bulk Air Flow (Center of Baffle Plate is at z = 15 and y =40 and Initial Jet Velocity is 17.3 m/s)

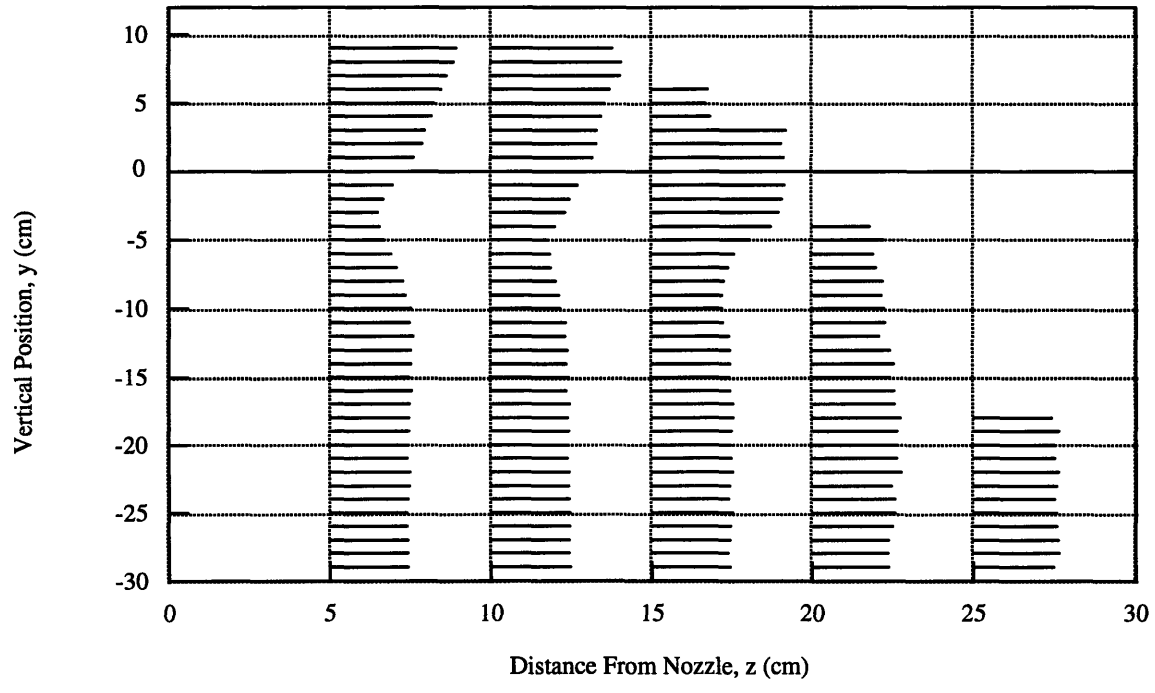

Figure 4.14: SMD distribution at 100 psi along the vertical center plane of the spray (B-50 clean nozzle). (The length of each line is proportional to the magnitude of the SMD which ranges from 14 - 107 microns.)

(a) In Still Air

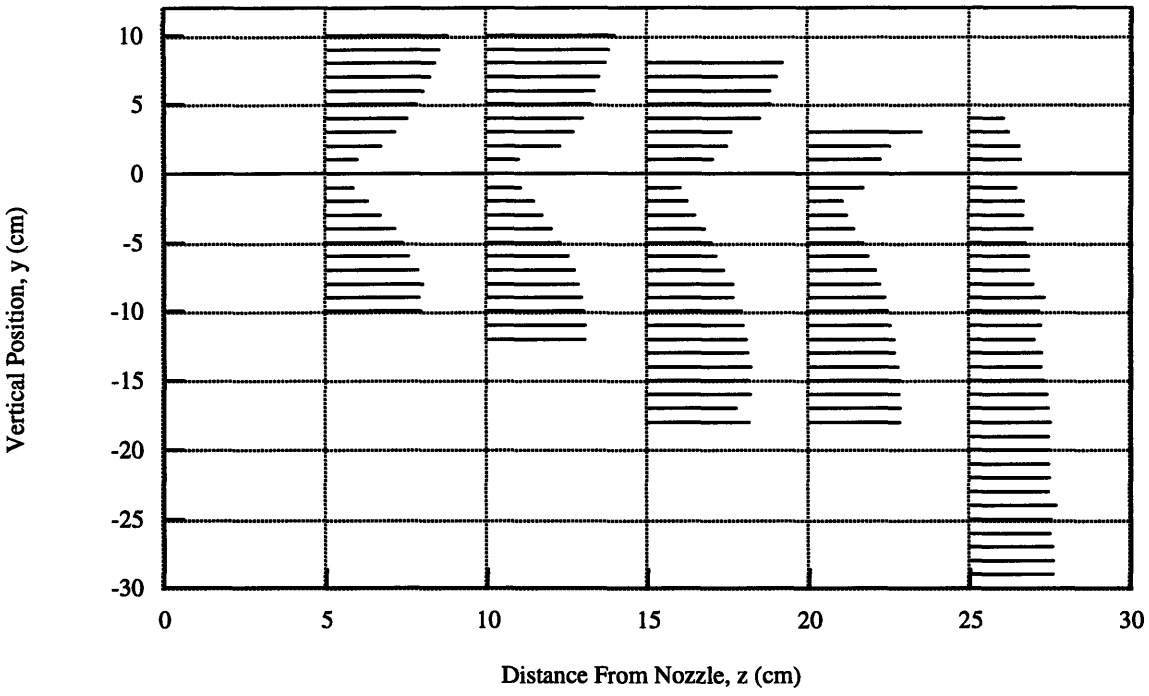

(b) In Bulk Air Flow (Center of Baffle Plate is at z = 15 and y =40 and Initial Jet Velocity is 21.4 m/s)

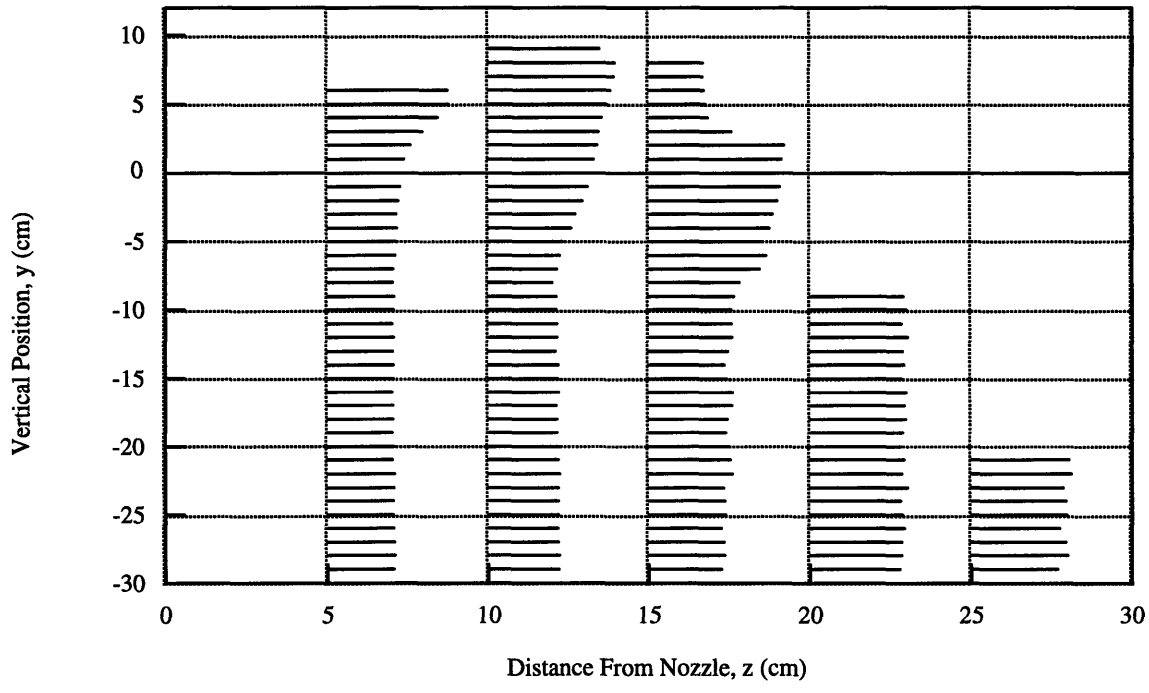

Figure 4.15: SMD distribution at 100 psi along the vertical center plane of the spray (B-50 clean nozzle). (The length of each line is proportional to the magnitude of the SMD which ranges from 14 - 107 microns.)

4.2.2 Droplet Velocity

Figures 4.7, 4.16, and 4.17 compare the z-velocity profile with and without air flow along the vertical center plane of the spray at three initial air jet velocities (13 m/s, 17.3 m/s, and 21.4 m/s, respectively). For all three air speeds the velocity profiles evolve from well defined peaks into nearly flat profiles of negligible velocity (less than 0.3 m/s). The final constant velocity profile occurs at a distance from the nozzle of z = 25 cm for all initial air jet speeds. For the air speed of 21.4 m/s the initial velocity profile at z = 5 cm is much flatter than those of the lower air speeds. The maximum velocity peak at z = 5 cm shifts downward as the initial air jet velocity is increased. The double peaks seen at distances of z = 5 cm and z = 10 cm from the nozzle for all three cases are again a consequence of nozzle aging as described in Section 4.1.2.

4.2.3 Droplet Validation Rate

Figures 4.11, 4.18, and 4.19 compare the validation rate profile with and without air flow along the vertical center plane of the spray at three initial air jet velocities (13 m/s, 17.3 m/s, and 21.4 m/s, respectively). For all three air speeds, as distance from the nozzle is increased, the profiles shift downward and flatten. At z = 20 cm and z = 25 cm the droplet flux for the measured area decreases with increasing air speed, indicating either a downward shift of droplets or increased evaporation of droplets.

Again it is evident that at an initial air jet velocity of 21.4 m/s, the spray is not fully developed before reaching the bulk air column. The elevated air speed of 21.4 m/s causes larger air velocities near the edges of the air jet, causing most of the droplets to be dragged to the bottom of the spray cone at a distance very close to the nozzle. For the other two air speeds the validation profile starts out with most of the droplets in the center of the cone, as distance from the center increases, the number of drops decreases. This fully developed structure is similar to the still air case. The smaller the initial air jet velocity, the greater this fully developed structure is preserved. Eventually this fully developed structure evolves into a flat profile with increasing flux corresponding to increasing distance below the nozzle.

Even though there are some differences seen in the droplet profiles with varying air jet speed, the discrepancies are minute. Increasing the initial air jet velocity from 13 m/s to 21.4 m/s does not have much of an effect on droplet dispersion or spray structure. However, perhaps greater changes in the initial air jet speed would show greater variance in spray dispersion and structure.

(a) In Still Air

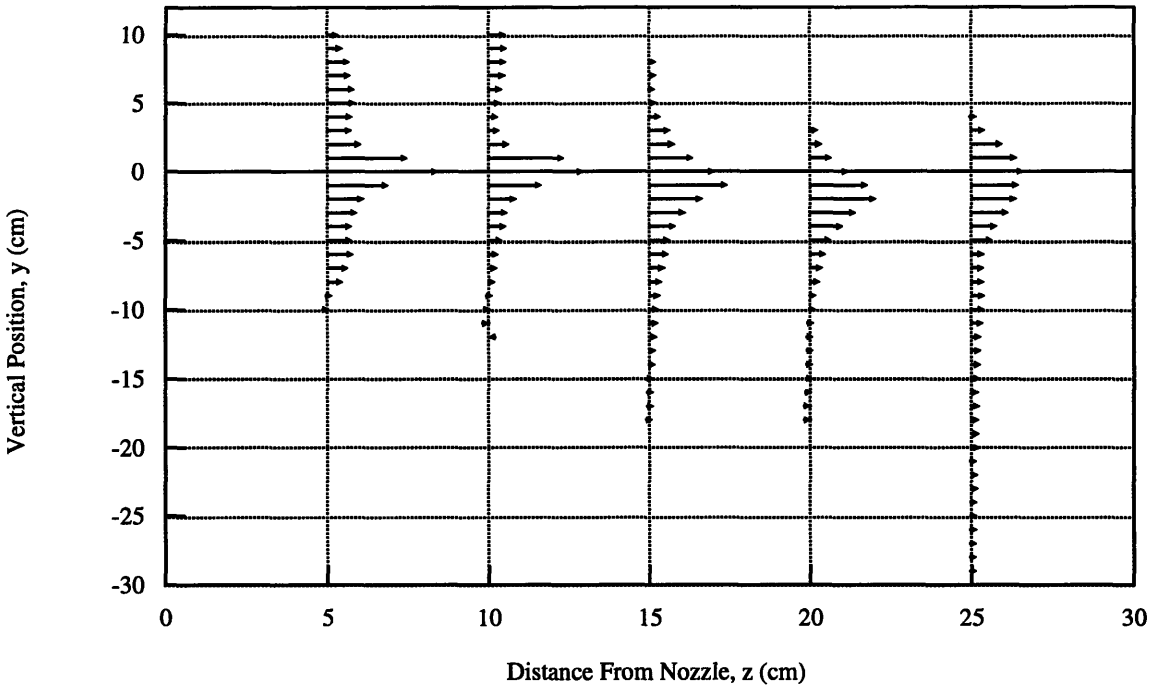

b) In Bulk Air Flow (Center of Baffle Plate is at z = 15 and y = 40 cm and Initial Jet Velocity is 17.3 m/s)

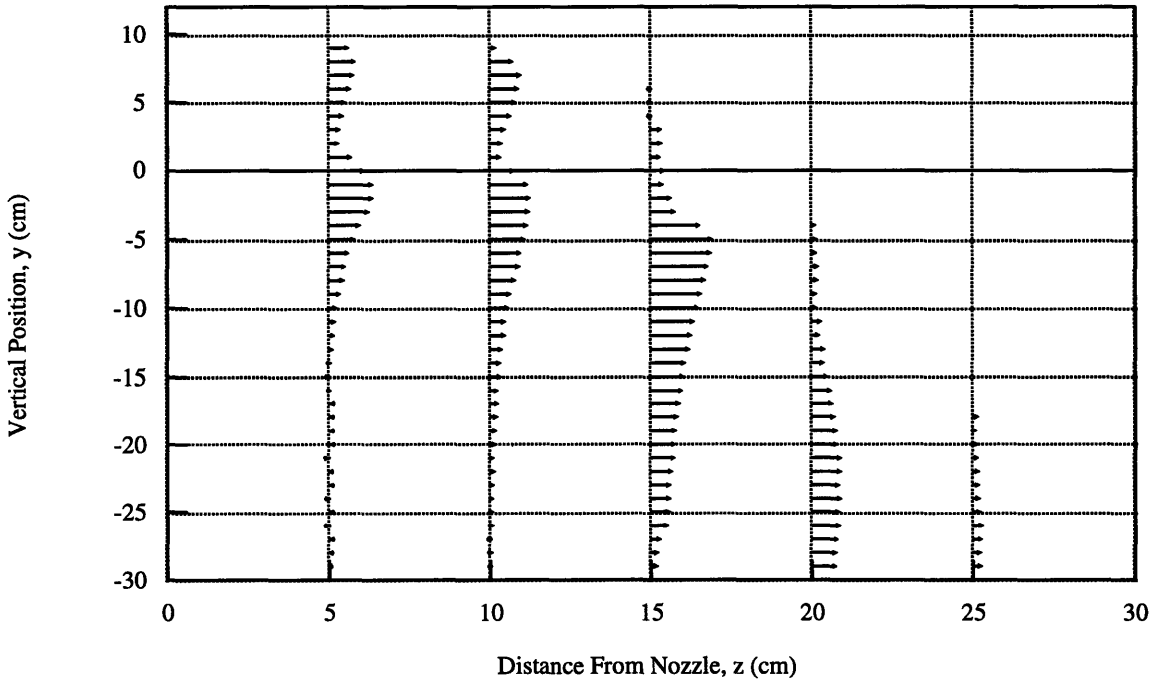

Figure 4.16: z-Velocity distribution at 100 psi along the vertical center plane of the spray (B-50 clean nozzle) (The length of each line is proportional to the magnitude of the velocity which ranges from 0 - 3.5 m/s.)

(a) In Still Air

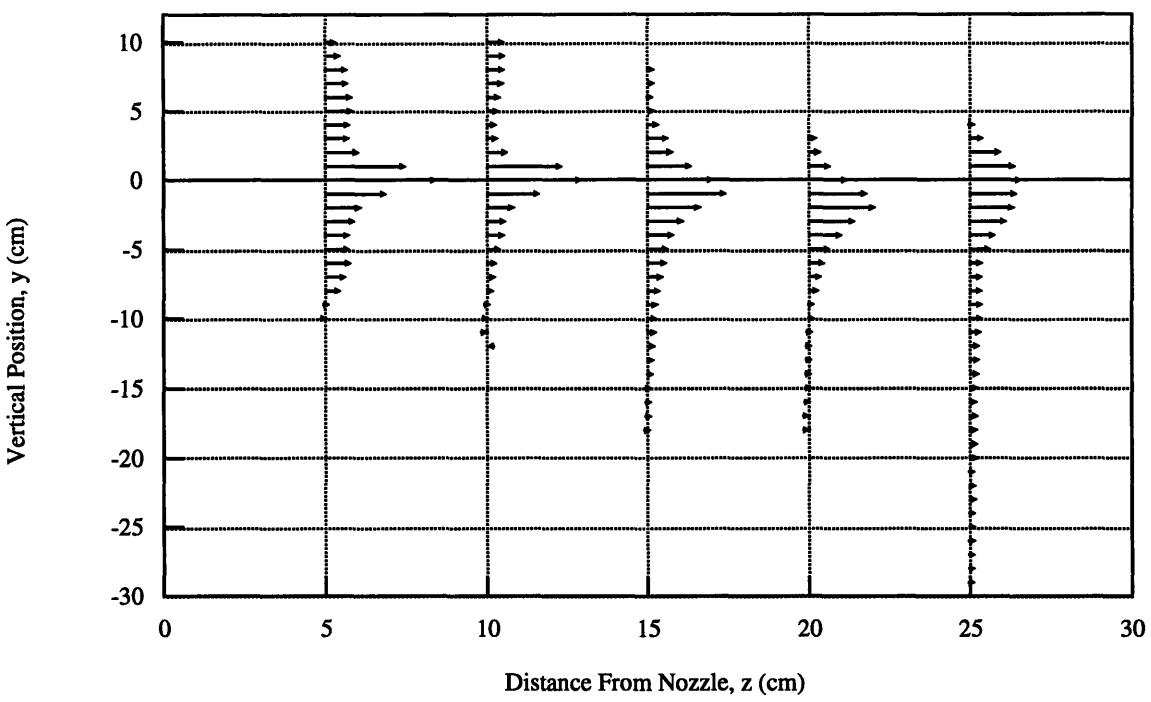

(b) In Bulk Air Flow (Center of Baffle Plate is at z = 15 and y = 40 cm and Initial Jet Velocity is 21.4 m/s)

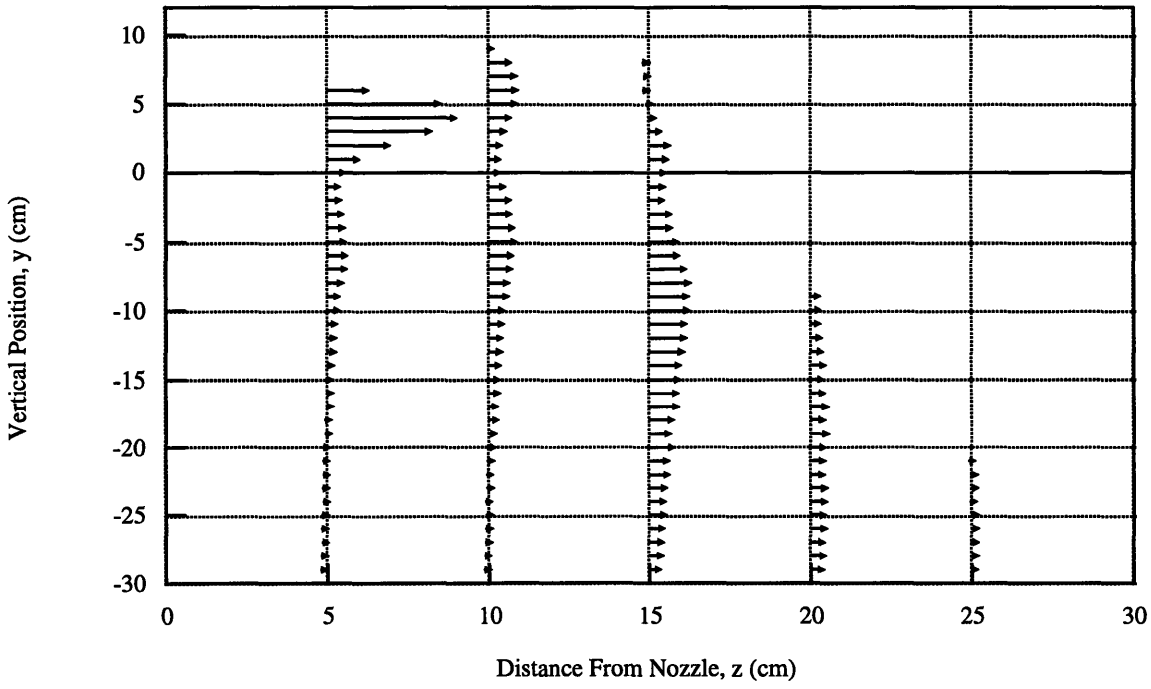

Figure 4.17: z-Velocity distribution at 100 psi along the vertical center plane of the spray (B-50 clean nozzle) (The length of each line is proportional to the magnitude of the velocity which ranges from 0 - 3.5 m/s.)

(a) In Still Air

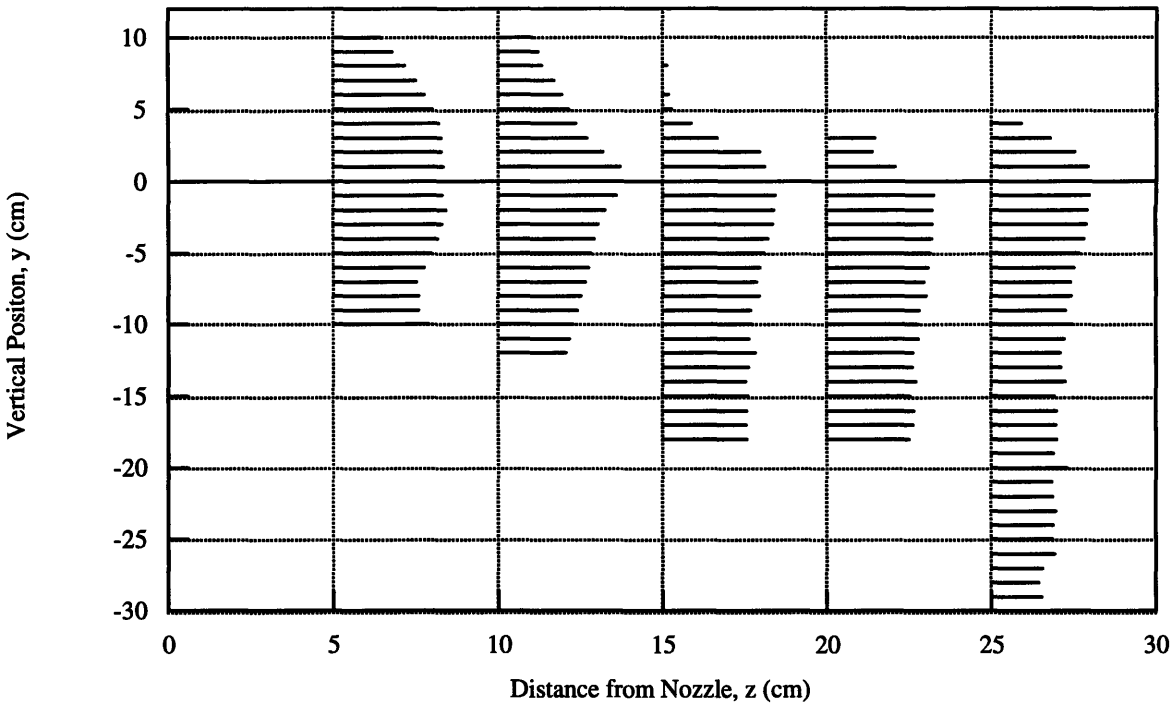

(b) In Bulk Air Flow (Center of Baffle Plate is at z = 15 and y= 40 cm and Initial Jet Velocity is 17.3 m/s)

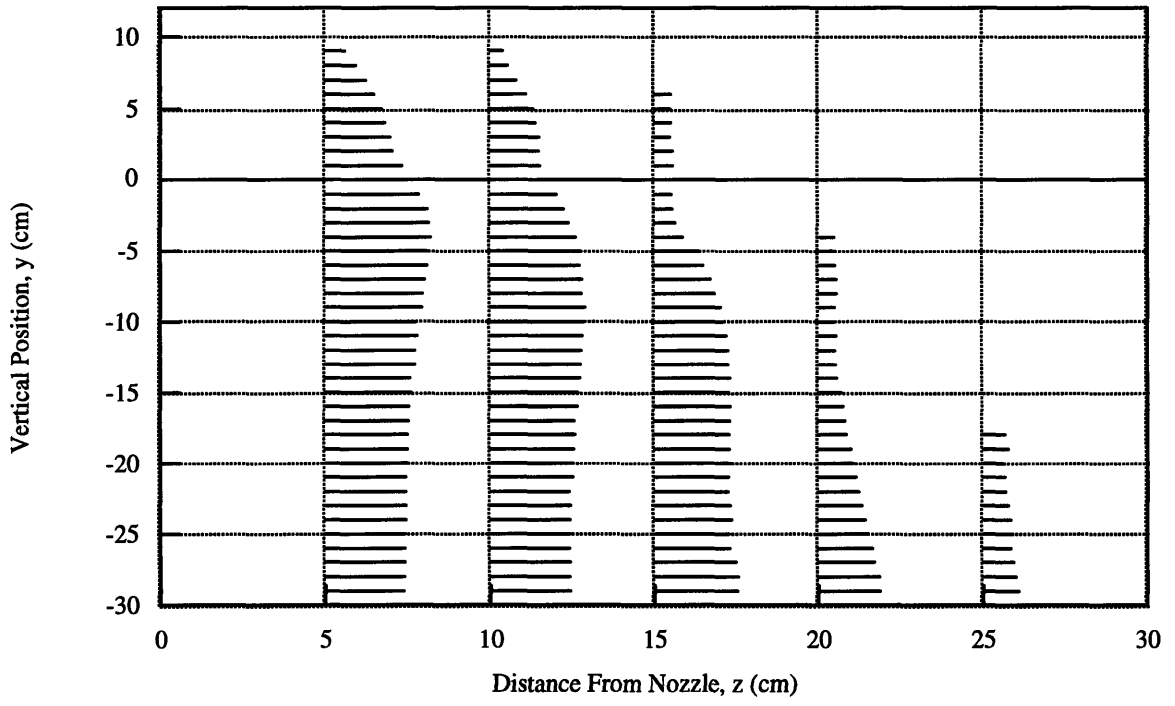

Figure 4.18: Validation Rate Profile at 100 psi along the vertical center plane of the spray (B50 clean nozzle)
(The length of each line is proportional to the magnitude of
Log_{10}(validations/sec) which ranges from 0 - 3.5.)

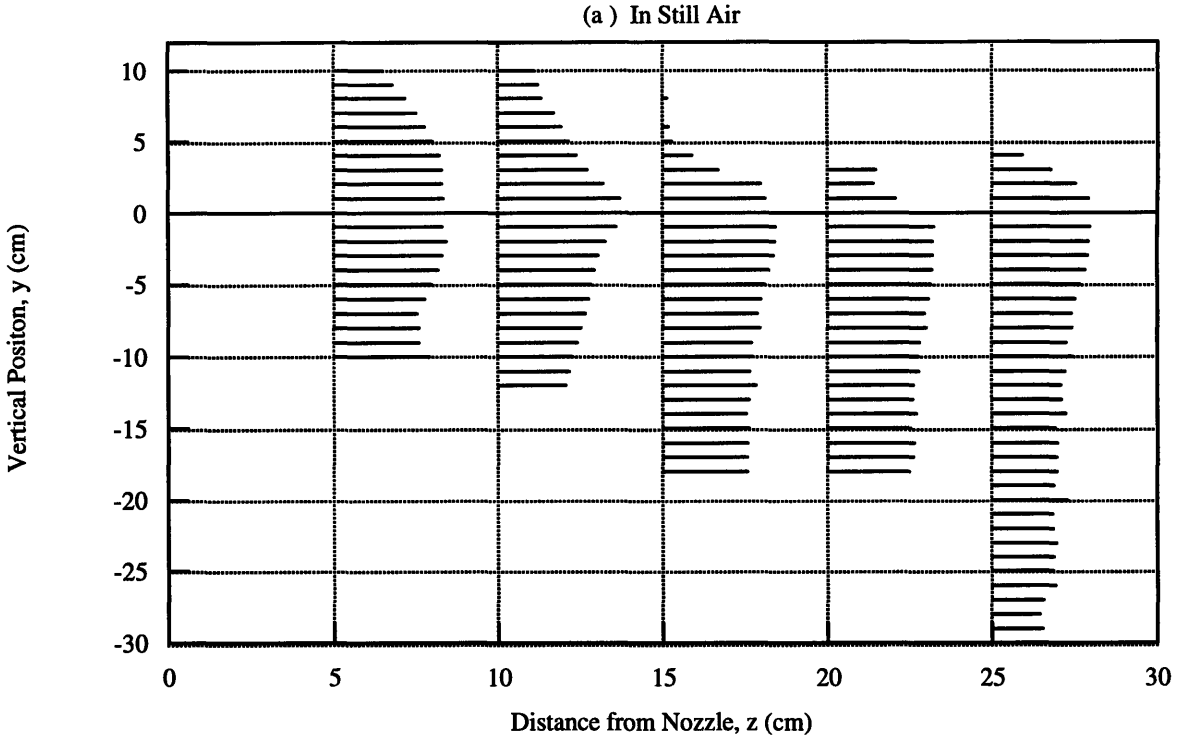

(b) In Bulk Air Flow (Center of Baffle Plate is at z = 15 and y= 40 cm and Initial Jet Velocity is 21.4 m/s)

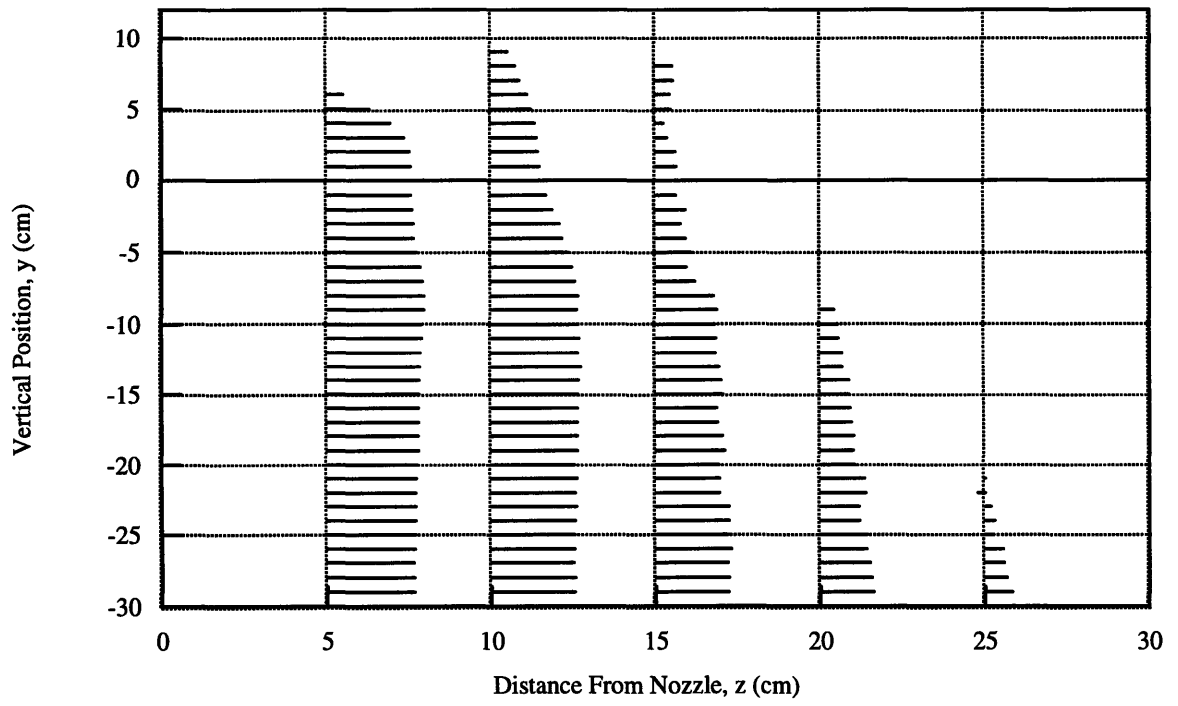

Figure 4.19: Validation Rate Profile at 100 psi along the vertical center plane of the spray (B50 clean nozzle)
(The length of each line is proportional to the magnitude of
Log_{10}(validations/sec) which ranges from 0 - 3.5.)

4.3 Flow Visualization

A flow visualization video was created to illustrate the effect of bulk air flow on spray dispersion. The images in the video were obtained by diluting a small amount of flourescein, sodium salt in the supply water. A 3 *watt* argon laser was used to create a light sheet that illuminated the droplets in a given plane. The laser was positioned 1.5 m from the test cell and the beam was passed through two half cylindrical lenses to produce a flat sheet, 4 mm thick. One side of the test chamber was removed to permit an unobstructed view of the flow field. The laser sheet was aligned with the nozzle centerline and could be rotated from a vertical plane to a horizontal plane by rotating the cylindrical lenses by 90°.

Video footage was obtained at a nozzle operating pressure of 690 kPa (100 psi), in both vertical and horizontal planes of the spray. In the vertical plane, data is recorded on the nozzle centerline where the center of the baffle plate is 10 cm, 15 cm, 20 cm, and 25 cm from the nozzle. Video footage in the horizontal plane is taken 3 cm above the nozzle, on the nozzle centerline, and 5 cm, 10 cm, and 20 cm below the nozzle centerline at a 15 cm separation between the nozzle and the center of the bulk air column. All above configurations are recorded for still air, a jet exit velocity of 13 m/s and for a jet exit velocity of 25 m/s.

Figure 4.20 contains sketches of the spray cloud shapes in the center vertical plane when the initial jet velocity is 13 m/s. The general structure of the spray in still air as illustrated in Figure 4.20 (a) consists of a central high velocity core that project out horizontally from the nozzle and a region where a large portion of the droplets have little horizontal velocity and rain out of the flow [1]. In the region close to the nozzle the flow is laminar and the streamlines are easily seen in the video. As distance is increased from the nozzle both in the horizontal and vertical directions, the spray becomes turbulent with many eddies.

The addition of the bulk air flow with a jet outlet velocity of 13 m/s causes the majority of the spray to be deflected downward and causes the turbulent eddies to form closer to the nozzle. The high velocity core is pushed downward by the bulk air drag force. As the bulk air flow is moved closer to the nozzle, the turbulent eddies form closer to the nozzle. At a separation of 10 cm, the initial streamlined, laminar region appears to have diminished completely. This verifies the observation that the spray does not have enough space to become fully developed before being swept down by the bulk air drag force. There is also some

(a) In still air

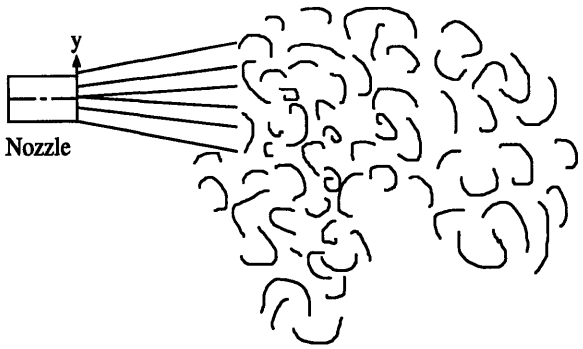

(b) The center of the bulk air flow is at z = 25 cm

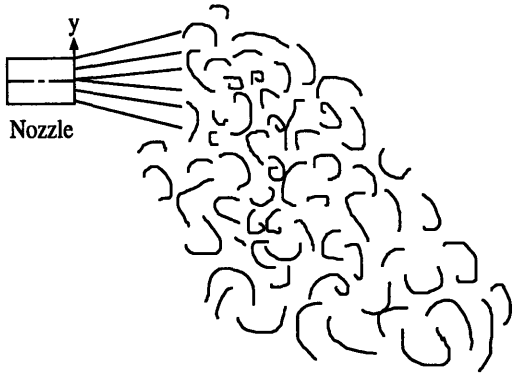

(c) The center of the bulk air flow is at z = 19 cm

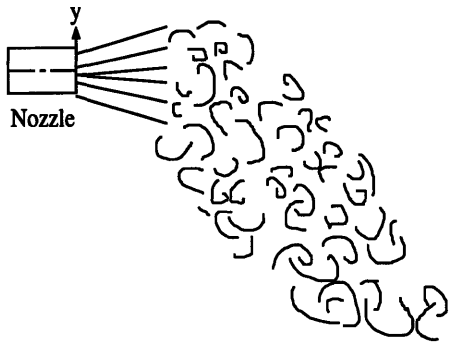

(d) The center of the bulk air flow is at z = 15 cm

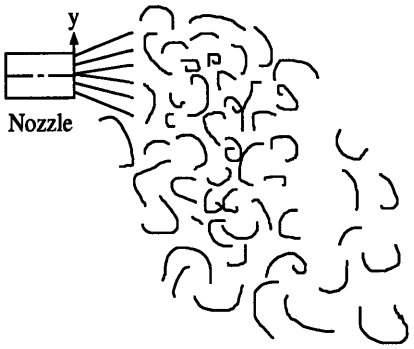

(e) The center of the bulk air flow is at z = 10 cm

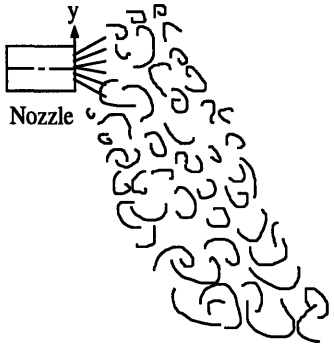

Note. The spray nozzle centerline is 40 cm below the baffle plate.
The jet exit velocity is 13 m/s.

Figure 4.20: B-50 nozzle spray structure.

recirculation of the spray from the floor of the nozzle test chamber.

Increasing the initial air jet velocity to 25 m/s increases the downward deflection of the spray and moves the turbulent eddies even closer to the nozzle. The streamlined laminar, region is only barely seen at a separation of 25 cm for this increased bulk air speed. The recirculation of the spray from the bottom of the nozzle testing chamber also greatly increases.

The measurements taken with the PDPA are confirmed with this flow visualization. It is evident from these observations that the bulk air flow dominates the behavior of the high velocity central core. The bulk air flow sweeps this core flow downward and destroys the laminar streamlined flow in the spray. Thus, the fiber induced air flow appears to entirely govern the dispersion of the droplets.

4.4 Summary

The following conclusions can be made about the spray structure of a Hago B-50 nozzle in bulk air flow.

1. When the spray cone encounters the down flowing air, it is deflected downward. The horizontal velocity decays while the vertical velocity grows.
2. The addition of the bulk air flow with an initial velocity of 13 m/s causes the majority of the spray to deflect downward and causes the turbulent eddies to form closer to the nozzle.
3. As the bulk air flow is moved closer to the nozzle, the turbulent eddies occur even closer to the nozzle.
4. The closer the bulk air flow is to the nozzle the earlier the SMD and validation profiles shift downward and flatten.
5. The velocity profiles evolve from well defined peaks into flat profiles that have negligible values of velocity as distance from the nozzle is increased.
6. As the separation of the air jet from the nozzle increases, the downward shift of the maximum velocity peak occurs more gradually.
7. A fully developed spray cone does not develop when the nozzle is located 10 cm from the center of the bulk air flow for an air jet exit velocity of 13 m/s.
8. The separation of 15 cm displays the best spray dispersion at an air jet exit velocity of 13 m/s.

9. Increasing the initial air jet velocity from 13 m/s to 21.4 m/s increases the downward deflection of the spray, reduces spray penetration into the air column and moves the turbulent eddies closer to the nozzle.

10. A fully developed spray cone does not develop at a separation of 15 cm when the initial air jet velocity is 21.4 m/s.

Chapter 5

Effect of Nozzle Supply Pressure Variations on Spray Characteristics in Bulk Air Flow

The effect of pressure variations is examined for four B-50 clean nozzles in a bulk air flow centered at z = 19 cm from the nozzle exit (Figure 4.1 (c) is a spatial description of the experimental configuration). The nozzle operating pressure is varied from 276 kPa (40 psi) to 1000 kPa (145 psi) at approximately 15 psi intervals. The measurements include the SMD, the velocity, the validation rate and the flow rate at four different positions within the vertical center plane of the spray. These four positions (1), (2), (3), and (4) were located at y = 0 and z = 10 cm, at y = -15 and z = 15 cm, at y = -30 and z =20 cm, and at y = -30 and z = 25 cm, respectively.

5.1 Droplet Diameter

Figures 5.1, 5.2, 5.3, and 5.4 show the variation of droplet SMD with pressure for four B-50 nozzles in a bulk air flow with an initial air jet speed of 13 m/s. For all four positions, the SMD's decrease with increasing pressure as seen for the nozzles in still air. The greatest range in SMD is seen for position (2) in Figure 5.2, where the SMD decreases from a value of approximately 115 μm at an operating pressure of 276 kPa (40 psi) to a value of about 50 μm at1000 kPa (145 psi). The greatest change in SMD occurs between 276 kPa (40 psi) and 690 kPa (100 psi) for positions (1) and (2), while for positions (3) and (4) the greatest change occurs between 276 kPa (40 psi) and 552 kPa (80 psi). In contrast to the scatter of SMD's observed

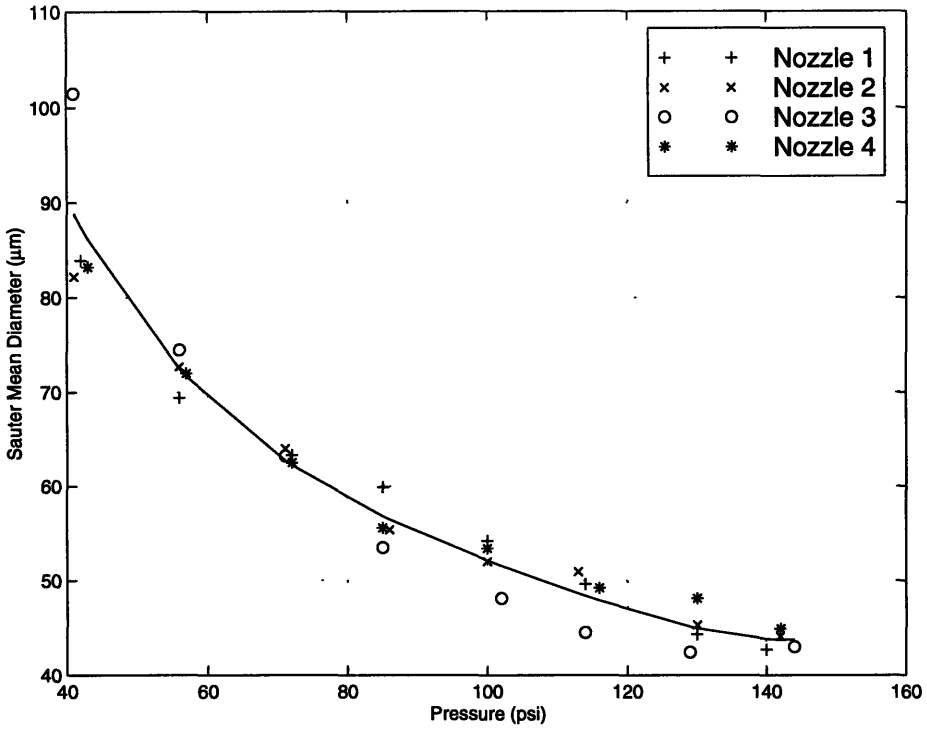

Figure 5.1: Hago B-50. Pressure vs. SMD at y = 0 and z = 10 cm in a bulk air flow.

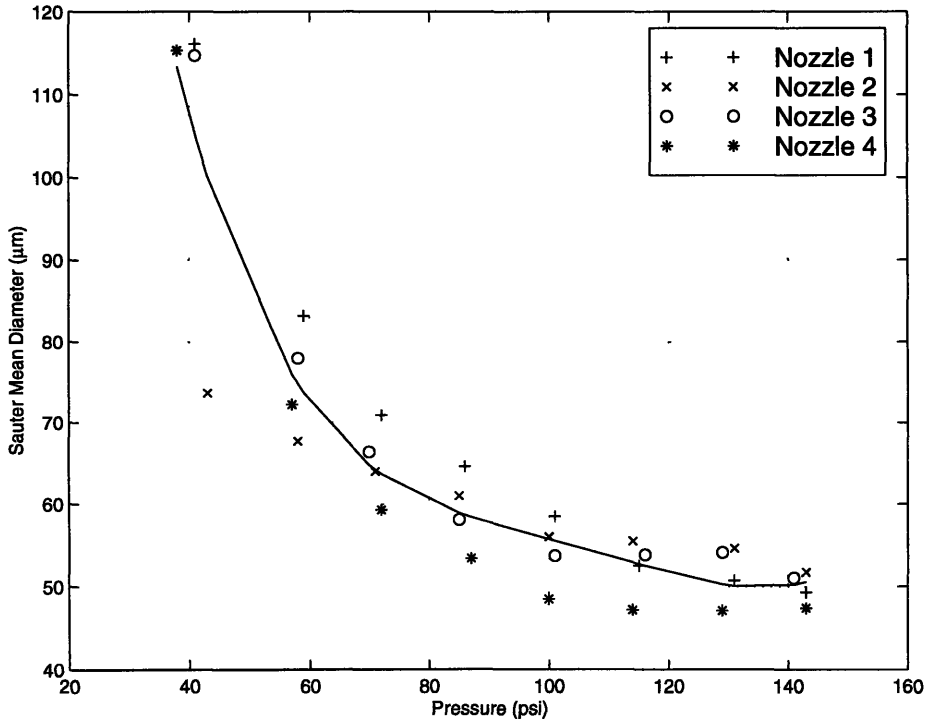

Figure 5.2: Hago B-50. Pressure vs. SMD at y = -15 and z = 15 cm in a bulk air flow.

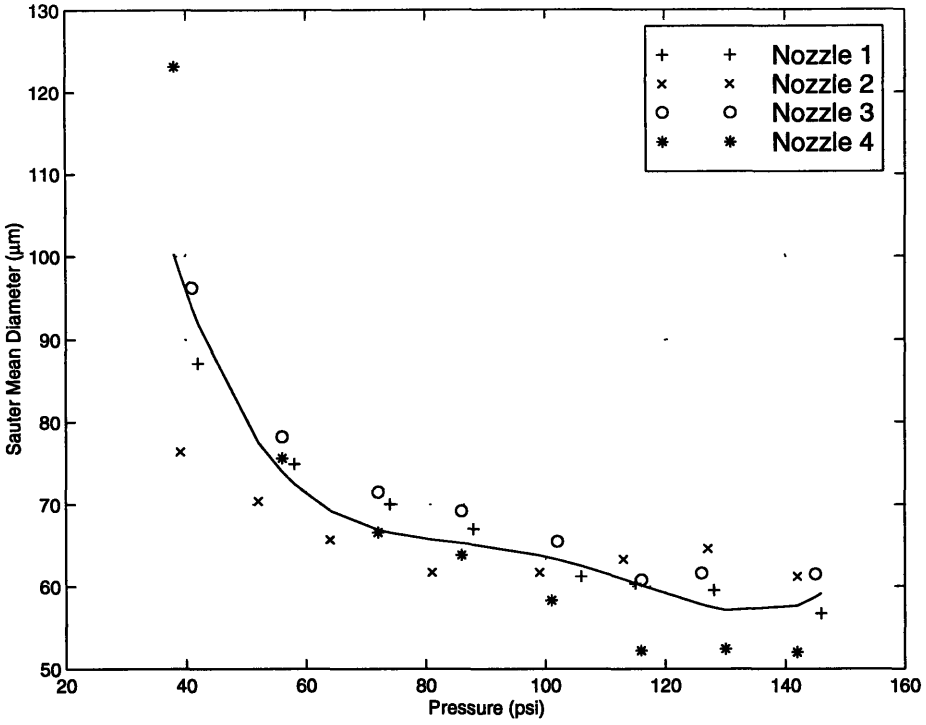

Figure 5.3: Hago B-50. Pressure vs. SMD at y = -30 and z = 20 cm in a bulk air flow.

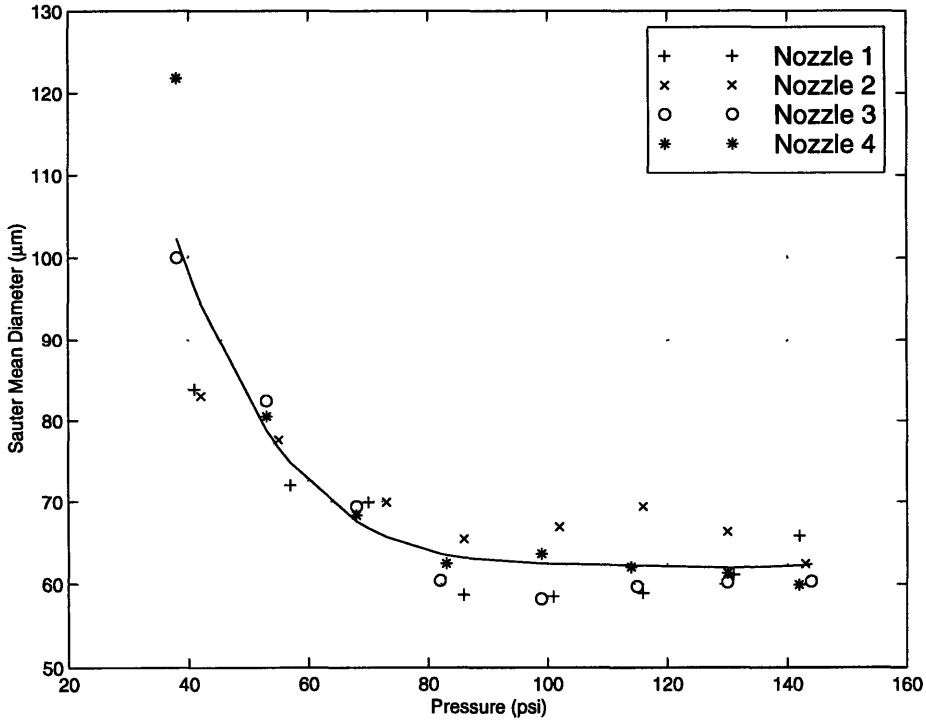

Figure 5.4: Hago B-50. Pressure vs. SMD at y = -30 and z = 25 cm in a bulk air flow.

in still air at a distance of 20 cm from the nozzle, very little scatter in SMD data is seen for these nozzles. The bulk air flow appears to reduce the variation between the SMD's of different nozzles as compared to the results for still air found by Sweetland [1].

5.2 Droplet Velocity and Flowrate

Figures 5.5, 5.6, 5.7, and 5.8 show the variation of the droplet z-velocity with pressure for four B-50 nozzles in bulk air flow. For all four positions, the velocities increase with increasing pressure as seen for the nozzles in still air. The greatest range in velocities is seen at the position closest to the nozzle, as distance from the nozzle increases the range of velocities decreases. The velocity at position (1), 10 cm from the nozzle increases from 0.75 m/s at an operating pressure of 276 kPa (40 psi) to 1.35 m/s at 1000 kPa (145 psi). While at position (4), 25 cm from the nozzle, the velocity only increases from 0.1 m/s at an operating pressure of 276 kPa (40 psi) to 0.25 m/s at 1000 kPa (145 psi). The most scatter in velocity data is seen at position (4) probably due to the small range of velocities at that position, while there is barely any scatter at position (2).

Figure 5.9 shows the variation of nozzle flow rate with pressure. The equation derived from basic inviscid theory relating pressure and flow rate for the Hago B-50 nozzle is [1],

$$Q = 4.09\sqrt{\Delta P} \tag{5.1}$$

where Q is in ml/min and P is in psi and the coefficient 4.09 in fitting from experimental data. Equation (1) is plotted in Figure 5.9 along with the pressure and flow rate data.

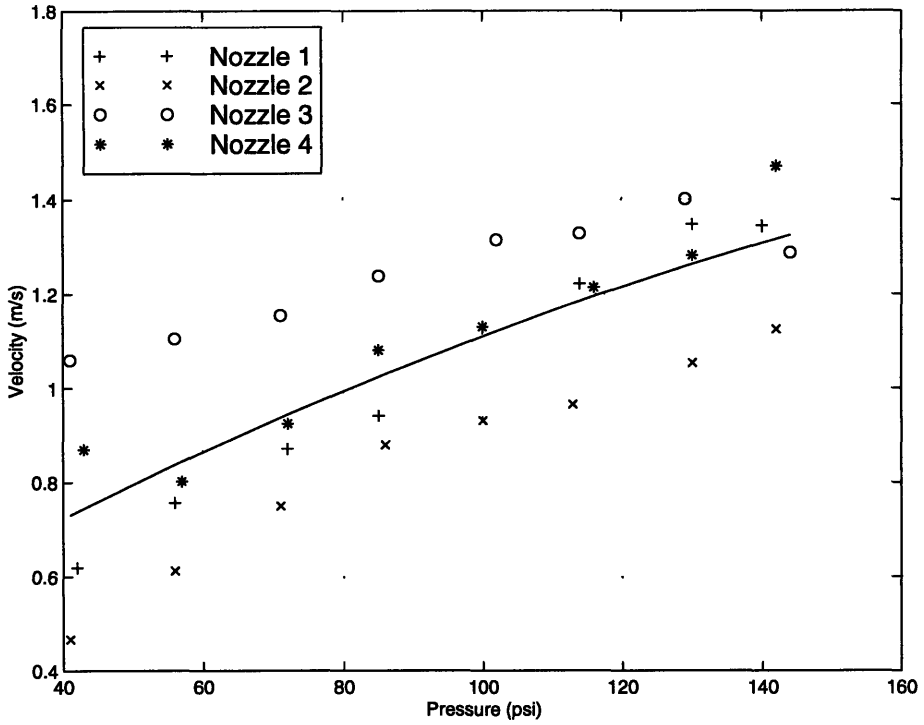

Figure 5.5: Hago B-50. Pressure vs. velocity at y = 0 and z = 10 cm in a bulk air flow.

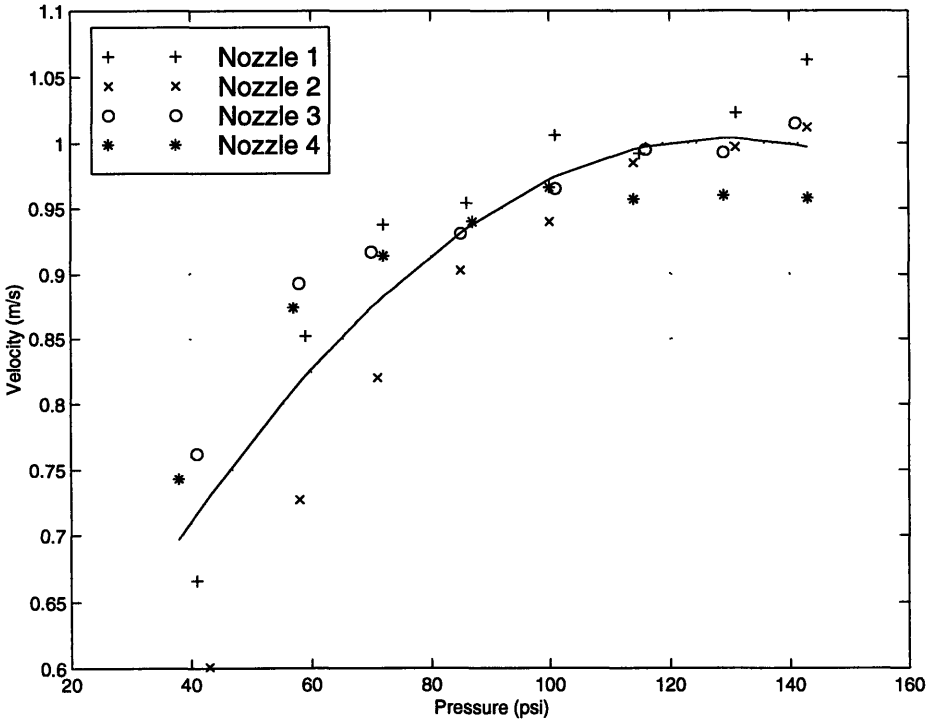

Figure 5.6: Hago B-50. Pressure vs. velocity at y = -15 and z = 15 cm in a bulk air flow.

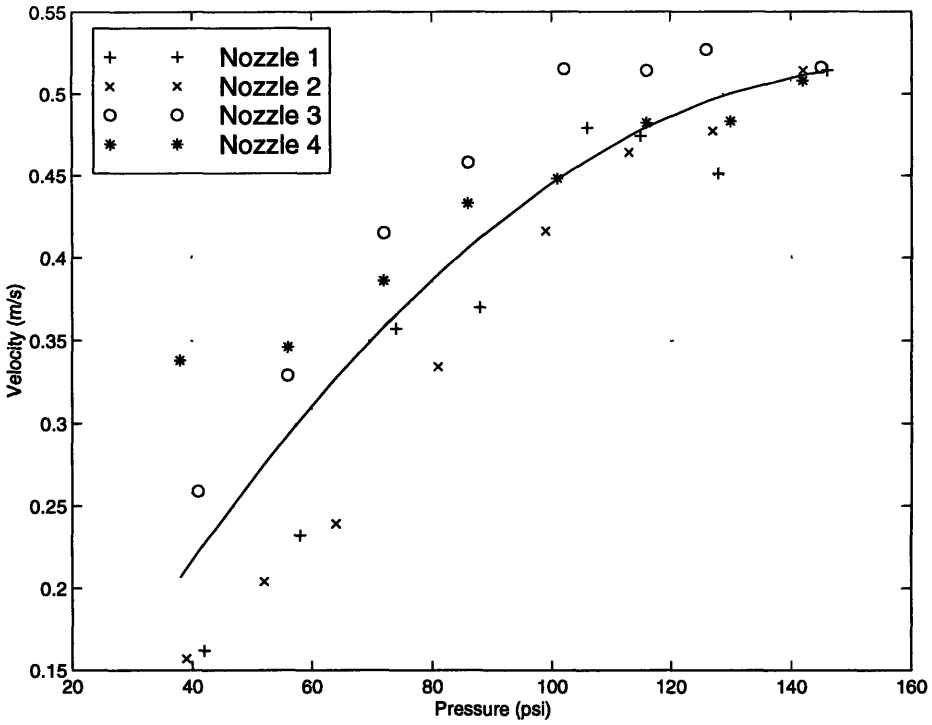

Figure 5.7: Hago B-50. Pressure vs. velocity at y = -30 and z = 20 cm in a bulk air flow.

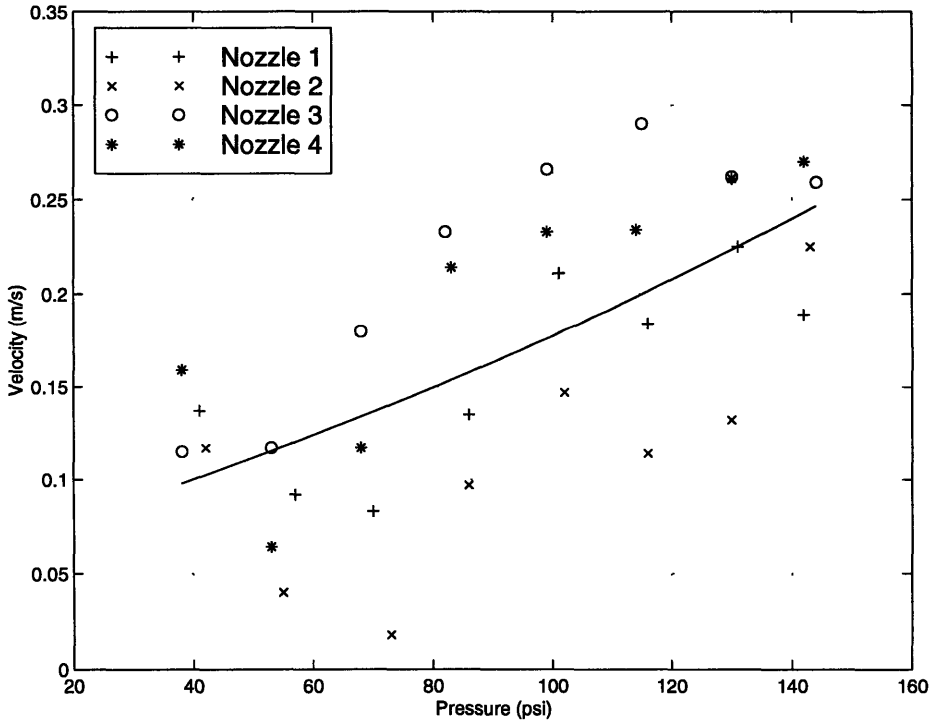

Figure 5.8: Hago B-50. Pressure vs. velocity at y = -30 and z = 25 cm in a bulk air flow.

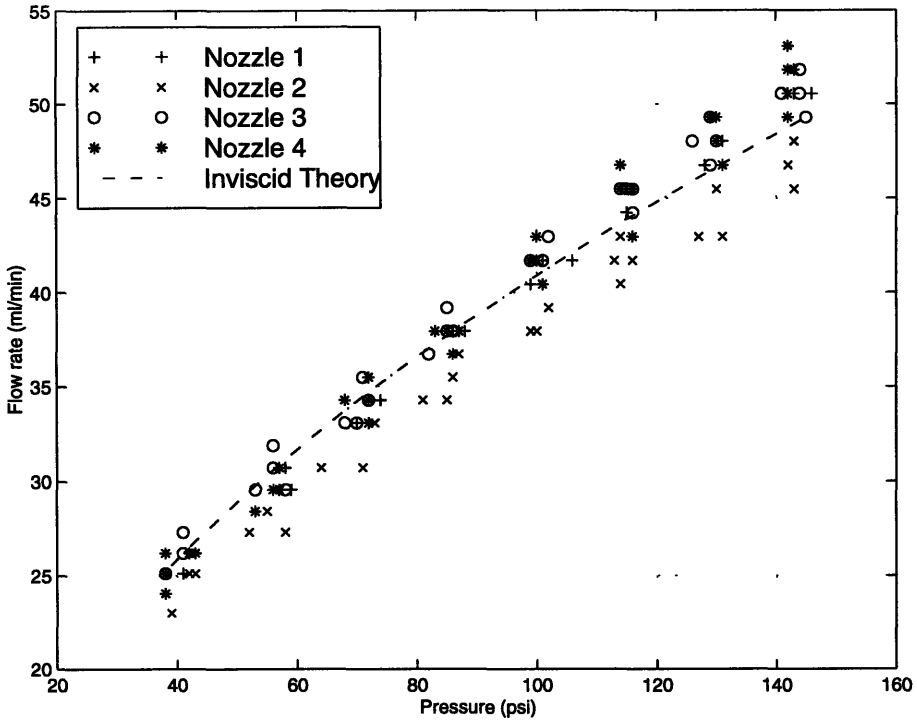

Figure 5.9: Hago B-50. Pressure vs. flow rate.

5.3 Droplet Validation Rate

Figures 5.10, 5.11, 5.12, and 5.13 show the variation of droplet validation rate with pressure for four B-50 nozzles in bulk air flow. For all four positions, the validation rates increase with increasing pressure as seen for the nozzles in still air. The increase in validation rate can be attributed to the production of a smaller SMD spray, yielding more droplets. The largest range in validation rate was seen in the positions closest to the nozzle. For positions (1) and (2), the validation rate increases approximately 200 validations/sec from 276 kPa (40 psi) to 1000 kPa (145 psi), while the increase for positions (3) and (4) was only 30 and 5 validations/sec, respectively. This indicates that at distances farther than 15 cm from the nozzle even an increase in operating pressure can not project the droplets farther into the bulk air column.

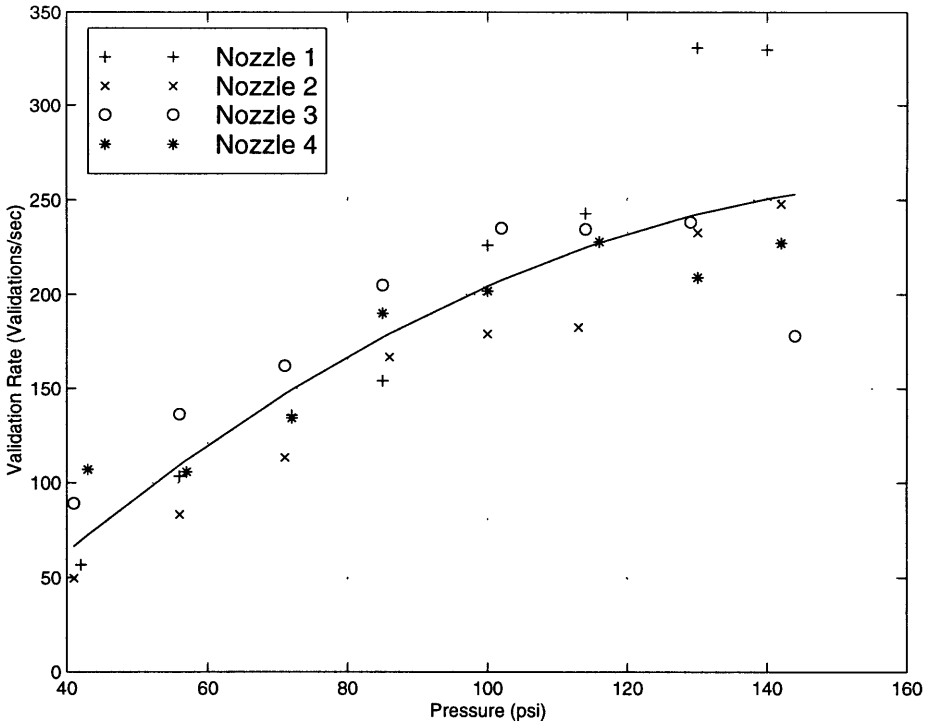

Figure 5.10: Hago B-50. Pressure vs. validation rate at y = 0 and z = 10 cm in a bulk air flow.

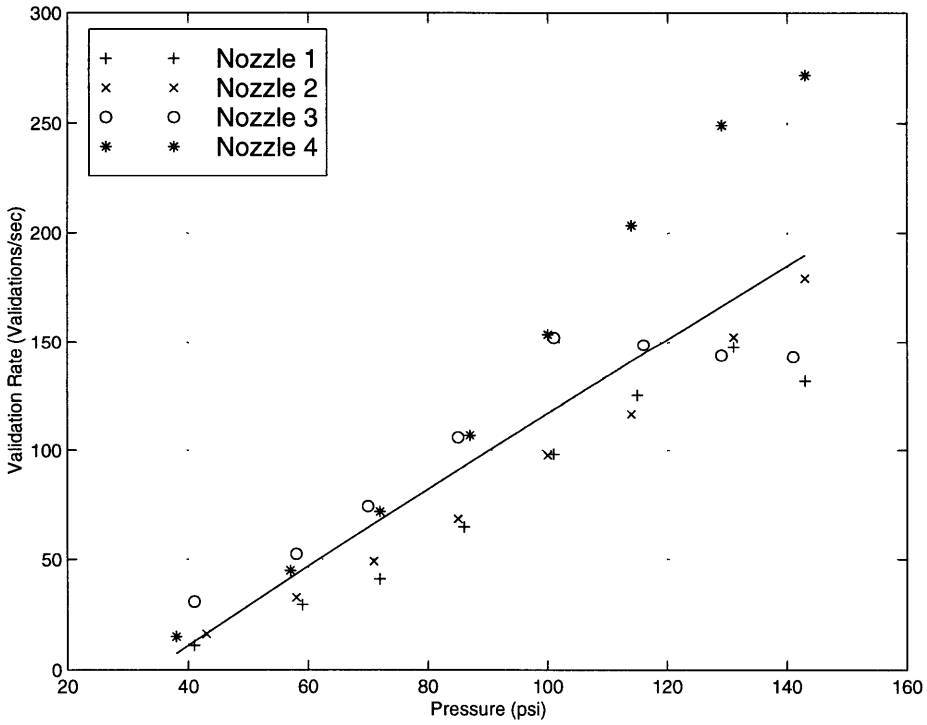

Figure 5.11: Hago B-50. Pressure vs. validation rate at y = -15 and z = 15 cm in a bulk air flow.

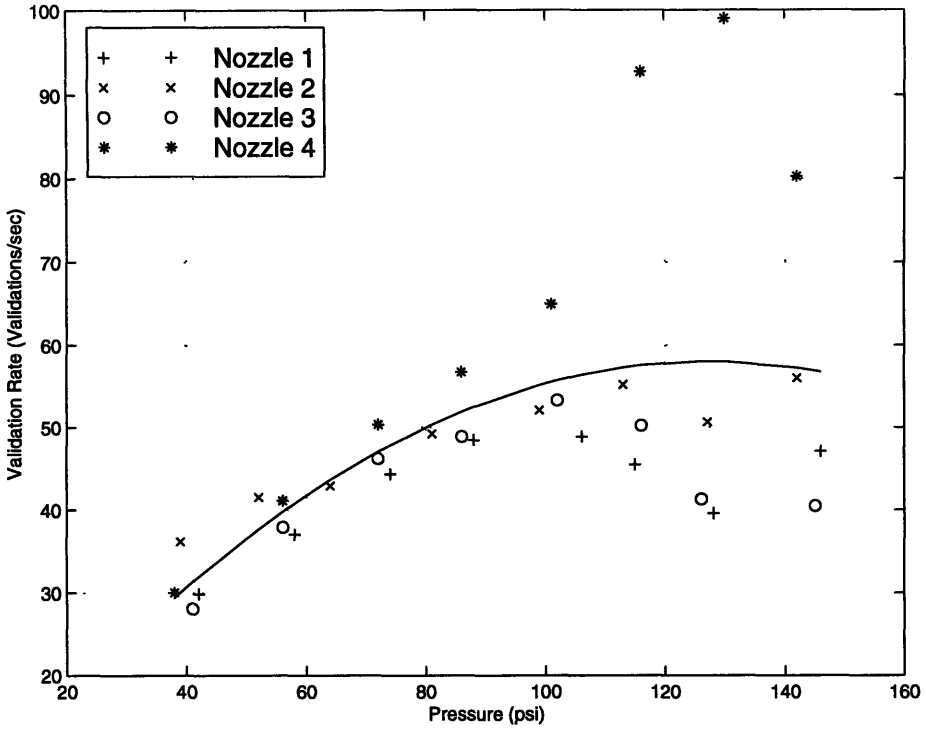

Figure 5.12: Hago B-50. Pressure vs. validation rate at y = -30 and z = 20 cm in a bulk air flow.

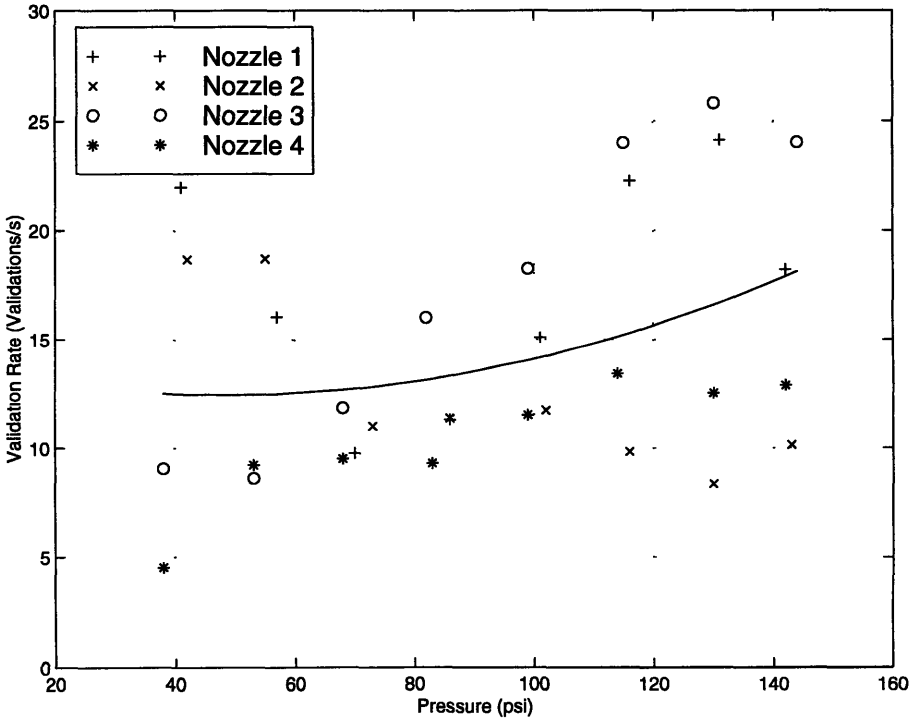

Figure 5.13: Hago B-50. Pressure vs. validation rate at y = -30 and z = 25 cm in a bulk air flow.

5.4 Summary

The following conclusions can be made about the spray structure of a Hago B-50 nozzle in bulk air flow.

1. The bulk air flow appears to reduce the variation of the SMD's between different nozzles relative to still air.
2. The greatest change in velocity with varying pressure is seen at the position closest to the nozzle. As distance from the nozzle increases, the range of velocity decreases.
3. The downward drag force of the air jet prevents the droplets from traveling far from the nozzle, even at elevated operating pressures.

Chapter 6

Effect of Aging on Spray Nozzles

This chapter describes the effect of aging on the Hago B-50 nozzles used in PPG Industries glass fiber production lines. As nozzles are aged, several regions of the nozzles become corroded. The areas that are affected by corrosion are the outer covering, the tangential slots, the orifice and the filter of the nozzle. The corrosion on the outside of the nozzle adapter is the most serious due to exposure to the environment. The effect of nozzle pressure variations on spray characteristics is examined for nozzles that are aged zero, two, four and six weeks.

6.1 Effect of Pressure Variations on Spray Characteristics of Aged Nozzles

The effect of pressure variations is examined for five B-50 nozzles aged two weeks, six nozzles aged four weeks and for six nozzles aged six weeks. The data for one two week nozzle could not be obtained because the nozzle orifice was completely blocked. The nozzle operating pressure is varied from 276 kPa (40 psi) to 1000 kPa (145 psi) at approximately 15 psi intervals. The measurements include the SMD, the velocity, the PDPA validation rate and the flow rate at three different positions in the spray cone. The positions are along the centerline (y = 0) of the nozzle and distances of z = 5 cm and z = 20 cm away from the nozzle and in the nozzle rain-out region (z = 20 cm away from the nozzle and y = –20 cm (below) the nozzle centerline). This data is compared to the results for clean nozzles previously described by Sweetland [1].

6.1.1 Droplet Diameter

Figures 6.1 through 6.4 show the variation of droplet SMD with pressure along the nozzle centerline 5 cm away from the outlet for the B-50 nozzles aged zero, two, four and six weeks, respectively. The aged nozzles' quality of atomization is much less than that of the clean nozzles'. The aged nozzles produce larger and fewer droplets. The average SMD range for the clean nozzles is 15 μm to 30 μm, while for the 2 week aged nozzles this range is 30 μm to 80 μm and for both the four and six week aged nozzles this range is 20 μm to 50 μm. There is much more scatter in data for the aged nozzles than for the clean nozzles. Both the clean nozzles and all the aged nozzles exhibit a decrease in SMD with increasing pressure, the largest decrease occurring between 276 kPa (40 psi) and 690 kPa (100 psi). This shows that operating above a pressure of 690 kPa (100 psi) does not improve atomization in nozzles aged up to six weeks.

Figures 6.5 through 6.8 show the variation of droplet SMD with pressure along the nozzle centerline 20 cm away, for the B-50 nozzles aged zero, two, four and six weeks, respectively. The SMD's of the aged nozzles fall in the range of 40 μm to 70 μm while the clean nozzles SMD's are in the smaller range of 25 μm to 35 μm. All nozzles exhibit decreasing SMD with increasing pressure. After a pressure of 690 kPa (100 psi) the SMD is constant for both clean and aged nozzles.

Figures 6.9 through 6.12 show the variation of droplet SMD with pressure in the rain out region of the spray, for the B-50 nozzles aged zero, two, four and six weeks, respectively. These plots reveal much more scatter in the aged nozzles than seen in the clean nozzles. The SMD's of the aged nozzles fall in the range of 70 μm to 90 μm while the clean nozzles SMD's are in the smaller range of 60 μm to 80 μm. Again, there is a decrease in SMD with increasing pressure for all nozzles.

Three conclusions are reached from the above analysis. Aging of nozzles causes the quality of atomization to decrease, thus producing larger sized droplets. Also, a nozzle operating pressure of 690 kPa (100 psi) is sufficient to produce optimal atomization for both clean and aged nozzles. Lastly, aging causes more variation in the SMD data among the nozzles.

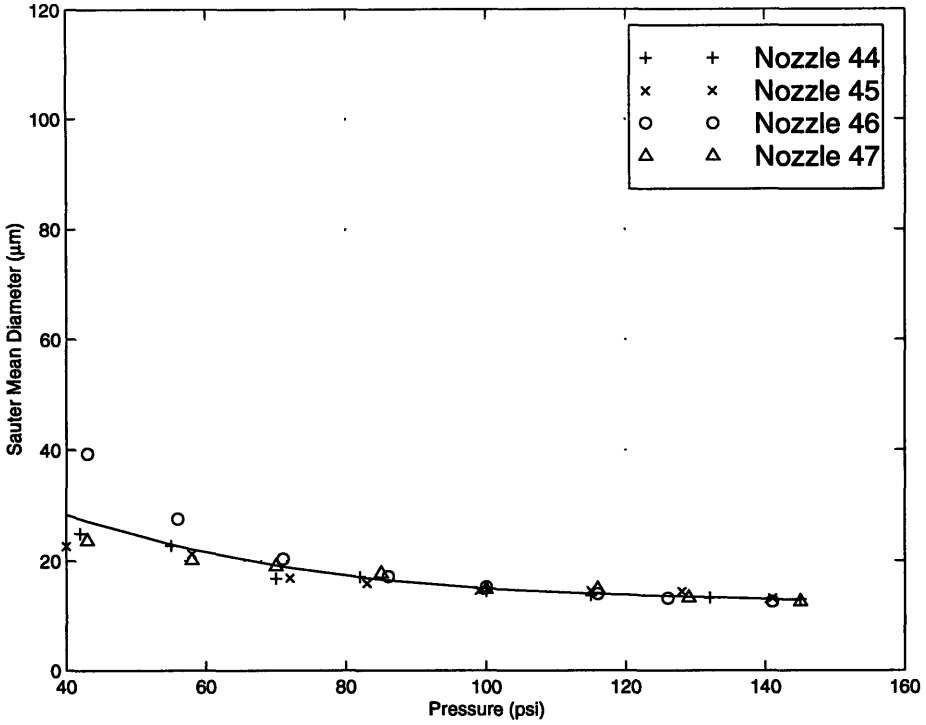

Figure 6.1: Hago B-50 clean nozzle. Pressure vs. SMD at y = 0 and z = 5 cm.

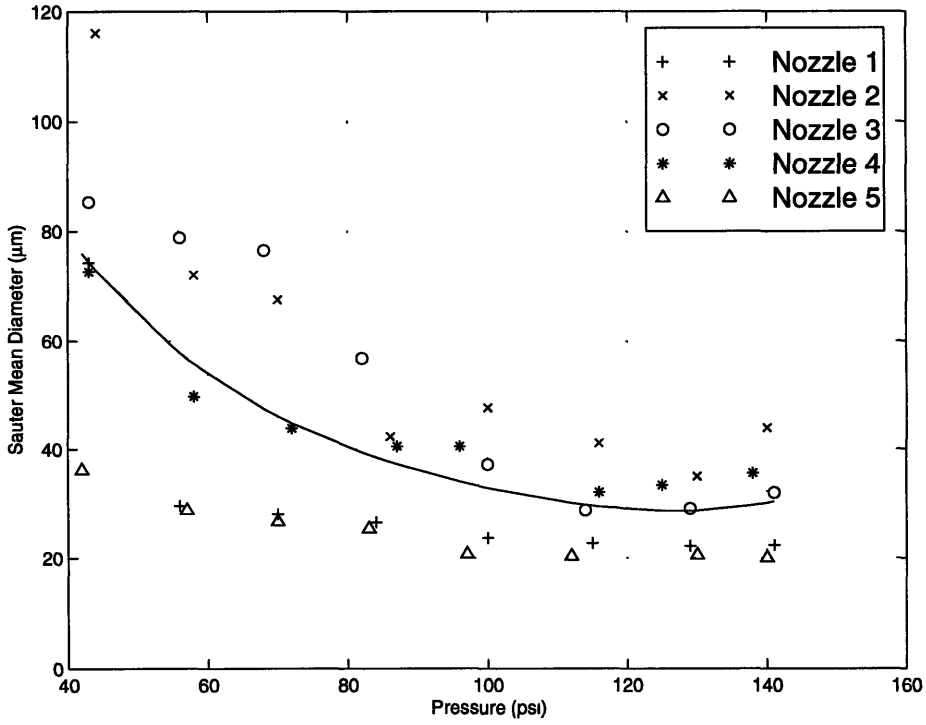

Figure 6.2: Hago B-50 aged 2 weeks. Pressure vs. SMD at y = 0 and z = 5 cm.

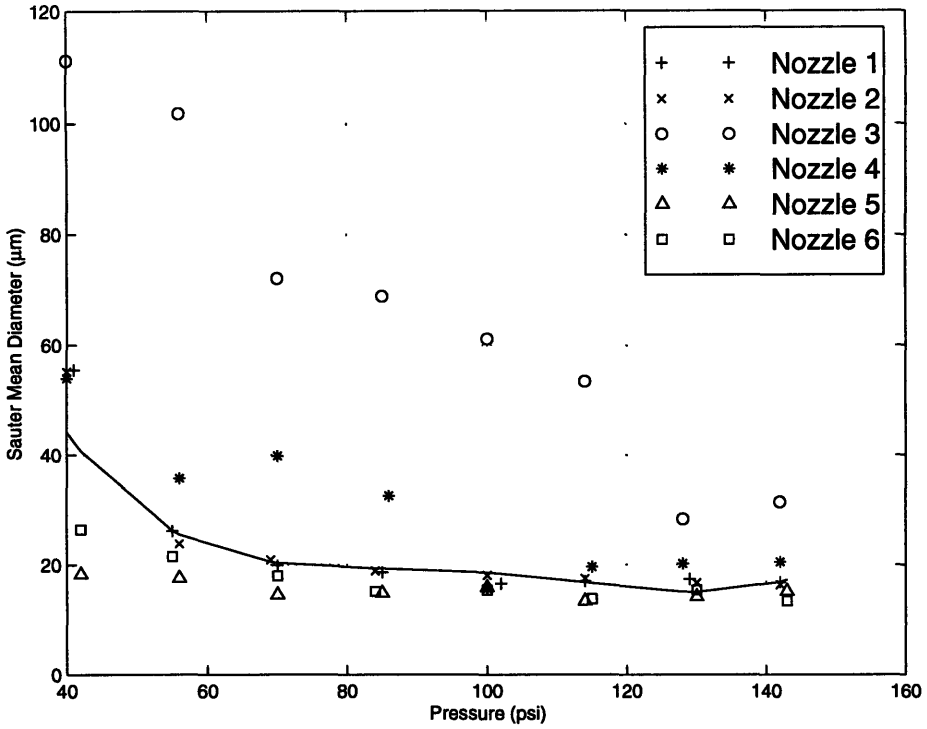

Figure 6.3: Hago B-50 aged 4 weeks. Pressure vs. SMD at y = 0 and z = 5 cm.

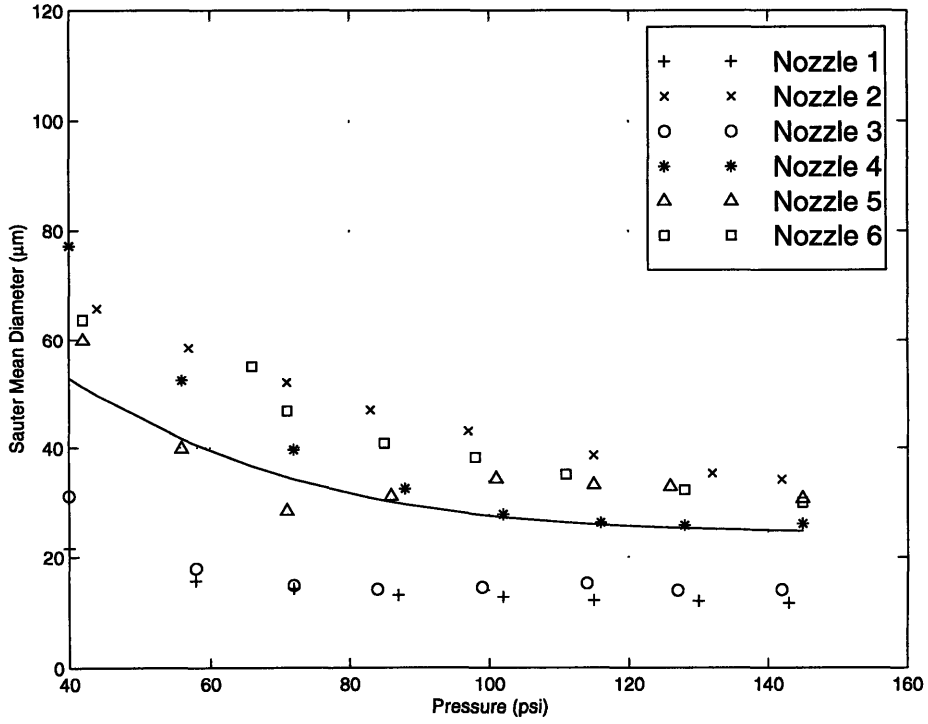

Figure 6.4: Hago B-50 aged 6 weeks. Pressure vs. SMD at y = 0 and z = 5 cm.

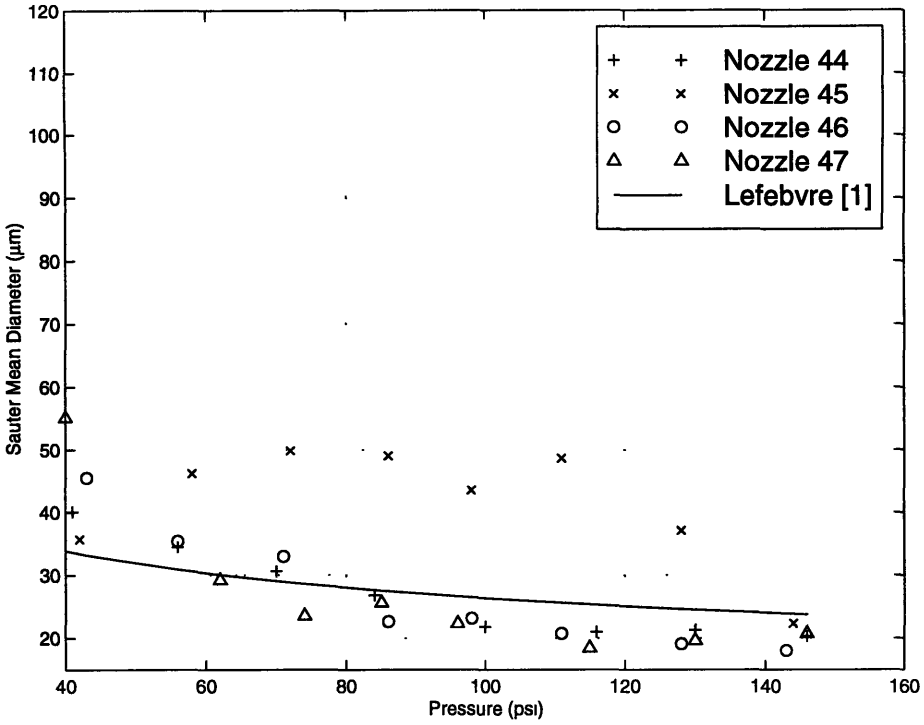

Figure 6.5: Hago B-50 clean nozzle. Pressure vs. SMD at y = 0 and z = 20 cm.

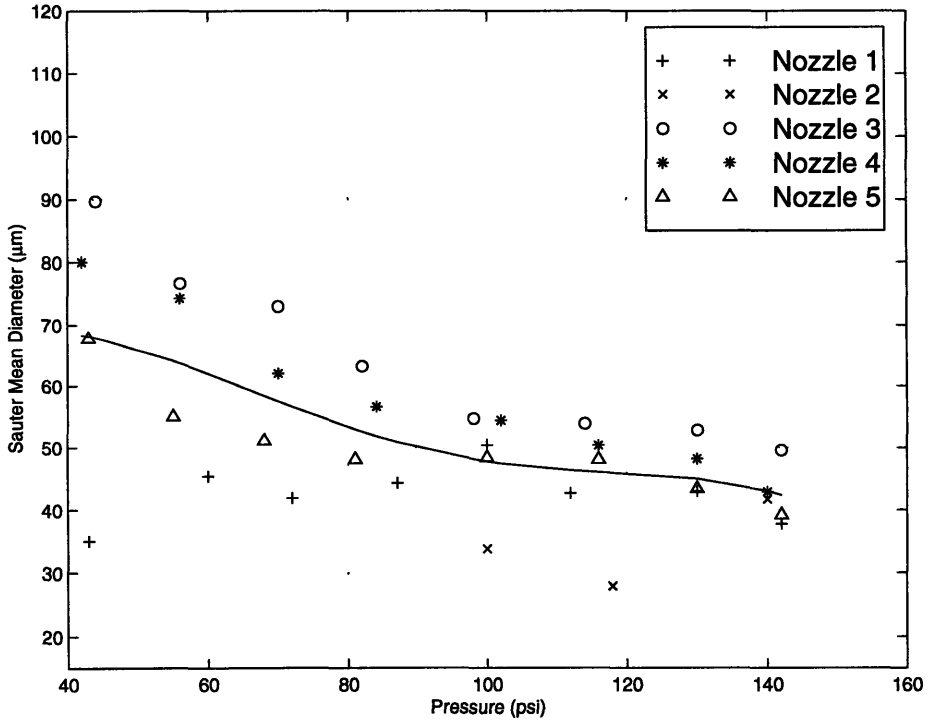

Figure 6.6: Hago B-50 Aged 2 weeks. Pressure vs. SMD at y = 0 and z = 20 cm.

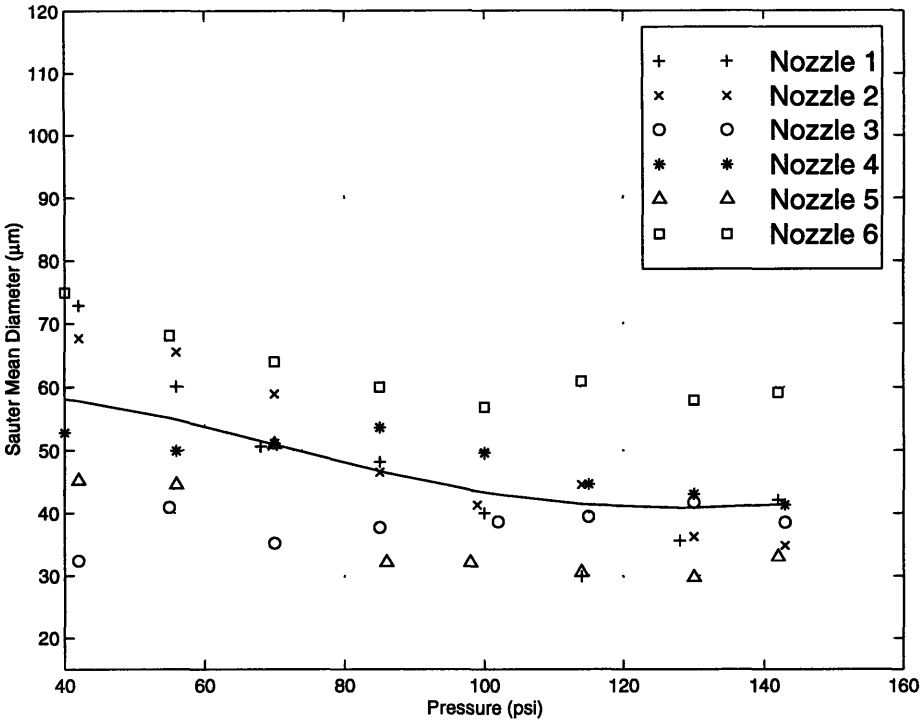

Figure 6.7: Hago B-50 Aged 4 weeks. Pressure vs. SMD at y = 0 and z = 20 cm.

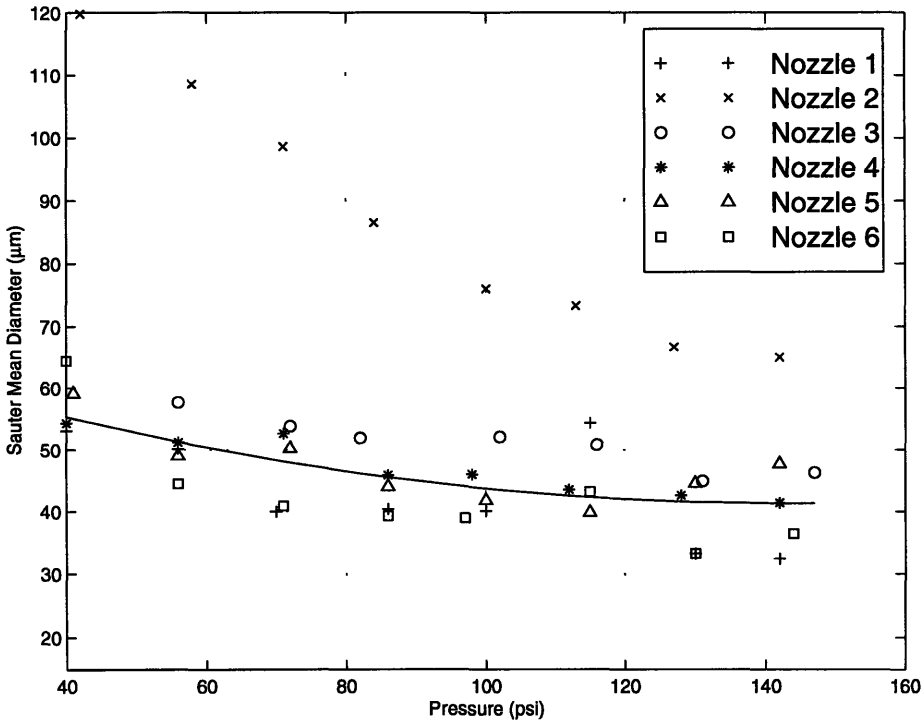

Figure 6.8: Hago B-50 Aged 6 weeks. Pressure vs. SMD at y = 0 and z = 20 cm.

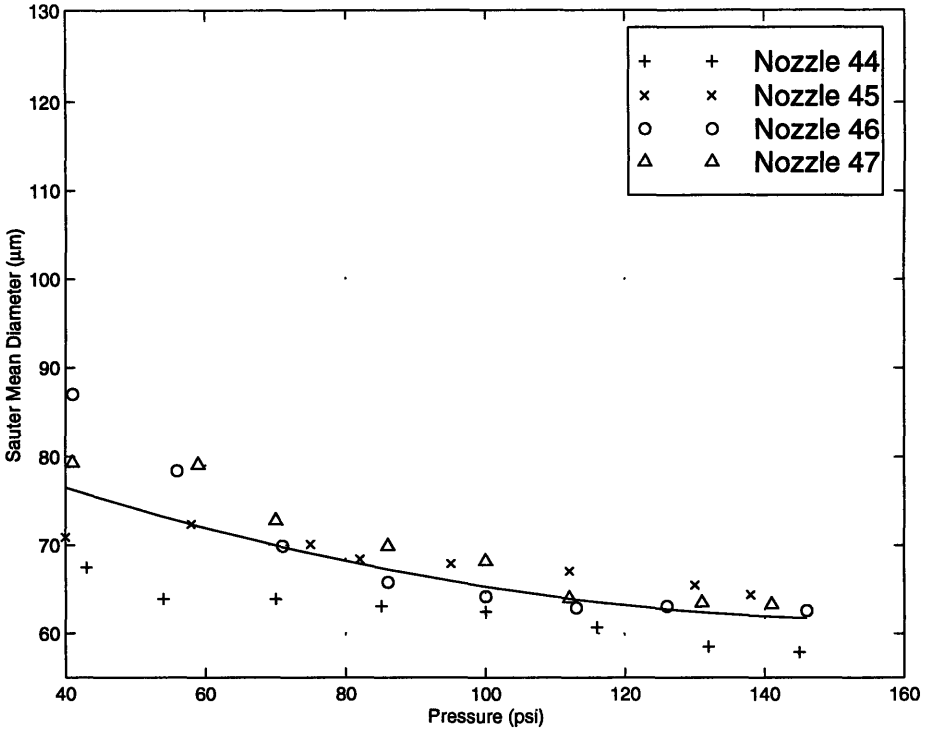

Figure 6.9: Hago B-50 clean nozzle. Pressure vs. SMD at y = -20 and z = 20 cm.

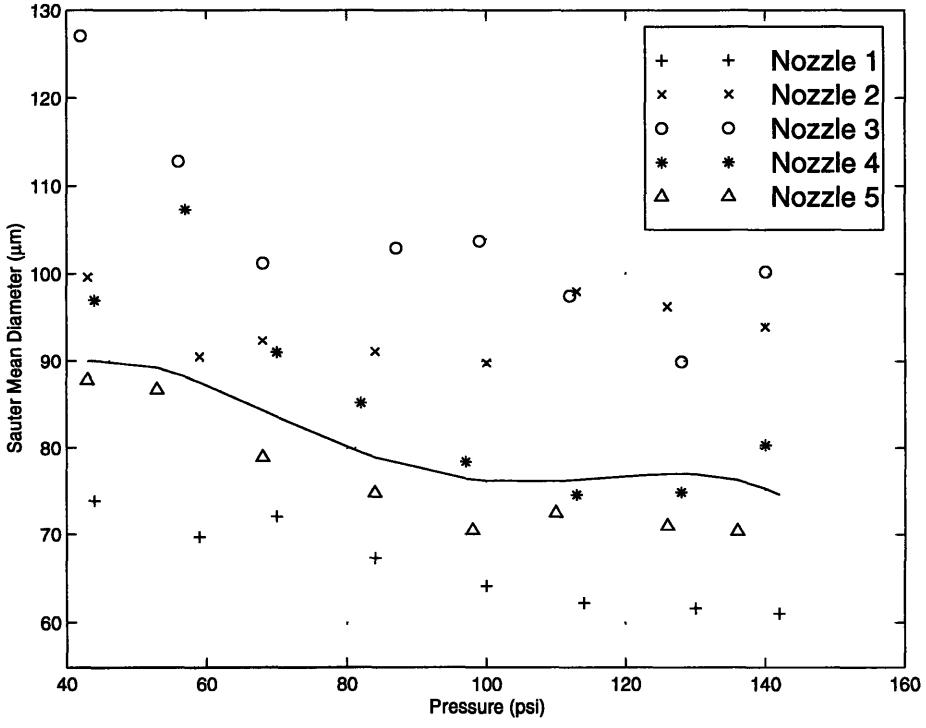

Figure 6.10: Hago B-50 aged 2 weeks. Pressure vs. SMD at y = -20 and z = 20 cm.

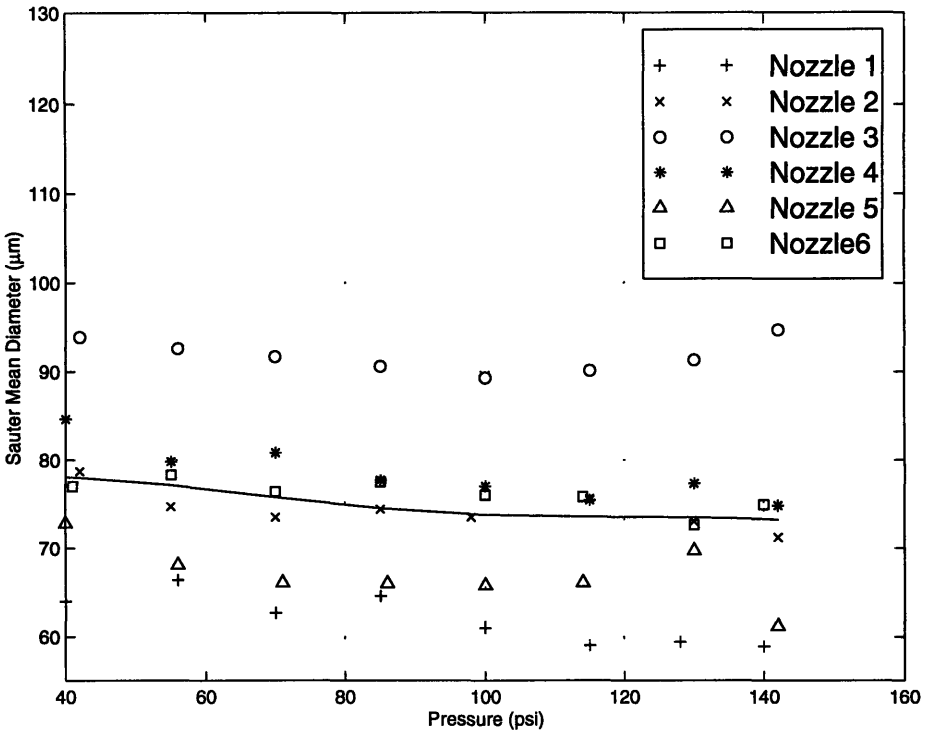

Figure 6.11: Hago B-50 aged 4 weeks. Pressure vs. SMD at y = -20 and z = 20 cm.

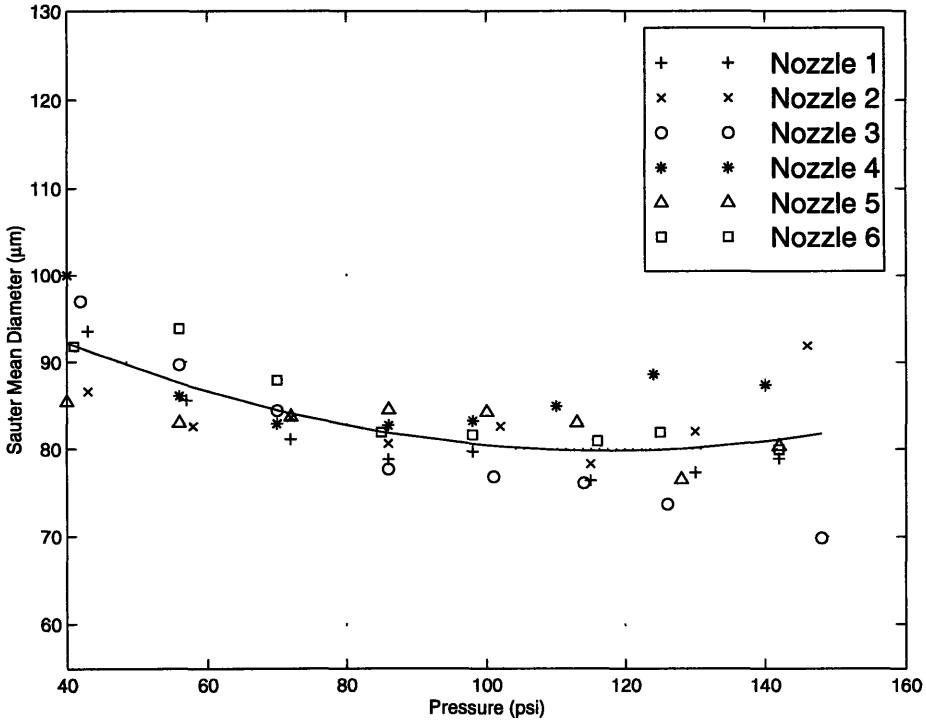

Figure 6.12: Hago B-50 aged 6 weeks. Pressure vs. SMD at y = -20 and z = 20 cm.

6.1.2 Droplet Velocity

Figures 6.13 through 6.16 show the variation of droplet velocity with pressure along the nozzle centerline 5 cm away, for the B-50 nozzles aged zero, two, four and six weeks, respectively. The aged nozzles display more scatter in velocity data than the clean nozzle. All nozzles show an increase in velocity with increasing pressure. After six weeks the increase in velocity with varying pressure is much less than that for the newer nozzles. The six week aged nozzles increase on average 0.8 m/s from 276 kPa (40 psi) to 1000 kPa (145 psi) while all other nozzles increase at least 1.5 m/s for the same pressure range.

Figures 6.17 through 6.20 show the variation of droplet velocity with pressure along the nozzle centerline 20 cm away, for the B-50 nozzles aged zero, two, four and six weeks, respectively. As pressure increases the velocity increases for both aged and clean nozzles. The velocity curve fits shift downward to lower values of velocity as the nozzles are aged. There is much more scatter in the six week data than in the other nozzles.

Figures 6.21 through 6.24 show the variation of droplet velocity with pressure in the rain out region of the spray, for the B-50 nozzles aged zero, two, four and six weeks, respectively. The plots for the clean nozzles and the two week aged nozzles reveal a steady velocity with increasing pressure, that decreases slightly after a pressure of 690 kPa (100 psi) is reached. In contrast, the curve fits for the four and six week nozzles show steadily decreasing velocity with pressure and more scatter than for the cleaner nozzles. While, the plots for the clean and two week aged nozzles display only positive velocities, negative velocities are seen for the older nozzles. These negative velocities are due to increased recirculation in the rain out region of the older nozzles.

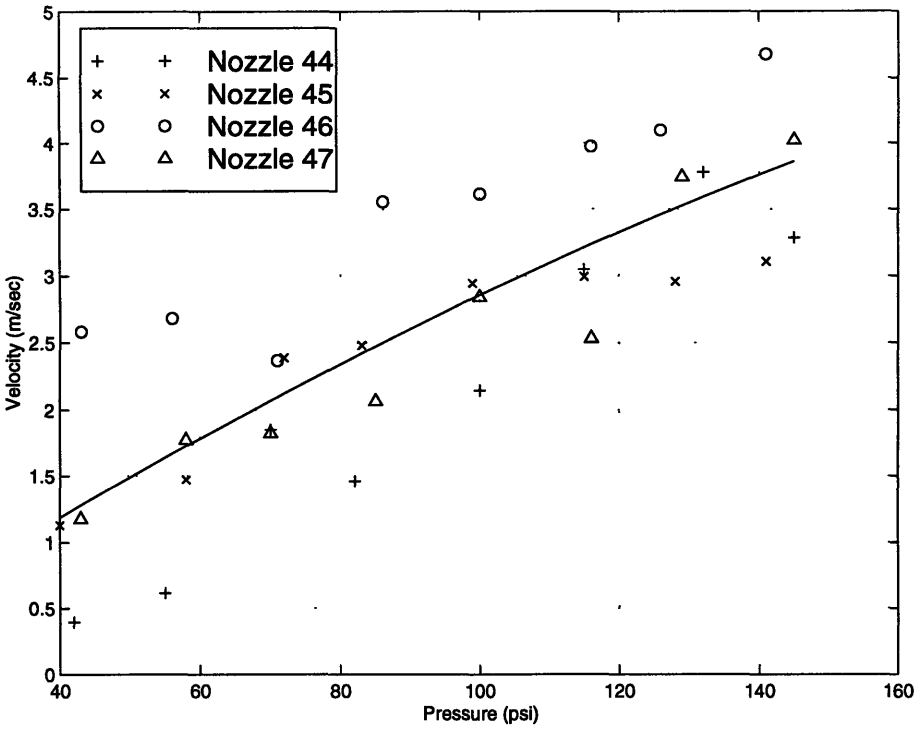

Figure 6.13: Hago B-50 clean nozzle. Pressure vs. velocity at y = 0 and z = 5 cm.

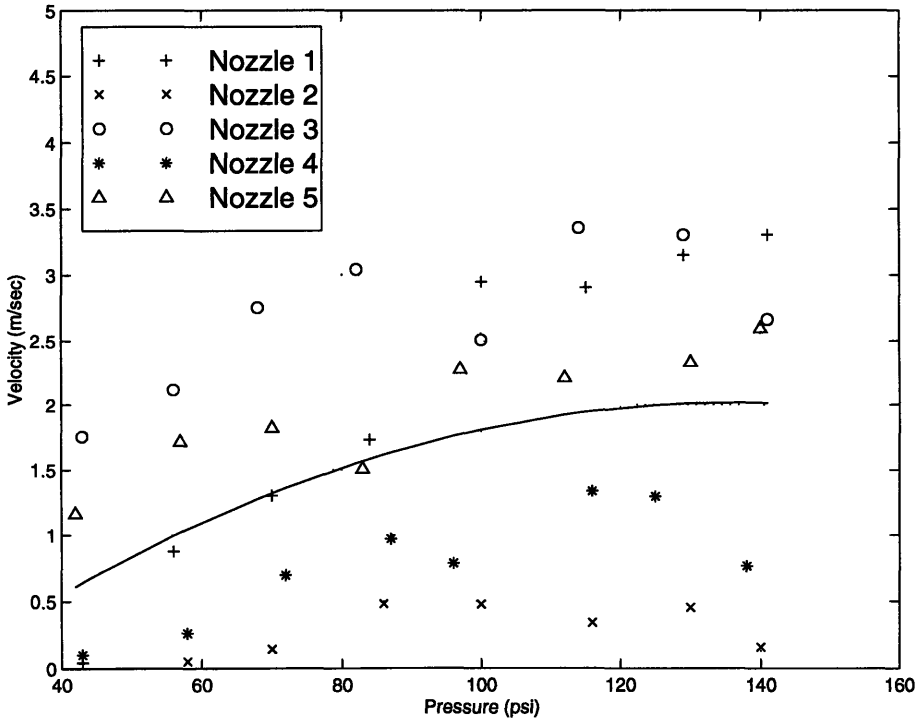

Figure 6.14: Hago B-50 aged 2 weeks. Pressure vs. velocity at y = 0 and z = 5 cm.

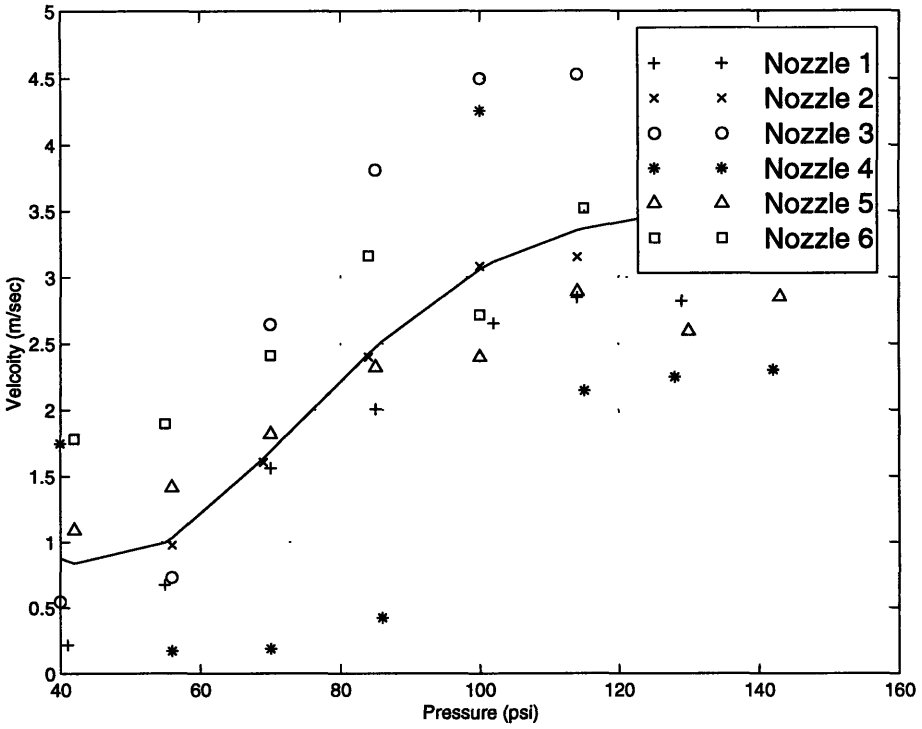

Figure 6.15: Hago B-50 aged 4 weeks. Pressure vs. velocity at y = 0 and z = 5 cm.

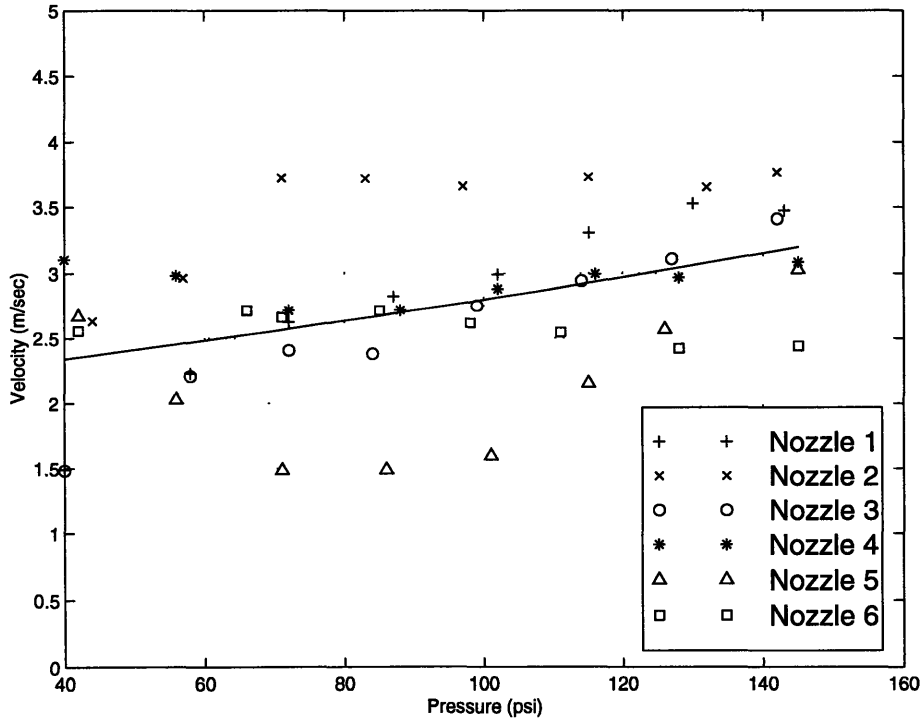

Figure 6.16: Hago B-50 aged 6 weeks. Pressure vs. velocity at y = 0 and z = 5 cm.

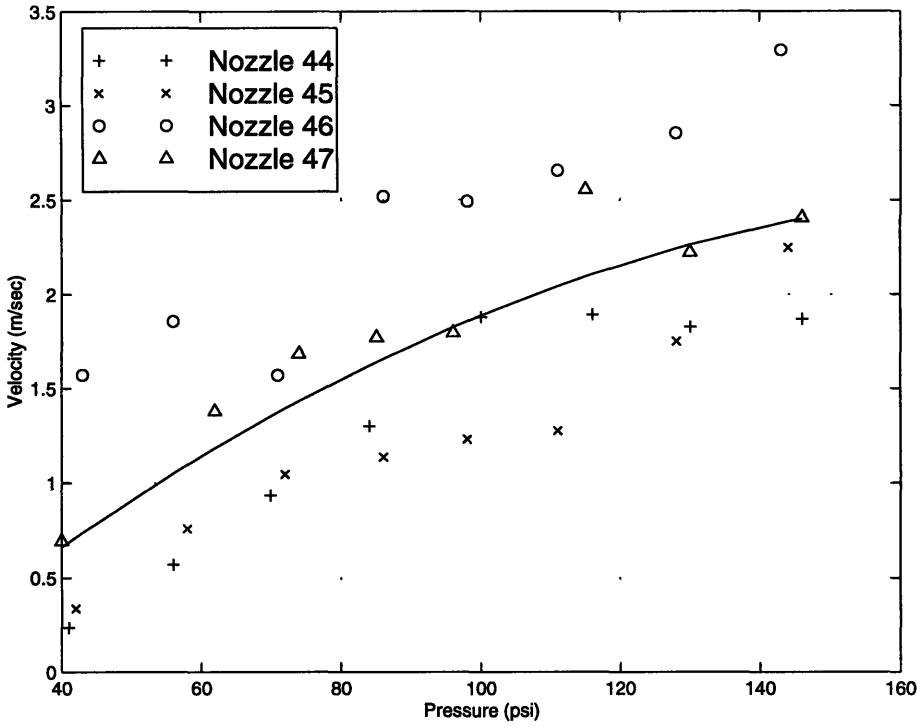

Figure 6.17: Hago B-50 clean nozzle. Pressure vs. velocity at y = 0 and z = 20 cm.

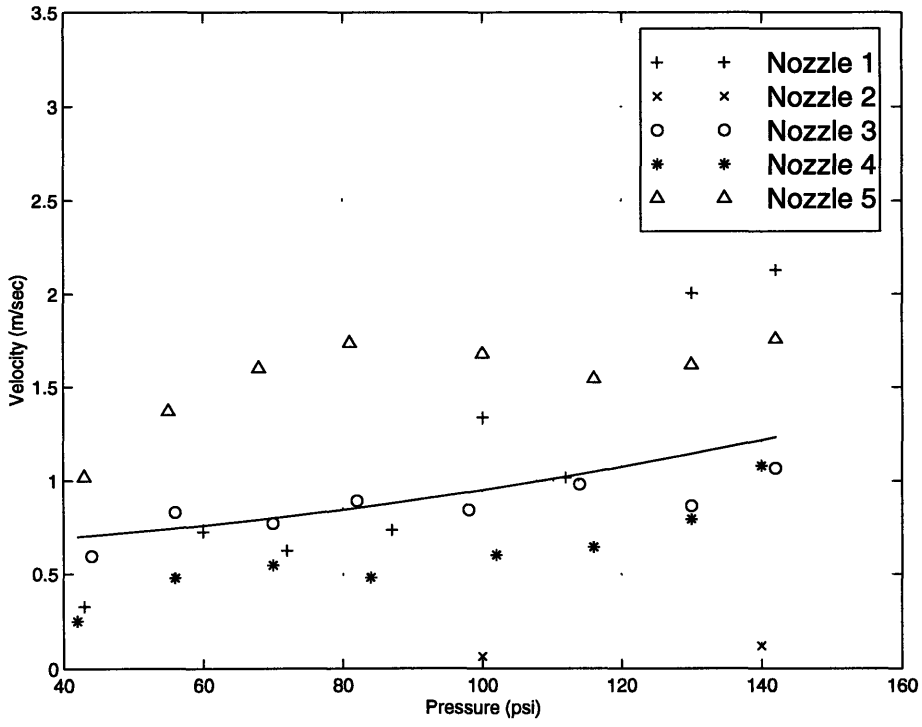

Figure 6.18: Hago B-50 aged 2 weeks. Pressure vs. velocity at y = 0 and z = 20 cm.

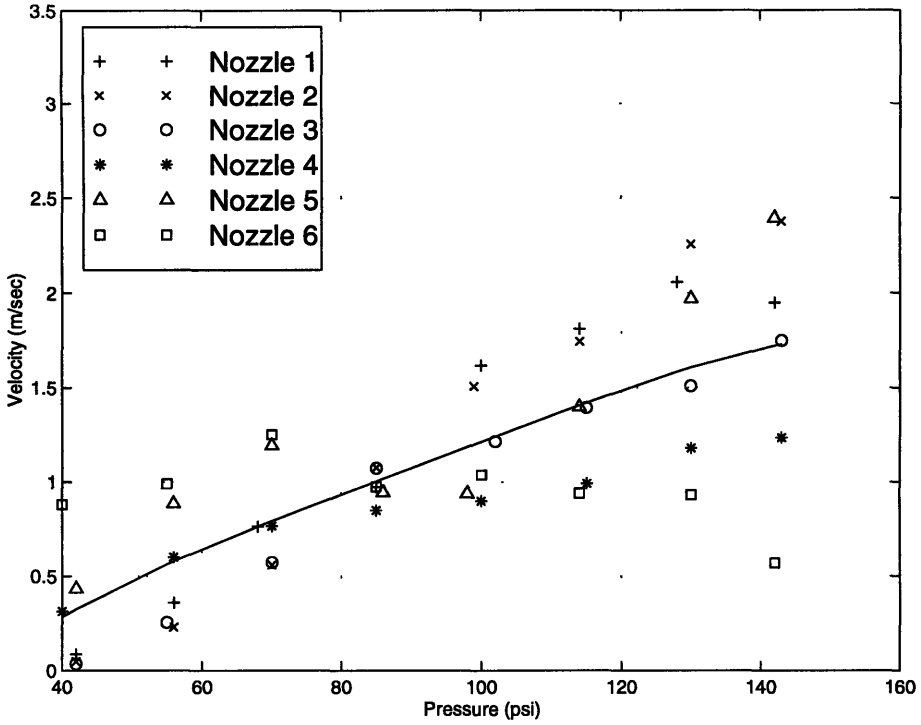

Figure 6.19: Hago B-50 aged 4 weeks. Pressure vs. velocity at y = 0 and z = 20 cm.

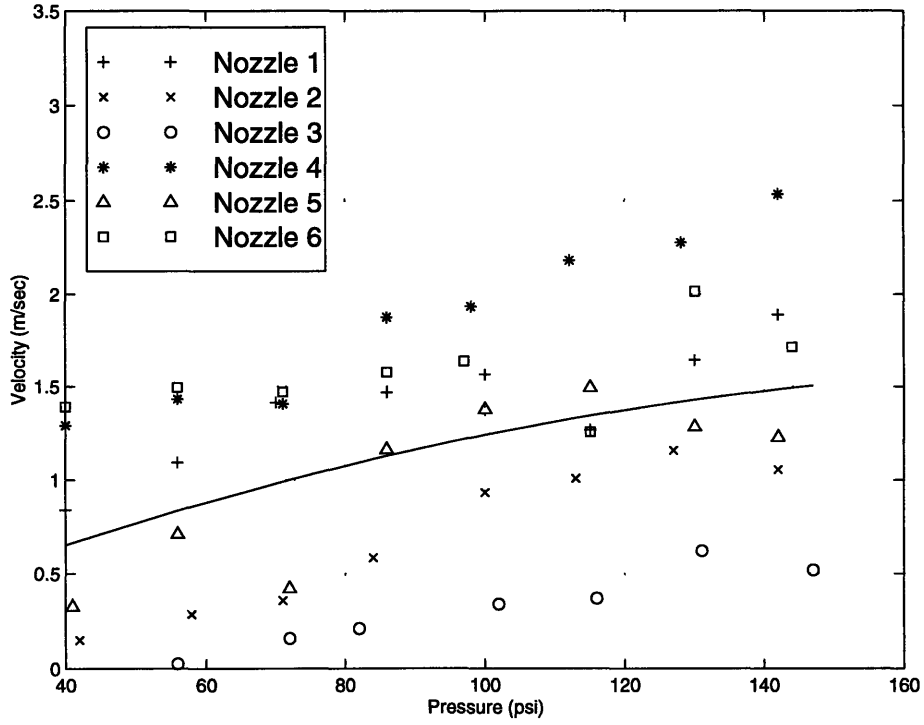

Figure 6.20: Hago B-50 aged 6 weeks. Pressure vs. velocity at y = 0 and z = 20 cm.

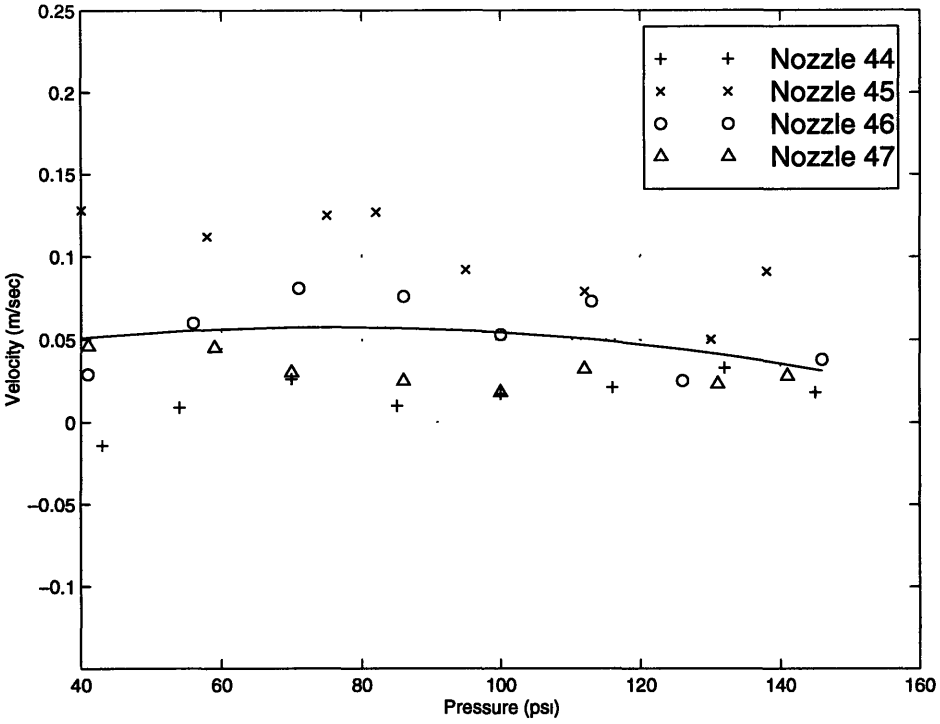

Figure 6.21: Hago B-50 clean nozzle. Pressure vs. velocity at y = -20 and z = 20 cm.

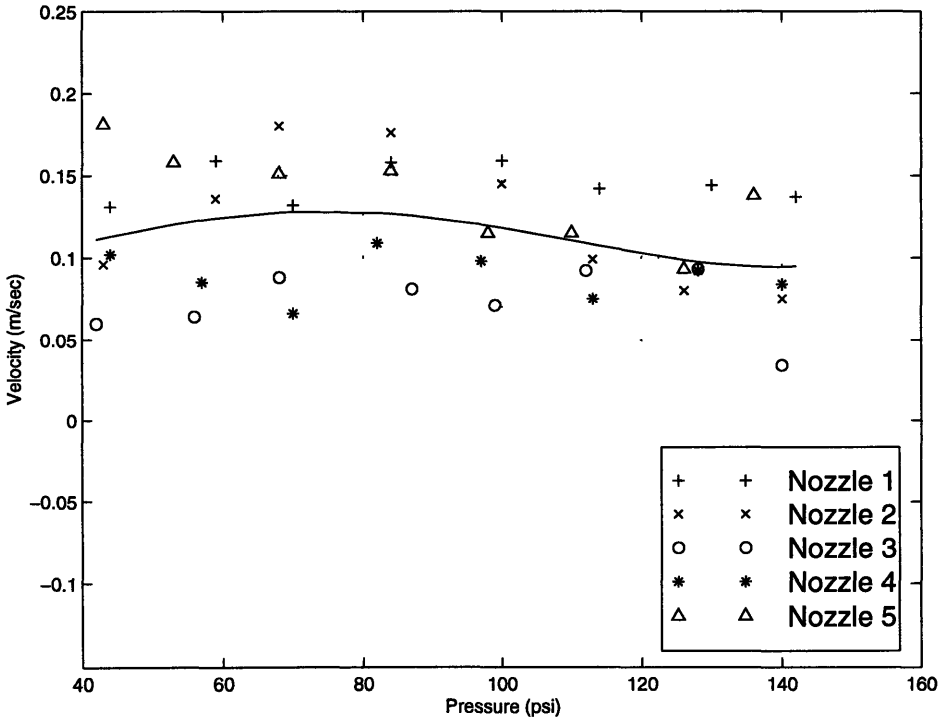

Figure 6.22: Hago B-50 aged 2 weeks. Pressure vs. velocity at y = -20 and z = 20 cm.

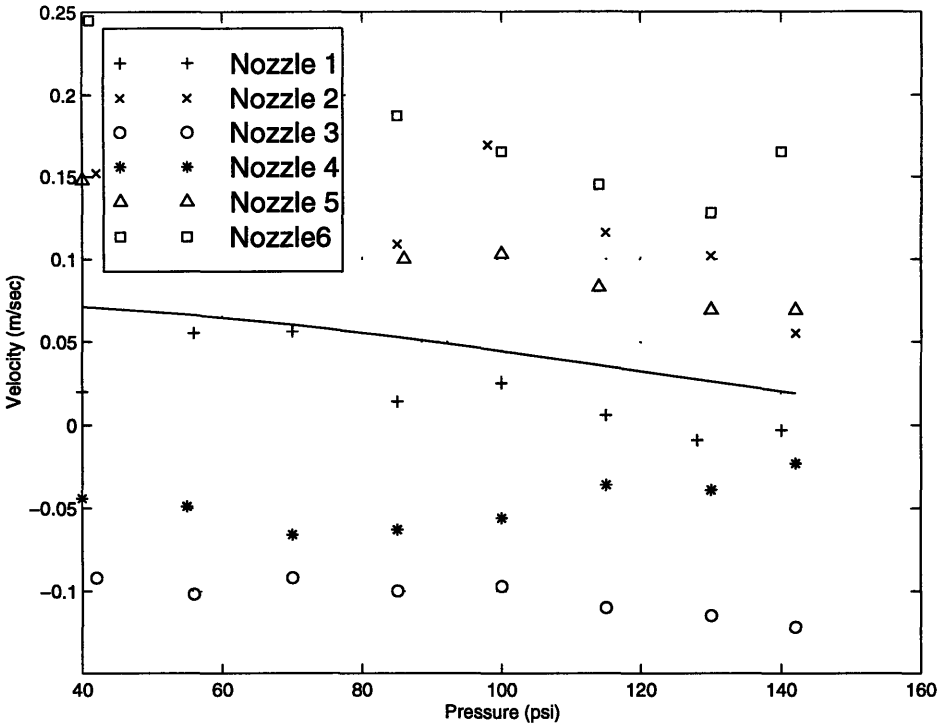

Figure 6.23: Hago B-50 aged 4 weeks. Pressure vs. velocity at y = -20 and z = 20 cm.

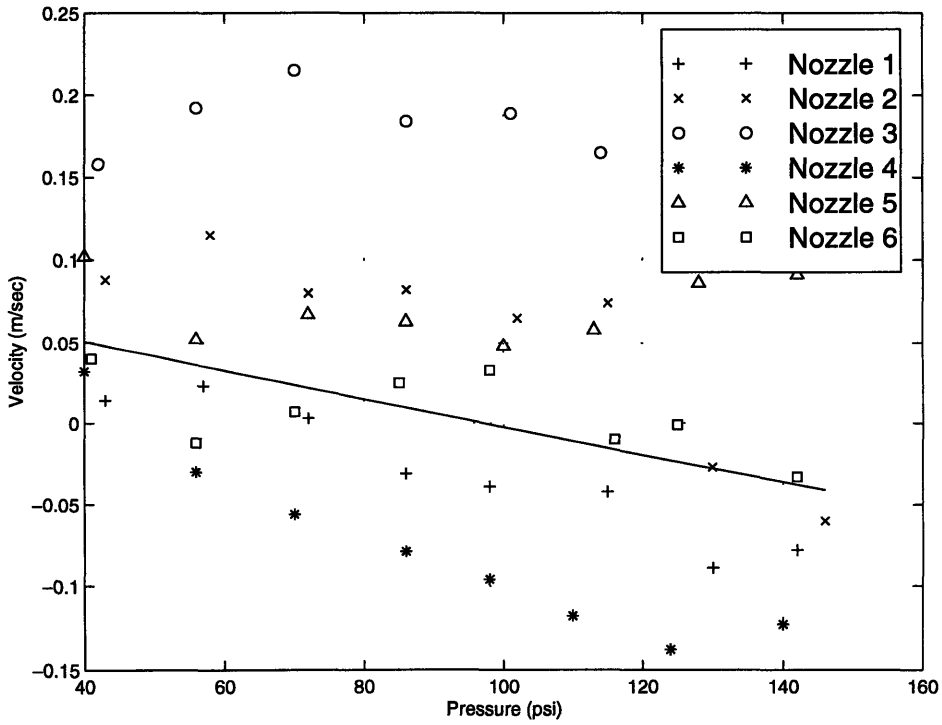

Figure 6.24: Hago B-50 aged 6 weeks. Pressure vs. velocity at y = -20 and z = 20 cm.

6.1.3 Droplet Validation Rate

As droplets pass through the measuring point of the PDPA, it produces an optical signal related to drop size and velocity. If the optical signal is within the proper specifications of velocity and diameter, the result is termed a validation. The droplet validation rate (number/sec) can be used as an indicator of the droplet flux through a region.

Figures 6.25 through 6.28 show the variation of droplet validation rate with pressure along the nozzle centerline 5 cm away, for the B-50 nozzles aged zero, two, four and six weeks, respectively. Figures 6.29 through 6.32 show the variation of droplet validation rate with pressure along the nozzle centerline 20 cm away, for the B-50 nozzles aged zero, two, four and six weeks, respectively. The plots along the centerline of the nozzle show the same general trend as the nozzles are aged. All nozzle plots show continuously increasing validation rates with increasing nozzle operating pressure. However, the increase in validation rate with increasing pressure for the clean and two week aged nozzles is much greater than for the four and six week aged nozzles. The maximum validation rates decrease as the nozzles are further aged. The validation rate data becomes more scattered as the nozzles are aged.

While the centerline plots displayed similar results, the data in the rain out region of the spray showed a very different pattern. Figures 6.33 through 6.36 show the variation of droplet validation rate with pressure in the rain out region of the spray, for the B-50 nozzles aged zero, two, four and six weeks, respectively. For both clean and aged nozzles there is significant scatter in the validation rate data among nozzles. The droplet validation rate is barely sensitive to pressure, in all cases it increases slightly until a pressure of 690 kPa (100 psi) where it either becomes constant or decreases.

At all three positions, validation rate decreases as the nozzles are further aged. This result is in agreement with the observation that larger droplets are formed as the nozzles are further aged. Thus aging of nozzles causes fewer and bigger droplets yielding inferior atomization.

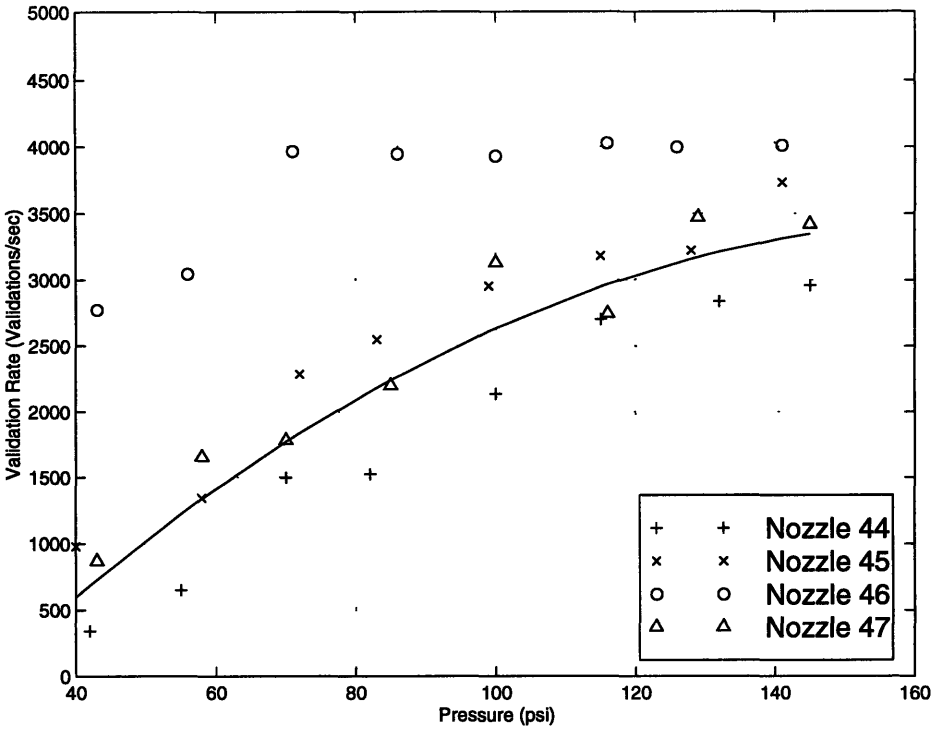

Figure 6.25: Hago B-50 clean nozzle. Pressure vs. validation rate at y = 0 and z = 5 cm.

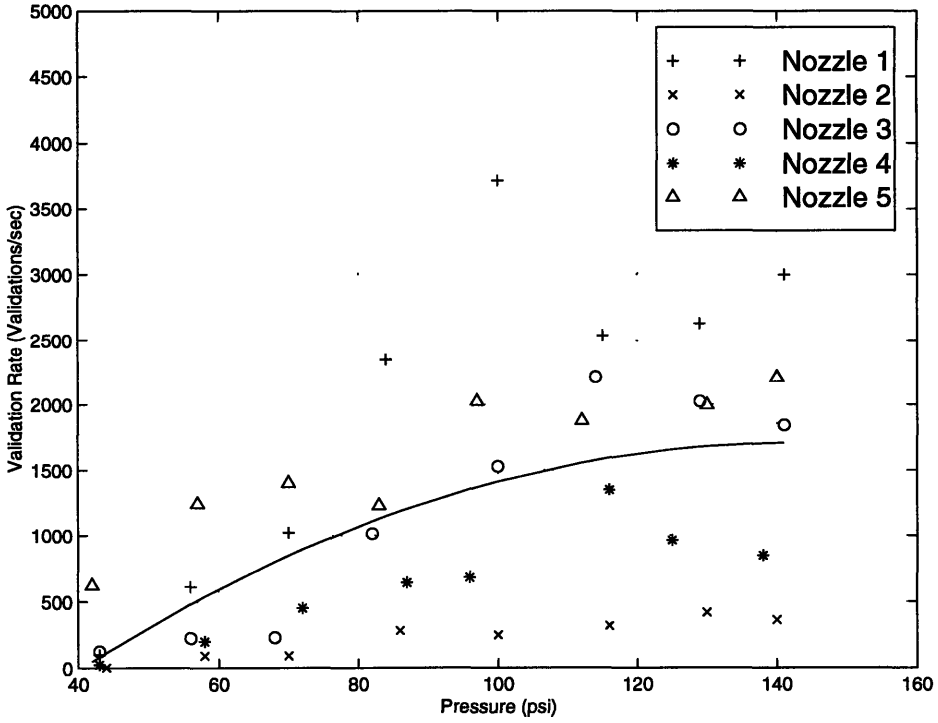

Figure 6.26: Hago B-50 aged 2 weeks. Pressure vs. validation rate at y = 0 and z = 5 cm.

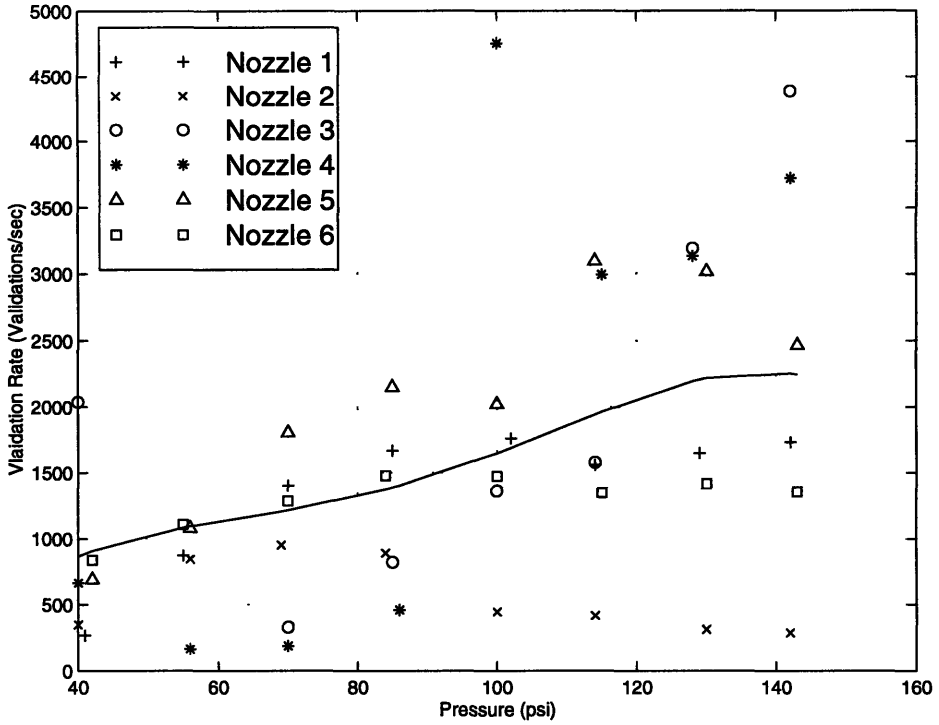

Figure 6.27: Hago B-50 aged 4 weeks. Pressure vs. validation rate at y = 0 and z = 5 cm.

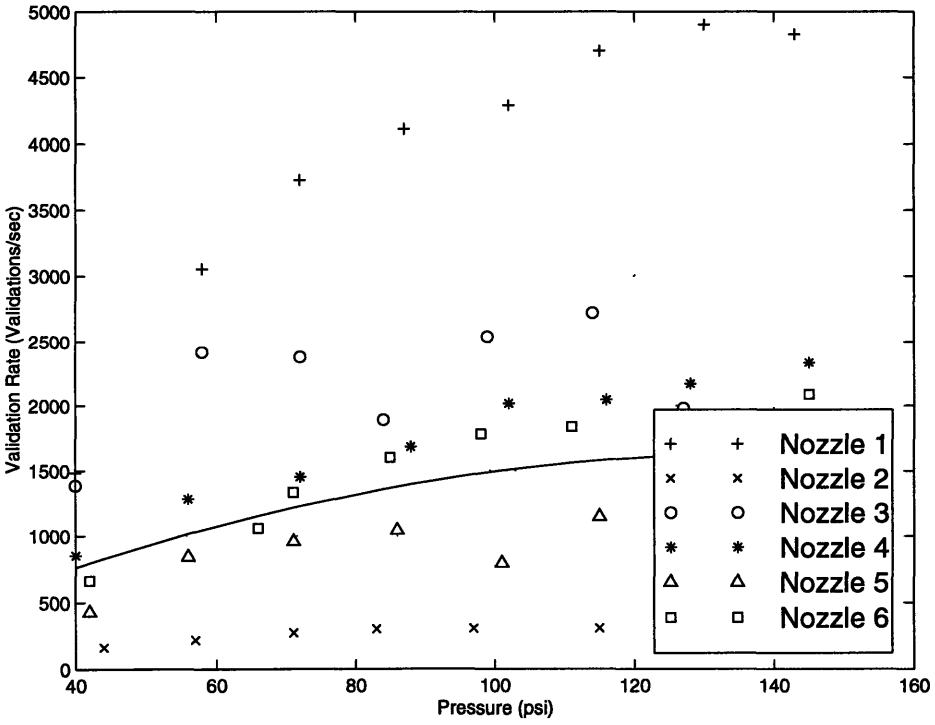

Figure 6.28: Hago B-50 aged 6 weeks. Pressure vs. validation rate at y = 0 and z = 5 cm.

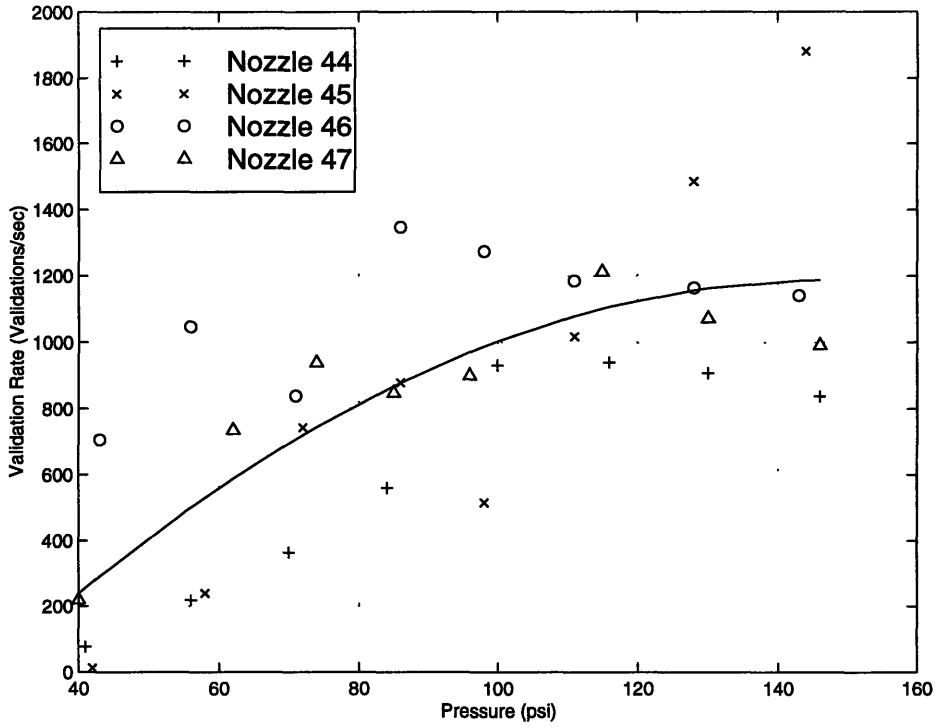

Figure 6.29: Hago B-50 clean nozzle. Pressure vs. validation rate at y = 0 and z = 20 cm.

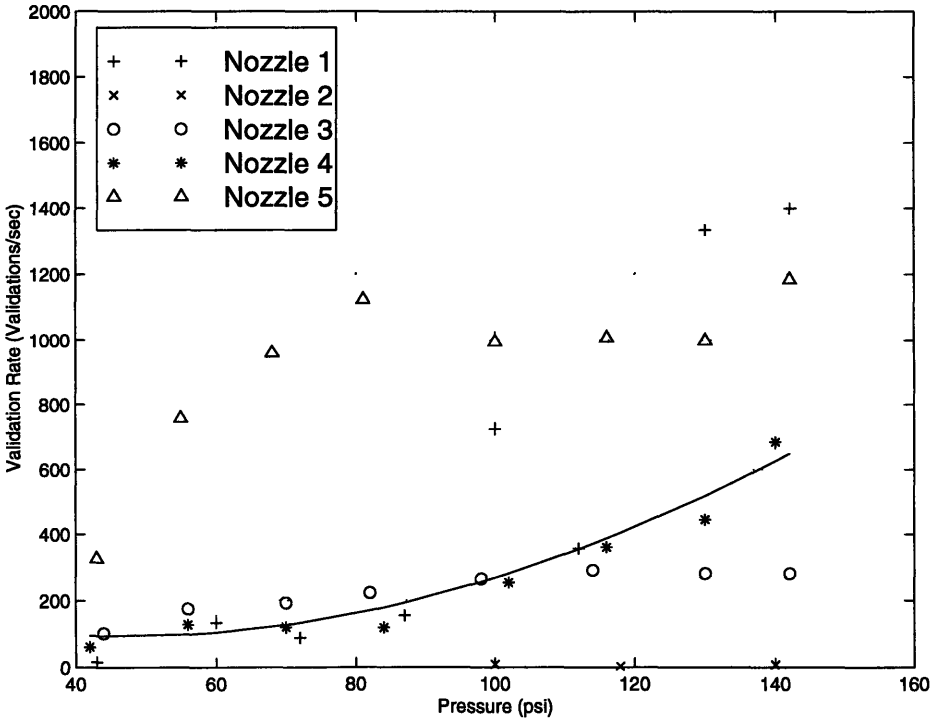

Figure 6.30: Hago B-50 aged 2 weeks. Pressure vs. validation rate at y = 0 and z = 20 cm.

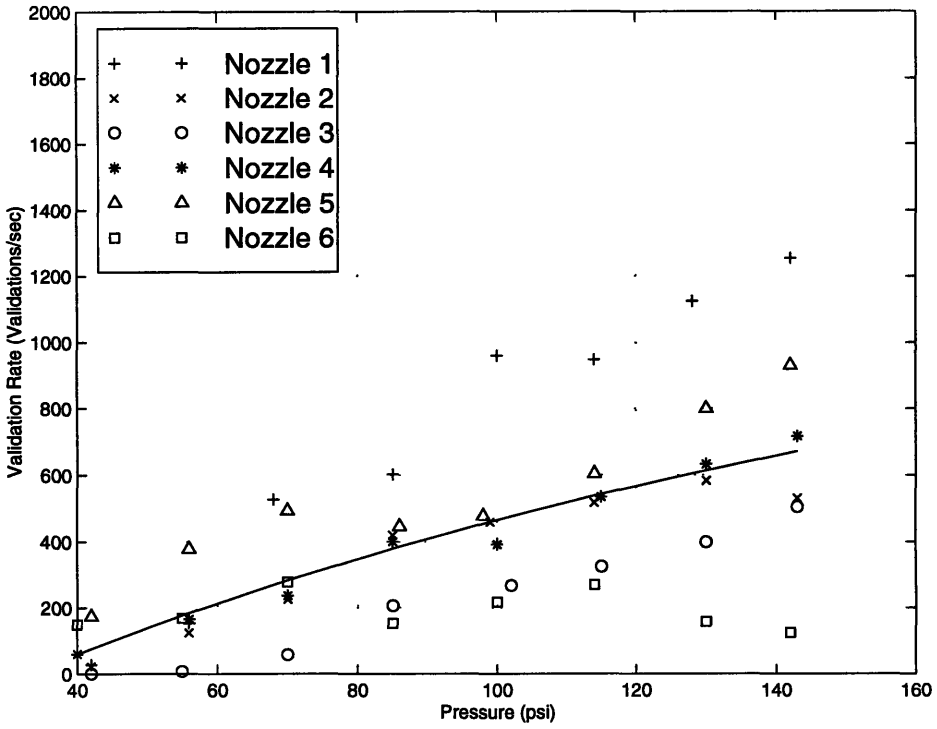

Figure 6.31: Hago B-50 aged 4 weeks. Pressure vs. validation rate at y = 0 and z = 20 cm.

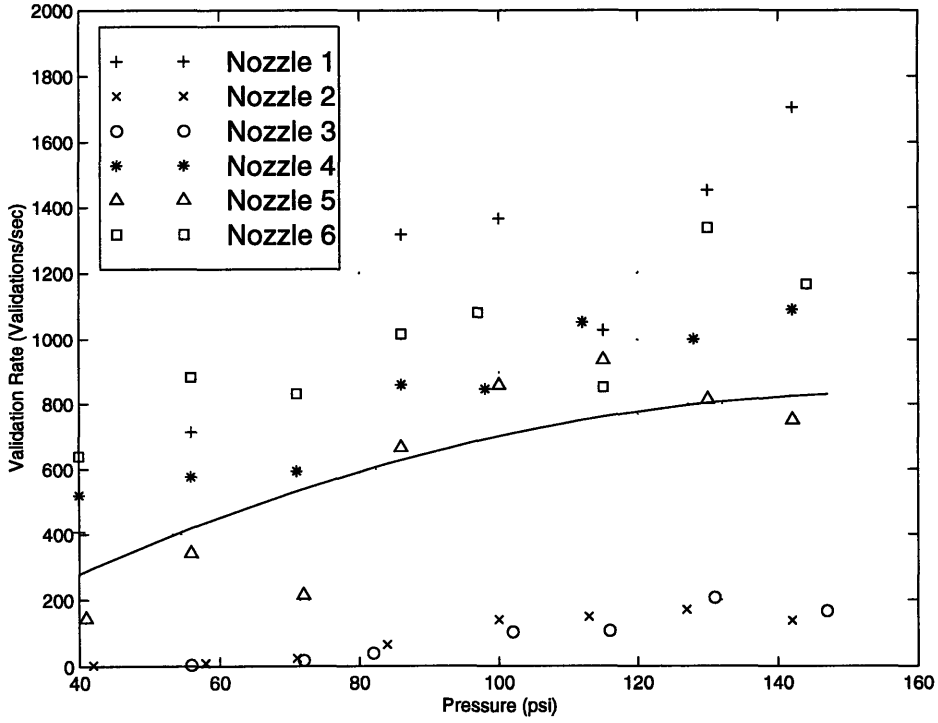

Figure 6.32: Hago B-50 aged 6 weeks. Pressure vs. validation rate at y = 0 and z = 20 cm.

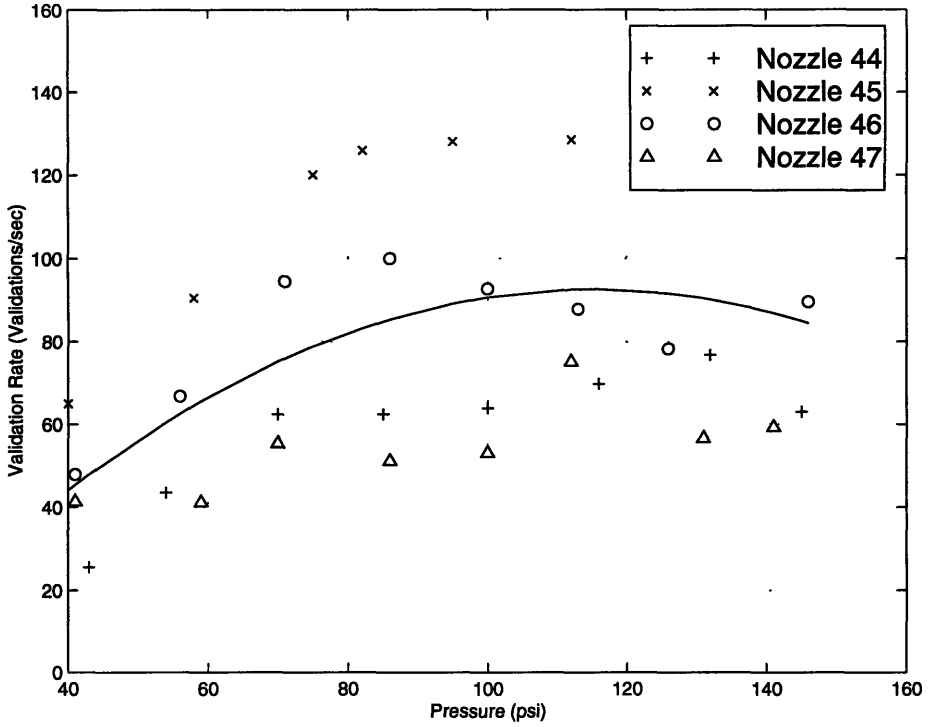

Figure 6.33: Hago B-50 clean nozzle. Pressure vs. validation rate at y = -20 and z = 20 cm.

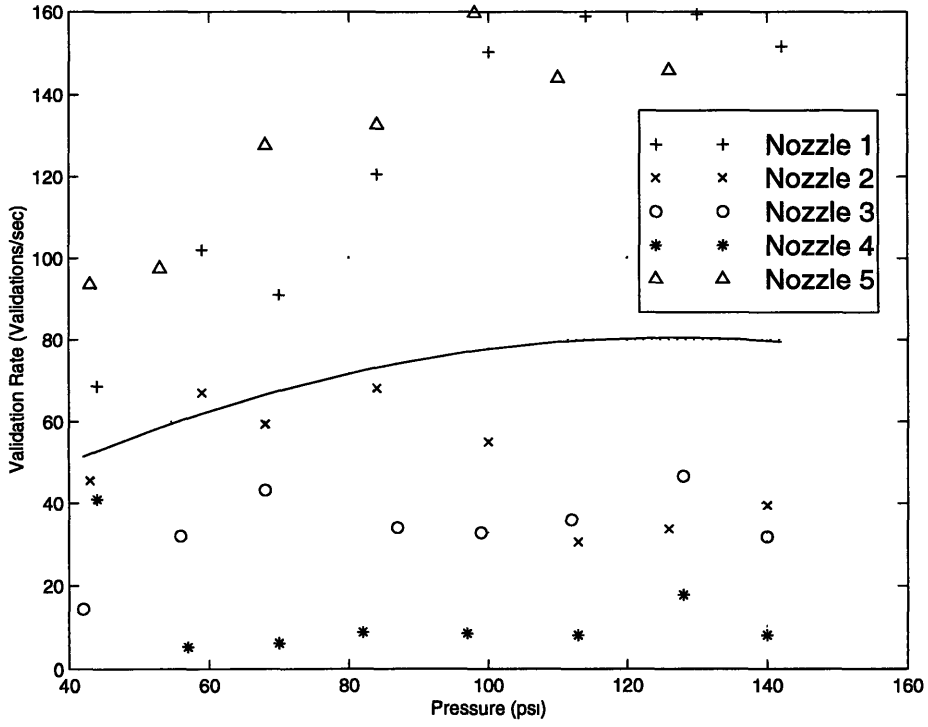

Figure 6.34: Hago B-50 aged 2 weeks. Pressure vs. validation rate at y = -20 and z = 20 cm.

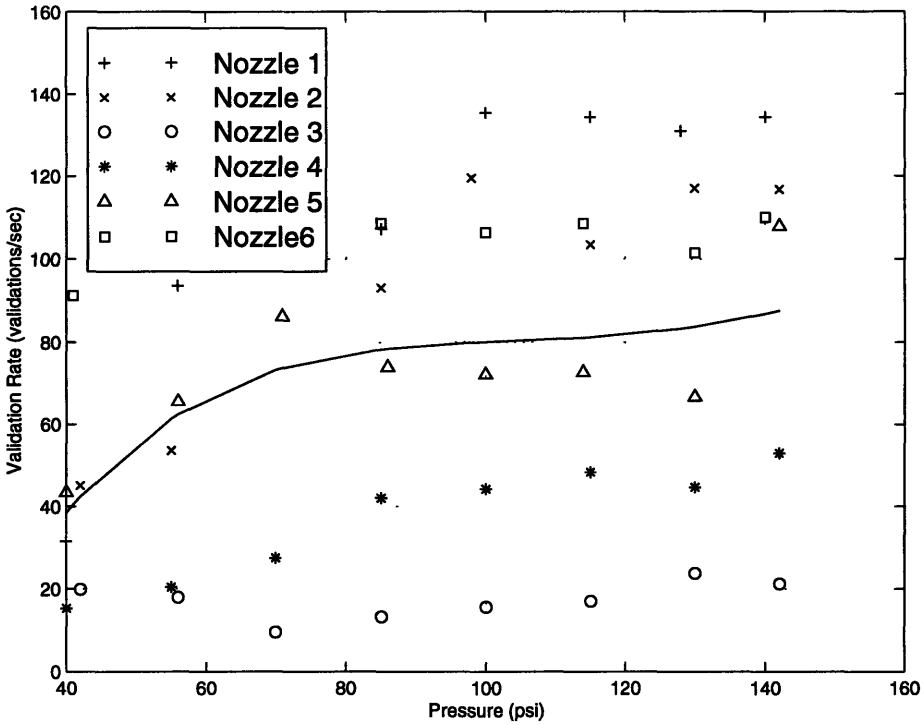

Figure 6.35: Hago B-50 aged 4 weeks. Pressure vs. validation rate at y = -20 and z = 20 cm.

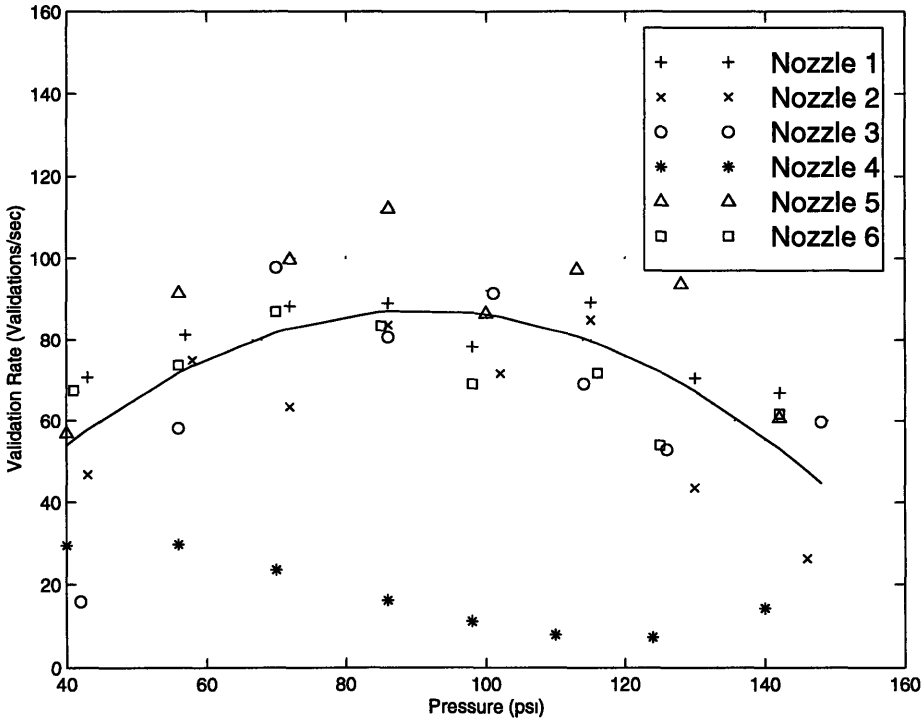

Figure 6.36: Hago B-50 aged 6 weeks. Pressure vs. validation rate at y = -20 and z = 20 cm.

Nozzle Age	A_c for ΔP in kPa	A_c for ΔP in psi
Clean	1.85	4.84
Aged Two Weeks	1.67	4.38
Aged Four Weeks	1.66	4.34
Aged Six Weeks	1.85	4.84

Table 6.1: Hago Nozzles' Constant, A_c.

6.1.4 Nozzle Flow Rate

Figures 6.37 through 6.40 show the variation of nozzle flow rate with pressure, for the B-50 nozzles aged zero, two, four and six weeks, respectively. Figure 6.41 is a juxtaposition of these four plots. The equation derived from basic inviscid theory between pressure and flow rate for the Hago B-50 nozzle [1] is,

$$Q = A_C\sqrt{\Delta P} \tag{6.1}$$

where A_c is a constant for a particular nozzle design, fluid and age, Q is the nozzle flow rate in ml/min and ΔP is the gage pressure in psi. The fitted values for A_c are listed in Table 6.1 for the clean and aged nozzles and for inputs of kPa and psi. The inviscid fit is plotted on all the flow rate graphs. The rotameter used to measure the flow rate is accurate to $\pm$ 2.2 ml/min.

The nozzles aged two and four weeks have approximately the same flow rate, while the clean and aged six weeks nozzles have the same flow rate which is higher than for the other nozzles. It is possible that as the nozzle are aged, the water flow path of the nozzle becomes partially obstructed by corrosion and scaling deposits (from the water) which reduces the flow rate of the nozzle. This would explain the decrease in flow rate from the clean nozzles to the nozzles aged four weeks. However, the reason the flow rate increased again after the nozzles were aged six weeks is not clear. Perhaps, after the nozzles are aged six weeks, the flow path expands due to erosion which yields an increased flow rate. Alternatively, it may be that some of the new nozzles have defects that promote clogging and that they become clogged after a few weeks and are removed from service before six weeks elapse. This sort of "infant mortality" is common in other areas of reliability engineering.

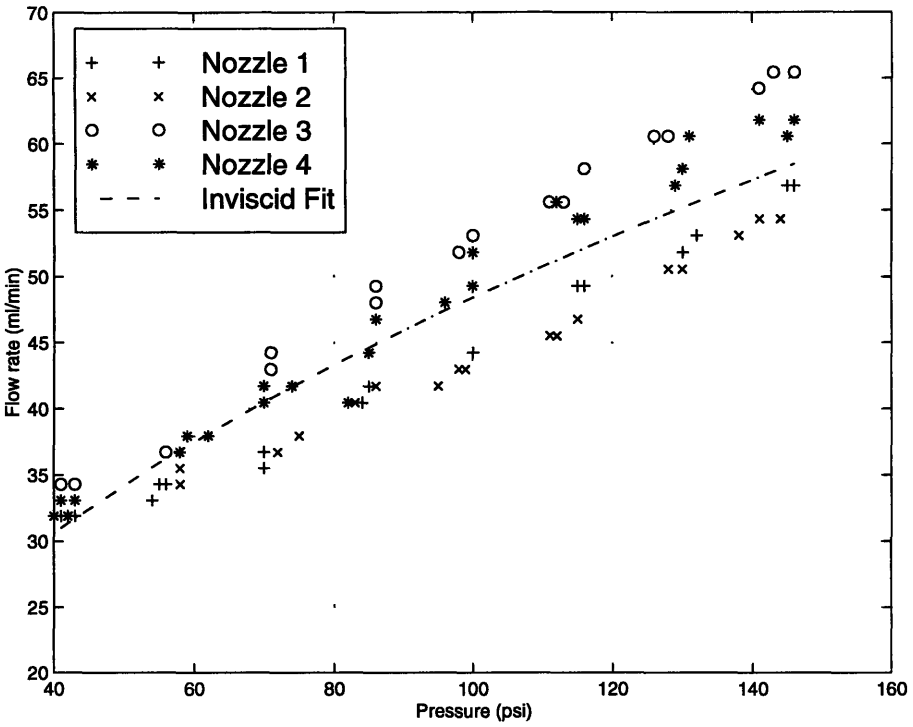

Figure 6.37: Hago B-50 clean nozzle. Pressure vs. flowrate.

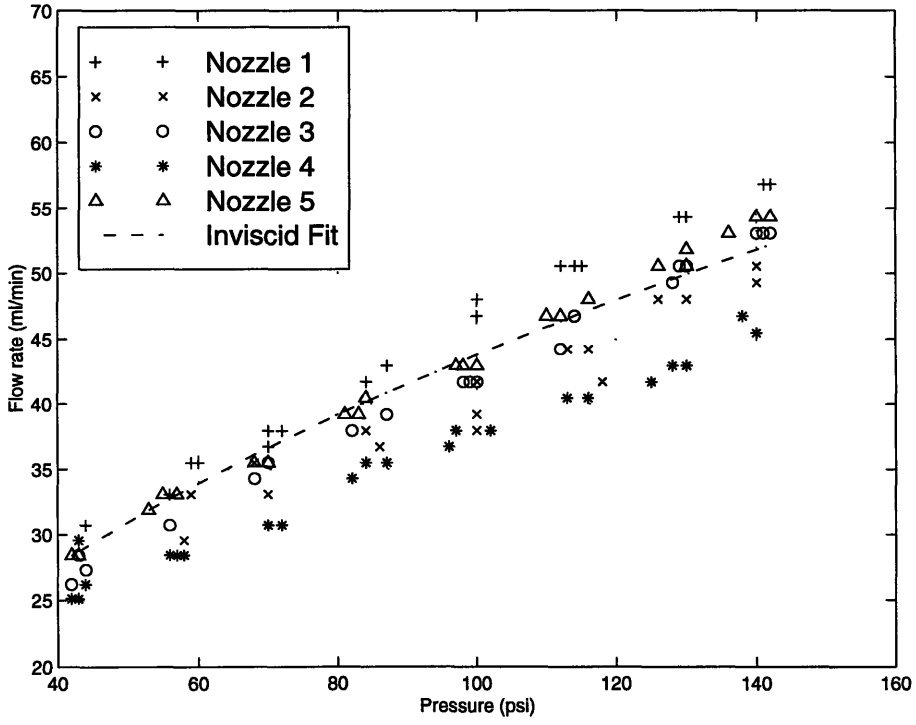

Figure 6.38: Hago B-50 aged 2 weeks. Pressure vs. flowrate.

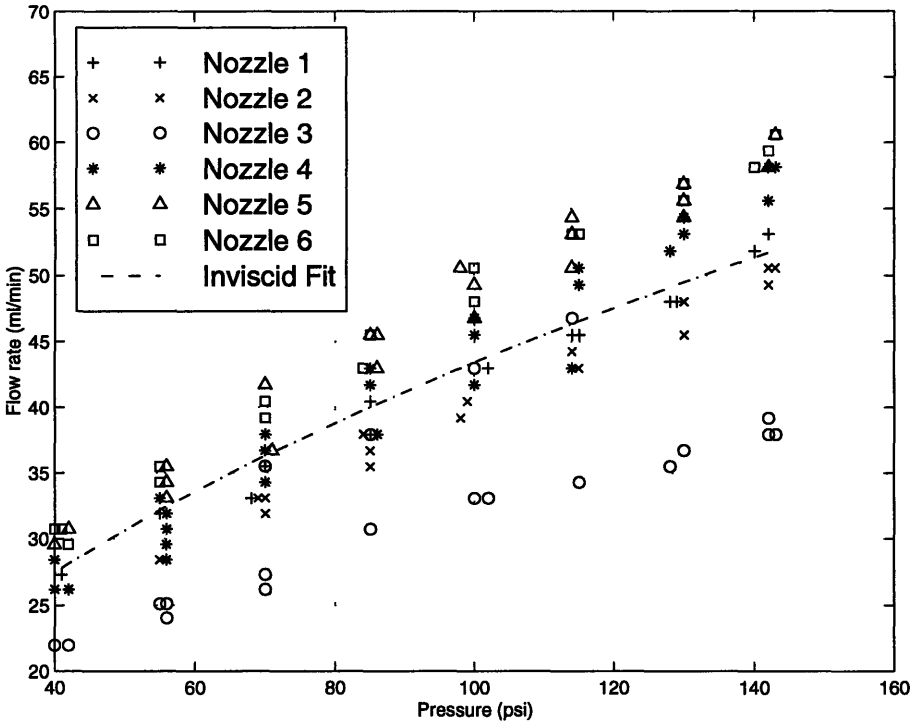

Figure 6.39: Hago B-50 aged 4 weeks. Pressure vs. flowrate.

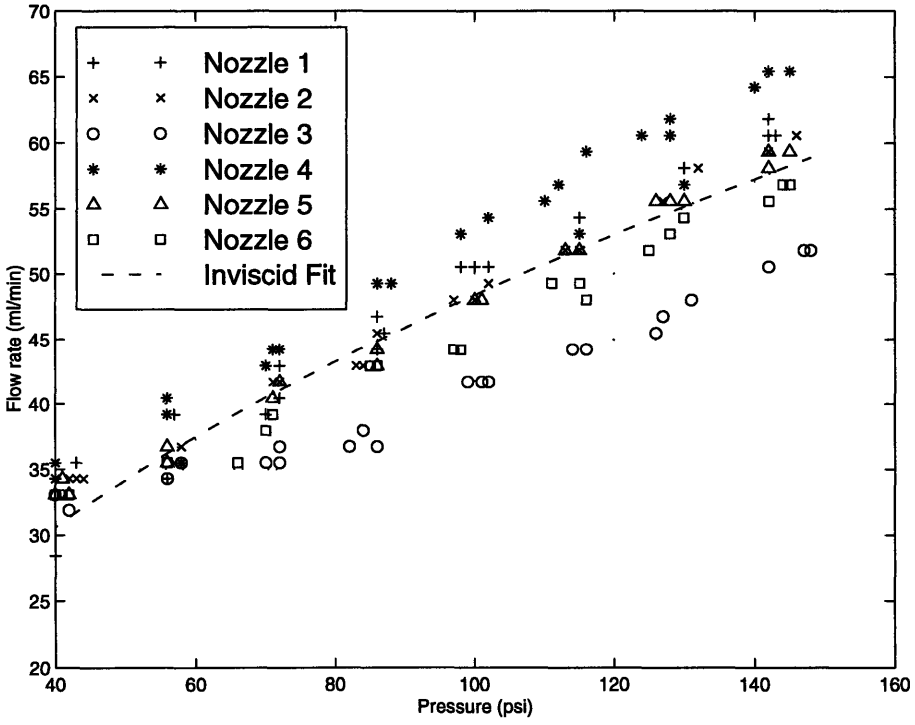

Figure 6.40: Hago B-50 aged 6 weeks. Pressure vs. flowrate.

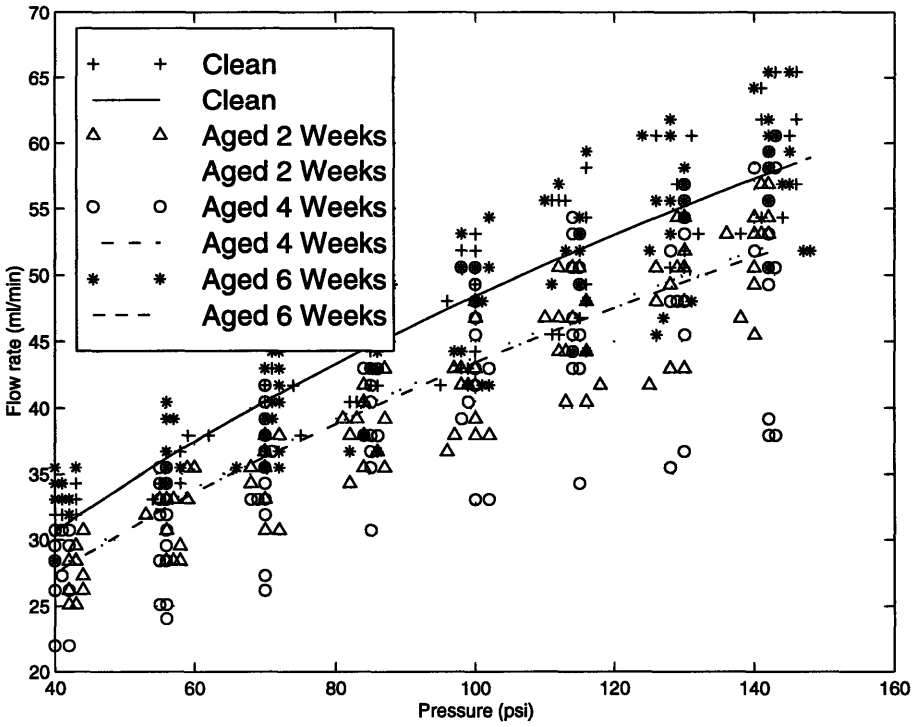

Figure 6.41: Hago B-50 aged nozzles comparison. Pressure vs. flowrate.

Mean Mean	Clean	Aged 2 Weeks	Aged 4 Weeks	Aged 6 Weeks
SMD	14.8	33.94	23.8	28.4
Velocity	2.89	1.8	3.27	2.75
Validation Rate	3036.5	1636.3	1968.5	1955
Flow Rate	46.38	44.23	45.06	48.23

Table 6.2: Hago B-50 Nozzles at a Pressure of 100 psi and at a Position of z = 5 and y = 0 cm.

Mean	Clean	Aged 2 Weeks	Aged 4 Weeks	Aged 6 Weeks
SMD	26.68	48.34	43.07	46.17
Velocity	1.85	.9042	1.2	1.3
Validation Rate	904.7	448.9	462.3	731.9
Flow Rate	46.75	43.98	43.63	48.02

Table 6.3: Hago B-50 Nozzles at a Pressure of 100 psi and at a Position of z = 20 and y = 0 cm.

Mean	Clean	Aged 2 Weeks	Aged 4 Weeks	Aged 6 Weeks
SMD	65.7	81.3	73.77	81.35
Velocity	.045	.118	.052	.033
Validation Rate	84.4	81.26	82.16	66.96
Flow Rate	46.7	44.47	43	48.02

Table 6.4: Hago B-50 Nozzles at a Pressure of 100 psi and at a Position of z = 20 and y = -20 cm.

6.2 Conclusions and Recommendations

Tables 6.2 through 6.4 show the mean droplet SMD, velocity, validation rate and flow rate at a pressure of 690 kPa (100 psi) for the B-50 nozzles aged zero, two, four and six weeks at the three positions previously mentioned (z = 5, y = 0 cm and z = 20, y = 0 cm and z = 20, y = -20 cm, respectively). The SMD and validation rate averages in the tables above reaffirm that aged nozzles produce larger and fewer droplets than the clean nozzles. However, concrete relationships can not be made regarding the variation of mean droplet SMD and mean validation rate with time, particularly in light of the high scatter of the data sets. Thus, the data analyzed in this report does not clearly indicate the maximum service life of nozzles on PPG's glass fiber production lines.

It is evident from the analysis that nozzle aging reduces the quality of atomization. Reduced

atomization is characterized by larger and fewer droplets, which reduces the total surface area of water. Hence, the evaporation rate and spray cooling effect are decreased and more water must be used for a given cooling load.

Once nozzle atomization becomes very poor, nozzles are replaced. The replacement of aged nozzles expends time and money. The life of a nozzle on a PPG production line is approximately three to eight weeks. This time period can be prolonged if corrosion and scale build-up from the water is reduced. Corrosion strongly depends on the concentration of mineral salts in the water. Softening the water will reduce the concentration of minerals in the water, thus decreasing corrosion and scale build-up. Another solution may be to manufacture the nozzles from a more corrosion resistant material. Presently, the nozzles are manufactured from 416 stainless steel and the nozzle adapters are manufactured from 303 stainless steel. Increased concentrations of nickel and molybdenum improves corrosion resistance in stainless steel [12].

Another possible factor affecting nozzle lifetime is an "infant mortality" in which some defective nozzles clog rapidly and are removed from service. Our studies have not used a large enough population of nozzles to verify such an effect, although they do suggest it. However, even the nozzles surviving to six weeks show degraded atomization implying lowered cooling efficiency.

6.3 Summary

1. The areas that are affected by corrosion are the outer covering, the tangential slots, the orifice and the filter of the nozzle.
2. Aging of nozzles causes fewer and larger droplets, yielding inferior atomization.
3. Operating above a pressure of 690 kPa (100 psi) does not significantly reduce SMD in nozzles of any age up to six weeks.
4. Aging causes more scatter in SMD, velocity, validation rate, and flow rate data among nozzles.
5. The increase in validation rate with increasing pressure for the clean and two week aged nozzles is much greater than for the four and six week aged nozzles along the nozzle centerline.
6. Validation rate decreases as the nozzles are further aged.
7. The nozzles aged two and four weeks have approximately the same flow rate, while the clean and six week aged nozzles have the same flow rate and have higher flow rates than the other nozzles.
8. Softening the water and/or manufacturing the nozzles from a more corrosion resistant material may reduce corrosion and mineral scale.
9. The maximum service life of nozzles on PPG's glass fiber production lines can not be concluded in this report. It is possible that testing a large sample of nozzles might reveal statistically significant trends in the mean nozzle characteristics as a function of age.

Chapter 7

Summary

The goal of this work was to investigate the entrainment of water sprays into the air flow induced in the manufacturing process of glass fibers. The spray atomization qualities and the spray dispersion patterns of the nozzles used on the glass production lines were examined. The droplet diameter, velocity and number flux were measured with a Phase Doppler Particle Analyzer.

During the manufacturing process, glass fibers move at very high velocities and generate a bulk air flow around the fiber bundle. An experimental apparatus was designed to generate various velocity profiles representative of the velocity fields on the actual glass fiber production lines. This test apparatus was used to measure the entrainment of the spray into a transverse air jet (simulated fiber air flow). The effect of aging on the spray nozzles was also examined in still air.

7.1 Spray Dispersion Analysis

Spray dispersion into a transverse air jet was studied for several different configurations of spray nozzles at various positions with different supply pressures. It was found that the air flow is a determining factor in the dispersion of the spray into the fiber bundle. When the spray cone comes in contact with the transverse air jet, the cone is deflected downward and the formed turbulent eddies are closer to the nozzle than in the still air case. As the nozzle is moved closer to the air flow, it is deflected further downward and turbulent eddies occur even closer to the nozzle. The air flow was found to have significant effects on the SMD, velocity and validation rate profiles of the spray. The measurements taken in the vertical center plane of the spray for various configurations of air jet speed and position captured these effects. Four different separations between

the nozzle and the bulk air flow were studied. For one of these separations, the effect of varying air velocity on spray dispersion was examined. Spray characteristics were also investigated for varying spray nozzle operating pressure.

7.1.1 Spray Dispersion into Air Flows of Various Speeds and Separations

The spray dispersion was examined at separations of 10 cm, 15 cm, 19 cm, and 25 cm; between the nozzle and the center of the bulk air flow at an jet exit velocity of 13 m/s. The results were compared to those of still air. In still air the SMD and validation rate profiles shift downward due to gravity and flatten with increasing distance from the nozzle. The addition of bulk air flow increased both these trends. The closer the bulk air flow was to the spray nozzle, the earlier the SMD and validation rate profiles shifted downward and flattened. In still air, the initial velocity profiles are characterized by well defined peaks that flatten with distance from the nozzle. In bulk air flow, this flattening is increased until the profiles are uniform with negligible values of velocity. The bulk air flow also causes the velocity profiles to shift downward. As the separation of the air jet from the nozzle increases, the downward shift of the maximum velocity peak occurs more gradually. It was also found that if the vertical air velocities near the nozzle were high enough, the spray would not develop into a fully developed spray cone, as was the case for a separation of 10 cm and a jet exit velocity of 13 m/s. The best spray dispersion for the initial jet velocity of 13 m/s was exhibited at a separation of 15 cm.

The spray dispersion was examined at a separation of 15 cm for the jet exit velocities of 13 m/s, 17.3 m/s and 21.4 m/s. Increasing the initial air jet velocity from 13 m/s to 21.4 m/s increased the downward deflection of the spray, reduced spray penetration into the air column and moved the turbulent eddies even closer to the nozzle. A fully developed spray cone did not develop at a separation of 15 cm when the initial air jet velocity was 21.4 m/s due to high air speeds in close vicinity to the nozzle.

These results suggest that the position of the spray nozzle as well as the speed of the air flow strongly influence the spray atomization and dispersion into the simulated fiber air flow. If the nozzle is placed too close to the air flow, poor atomization results because the spray does not fully develop. However, if the nozzle is placed too far from the fiber bundle most of the spray will be deflected downward before it reaches the fibers. Therefore, the nozzle most be placed in a position between these extremes in order to

optimize the spray cooling effects. For an initial air jet speed of 13 m/s, this position was determined to be 15 cm. However, the optimal position is dependent on air speed as was found when the initial air jet speed was increased to 21.4 m/s resulting in a spray cone that did not fully develop at the same position.

7.1.2 Effect of Nozzle Supply Pressure Variations on Spray Characteristics in Bulk Air Flow

The effect of pressure variations is examined for four spray nozzles in a bulk air flow centered at z = 19 cm from the nozzle exit. The nozzle operating pressure is varied from 276 kPa (50 psi) to 1000 kPa (145 psi) SMD, velocity and validation rate data is collected at four positions within the bulk air flow. As was the case with still air, increasing the nozzle operating pressure above 690 kPa (100 psi) did not significantly improve atomization. It was found that the bulk air flow appears to reduce the variation of the SMD's between different nozzles relative to still air. It was also observed that the downward drag force of the air flow prevented droplets from traveling far from the nozzle, even at elevated pressures.

7.1.3 Applications of This Work

The information gathered in this work provides a foundation for developing simplified models of the spray atomization qualities and the spray dispersion patterns. This type of information will be useful in predicting the heat transfer behavior on glass fiber production lines. Two important parameters needed to calculate the evaporative cooling effect of the spray are droplet SMD and droplet number density in the fiber bundle.

If the center of the bulk air flow is taken as the edge of the fiber bundle, the SMD can be estimated from the measurements taken at this position for each separation. In general the SMD profile was constant in the center of the bulk air flow, so a single average value could be used to estimate the SMD for each separation. It is interesting to note that in still air at distances of 25 cm or greater from the nozzle, the SMD profiles are also nearly constant with comparable magnitude to those observed in the center of the bulk air flow. As separation between the nozzle and the bulk air flow increased, the average SMD of this profile usually decreased. A decrease in SMD is also seen with increasing nozzle operating pressure. The droplet SMD did not change significantly in the center of the transverse air jet for the range of air velocities tested in this work.

In estimating droplet number density in the fiber bundle, significant parameters to consider include

nozzle flowrate, SMD, air velocity and the cross-sectional area of the air jet. This estimate would be affected by the following variables; air speed, separation, nozzle operating pressure and SMD. If the number flux (validation rate) measurements are assumed to be proportional to the number density estimates, presumptions can be made to estimate the effect of these variables on number density. The results of the number flux measurements indicated several trends. Increases in air speed and air jet area decreased the number flux of droplets that penetrated the air flow. An increase in nozzle flowrate and a decrease in droplet SMD were observed to increase the number flux. Changes in number flux with varying separation were harder to quantify because they depended on whether or not the spray becomes fully developed. It was found that if the spray becomes fully developed, the highest number flux occurred at the separation closest to the nozzle. These observations for number flux can be extended to number density. However, a more accurate model of number density would need to include the amount of spray that is actually entrained by the fiber air flow. It is possible that some of the droplets may be deflected in directions other than that of the fiber bundle before they are entrained into the air flow.

7.2 Aging Effects on Spray Nozzles

The effect of aging on the spray nozzles was examined. The spray characteristics were measured at three different positions within the spray cone for a range of operating pressures from 276 kPa (40 psi) to 1000 kPa (145 psi) for nozzles aged zero, two, four and six weeks on an actual glass fiber production line. It was found that increasing the nozzle operating pressure above 690 kPa (100 psi) did not provide significant improvement in spray atomization as was found in the bulk air flow case. Aging was found to cause inferior atomization characterized by fewer and larger droplets. Aging also caused more scatter in SMD, velocity, validation rate and flow rate data among nozzles. These effects are due to corrosion of the spray nozzles and to scale deposits within the nozzle water passage.

The maximum service life of a nozzle on a glass fiber production line could not be determined from this work. It is possible that testing a larger sample of nozzles might reveal statistically significant trends in the mean nozzle characteristics as a function of age.

Bibliography

[1] M. Sweetland. *Nozzle Analysis and Heat Transfer Model for Spray Cooling of Glass Fibers.* Massachusetts Insitute of Technology Thesis, Cambridge, 1998.

[2] A. H. Lefebvre. *Atomization and Sprays.* Hemisphere Publishing Corporation, New York, 1989.

[3] C. F. Edwards and K. D. Marx. Application of poisson statistics to the problem of size and volume flux measurement by phase-doppler anemometry. *Proceeding of the Fifth International Conference on Liquid Atomization and Spray Systems,* pages 653 - 660, 1991.

[4] H. C. Lewis, D. G. Edwards, M. J. Goglia, R. I. Rice, and L. W. Smith. Atomization of liquids in high velocity gas streams. *Ind. Eng. Chem.,* 40(1):67 - 74, 1948.

[5] H. Bruun. *Hot-wire Anemometry: Principles and Signal Analysis.* Oxford University Press, New York, 1995.

[6] Pitts and B. J. McCaffery. Response Behavior of Hot Wires and Films to Flows of Different Gases. *Journal of Fluid Mechanics*, 169:465-512, 1986.

[7] Freymuth and L. M. Fingerson. *Electronic Testing of Frequency Response for Thermal Anemometers.* TSI Technical Paper.

[8] R. Knystautas. The Turbulent Jet from a Series of Holes in Line. *The Aeronautical Quarterly,* 15:1-28, 1964.

[9] Stanley J. Kleis. The Effect of Exit Conditions on the Development of an Axisymmetric Turbulent Free Jet. Ph.D. Thesis, Michigan State University, 1974.

[10] James A. Fay. *Introduction to Fluid Mechanics.* M.I.T. Press, Cambridge, 1994.

[11] G.N. Abramovich. *The Theory of Turbulent Jets.* M.I.T. Press, Cambridge, 1963.

[12] William D. Callister, Jr. *Materials Science and Engineering.* John Wiley & Sons, New York, 1994.